

# The PLATO field selection process

## II. Characterization of LOPS2, the first long-pointing field

V. Nascimbeni<sup>\*1</sup>, G. Piotto<sup>2,1</sup>, J. Cabrera<sup>3</sup>, M. Montalto<sup>4</sup>, S. Marinoni<sup>5,6</sup>, P. M. Marrese<sup>5,6</sup>, C. Aerts<sup>7</sup>, G. Altavilla<sup>5,6</sup>, S. Benatti<sup>8</sup>, A. Börner<sup>9</sup>, M. Deleuil<sup>10</sup>, S. Desidera<sup>1</sup>, L. Gizon<sup>11</sup>, M. J. Goupil<sup>12</sup>, V. Granata<sup>1,2</sup>, A. M. Heras<sup>13</sup>, D. Magrin<sup>1</sup>, L. Malavolta<sup>2,1</sup>, J. M. Mas-Hesse<sup>14</sup>, H. P. Osborn<sup>15</sup>, I. Pagano<sup>4</sup>, C. Paproth<sup>9</sup>, D. Pollacco<sup>16</sup>, L. Prisinzano<sup>8</sup>, R. Ragazzoni<sup>2,1</sup>, G. Ramsay<sup>17</sup>, H. Rauer<sup>3,18</sup>, A. Tkachenko<sup>7</sup>, and S. Udry<sup>20</sup>

(Affiliations can be found after the references)

Submitted 20 September 2024 / Accepted 11 January 2025

### ABSTRACT

PLAnetary Transits and Oscillations of stars (PLATO) is an ESA M-class mission to be launched by the end of 2026 to discover and characterize transiting planets around bright and nearby stars, and in particular habitable rocky planets hosted by solar-like stars. Over the mission lifetime, an average of 8% of the science data rate will be allocated to Guest Observer programs (GOs) selected by ESA through public calls, hence it is essential for the community to know in advance where the observing fields will be located. In a previous paper, we identified two preliminary long-pointing fields (LOPN1 and LOPS1) for PLATO, respectively in the northern and southern hemisphere. Here we present LOPS2, a slightly adjusted version of the southern field that has recently been selected by the PLATO Science Working Team as the first field to be observed by PLATO for at least two continuous years, following the scientific requirements. In this paper, we describe the astrophysical content of LOPS2 in detail, including known planetary systems, bright/variable/binary stars, clusters and synergies with other current and future facilities.

**Key words.** Catalogues – Astronomical data bases – Techniques: photometric – Planetary systems – Planets and satellites: detection – Stars: clusters

### 1. Introduction

PLATO (PLAnetary Transits and Oscillations of stars; Rauer et al. 2024) is an ESA M-class mission primarily designed to detect a large number of planetary systems hosted by nearby and bright stars through the transit technique. Among many other aims, the goal of this mission is the discovery and confirmation of Earth-like planets, i. e., habitable rocky planets hosted by solar-type dwarfs (Heller et al. 2022; Matuszewski et al. 2023). Very accurate stellar parameters, including stellar age at 10% accuracy<sup>1</sup>, will be extracted from the light curves themselves through asteroseismological analysis (Cunha et al. 2021; Bétrisey et al. 2023). This will enable us to put the discovered planetary systems in a consistent evolutionary context. Furthermore, the follow-up and confirmation of candidate planets discovered by PLATO is part of the mission through the Ground-based Observation Program (GOP) of the PLATO Consortium. We refer the reader to Rauer et al. (2024) for a recent, detailed review of the mission.

During its nominal 4-year mission, PLATO will continuously monitor one or two pre-selected fields for at least two years each (during the so-called LOP: Long-duration Observing Phase). The mission has been designed to have the capability to observe additional fields for shorter intervals, at least two months each (SOP; Short-duration Observing Phase). The 24 “normal” cameras of PLATO (NCAMs) are not all co-aligned, but rather split in four groups with an angular offset ( $9.2^\circ$ ) with respect to the satellite bore-sight (Pertenais et al. 2021). As a consequence, the overall field of view (FOV) of about  $2\,149\text{ deg}^2$  is covered

by a variable number of NCAMs, from six to 24, depending on the specific line of sight considered, as illustrated by Fig. 1. In terms of sky area, approximately  $325\text{ deg}^2$  will be covered by 24 NCAMs,  $153\text{ deg}^2$  by 18 NCAMs,  $847\text{ deg}^2$  by 12 NCAMs and  $824\text{ deg}^2$  by 6 NCAMs (assuming a corrected FOV of  $19.2^\circ$  and CCD gaps of 1.3 mm; Pertenais et al. 2021) although the exact numbers could slightly change according to the actual optical performances once in flight.

Due to telemetry constraints, we will not be able to download full-frame images at high cadence<sup>2</sup>. Instead, PLATO will perform a significant part in the photometric analysis onboard. Only light curves, centroid data and a number of stamp-like “imaggettes” will be transmitted back to Earth, meaning that targets have to be selected in advance. PLATO targets are divided into four main samples, summarized in Table 1, with different requirements on magnitude, spectral type and noise-to-signal ratio (NSR): three of such samples are composed by main-sequence or subgiant stars with spectral type from F5 to K7 (P1, P2, P5), while a fourth one contains only M dwarfs (P4). The PLATO Scientific Requirement Document<sup>3</sup> (SciRD) identifies P1 ( $V < 11$ ,  $\text{NSR} < 50\text{ ppm}$  in one hour) as the highest-priority sample, and sets a requirement of at least 15 000 P1 targets to be observed during the LOPs. We refer to the SciRD, Nascimbeni et al. (2022) and Montalto et al. (2021) (hereafter quoted as N22 and M21) for a complete summary of the definitions and requirements on the PLATO samples.

PLATO is currently on schedule to be launched at the end of 2026, and to start its routine scientific operations in mid-

<sup>2</sup> Full-frame images will be acquired during the commissioning phase, at least once every 90 days.

<sup>3</sup> ESA reference: PTO-EST-SCI-RS-0150.

\* E-mail: valerio.nascimbeni@inaf.it

<sup>1</sup> For solar-like stars.

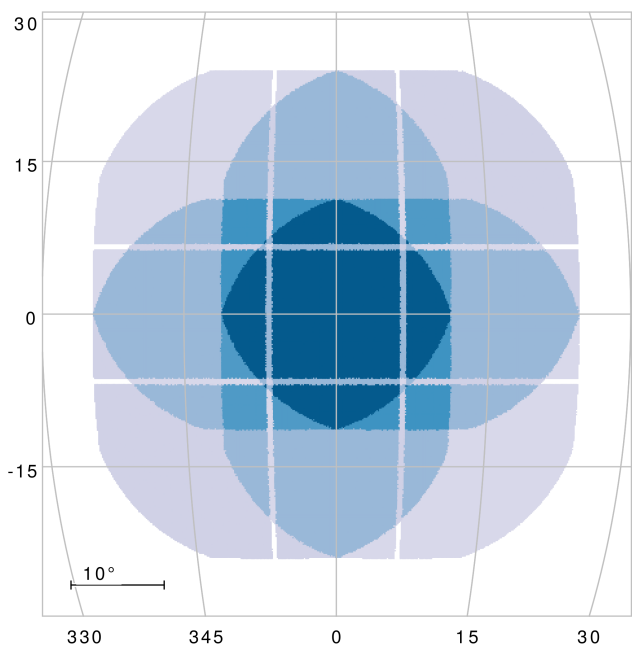


**Fig. 1.** Geometry of the PLATO field FOV. In this figure, the field is centered at the origin (0,0) of a generic spherical reference frame (units are degrees; projection is orthographic). The number of “normal” cameras covering a given line of sight is color-coded. The four blue shades, from dark to light, map the regions covering 325/153/847/824 deg<sup>2</sup> observed respectively with 24, 18, 12, six cameras (and corresponding to four, three, two, and one group of six co-pointing telescopes each).

2027. Most raw and calibrated data products from PLATO will be made publicly available as soon as possible<sup>4</sup>. The astronomical community has the opportunity to be deeply involved at different stages: preparation, data analysis, and follow-up. PLATO data products will be released quarterly. Each set of data from a three-month observation period will be made available approximately six months later. For around 20 000 bright targets prioritized for ground-based follow-up observations, the data products will be delivered roughly 1.2 years after the corresponding three-month observation period. On top of that, over the mission lifetime, an average of 8% of the PLATO science data rate will be allocated to Guest Observer programs (GOs) selected by ESA through open calls, so it is essential to select and communicate each field that is going to be pointed at with a proper time margin.

In a previous work (Paper I; N22), we described all the steps of the process that led to the identification of two provisional fields (labeled LOPN1 and LOPS1) as candidates for the LOP. Back then, it was still unknown which one would be selected as the first one. Also, it was anticipated that the final LOP fields could have had small changes in position and/or rotation angle. In this paper, we present LOPS2, the long-pointing field finally chosen by the ESA PLATO Science Working Team (PSWT) as the first field to be observed by PLATO. After summarizing the fine-tuning process and the general properties of LOPS2 in Section 2, we review and discuss its astrophysical content in Section 3. Finally, the conclusions and some prospects for the future work to be done are given in Section 4. A glossary of the most common acronyms used throughout this work is compiled in Table B.1 in the Appendix.

<sup>4</sup> With the exception of GO programs and reserved targets allocated to the Plato Mission Consortium, within their proprietary time.

## 2. The choice of the first long-pointing field

Paper I gave a very detailed description of the process that led to the selection of LOPS1 and LOPN1 as candidate long-duration fields for PLATO. In order to fine-tune their position/rotation angle and to help the SWT to select the first LOP, three main criteria were considered:

- *Duty cycle*: The PLATO attitude is defined by the pointing direction and the rotation around the mean line of sight. Because of the geometry of the overlapping cameras, different rotation angles result in different sets of stars observed with a given photometric precision (with a different number of cameras). For pointing directions with ecliptic latitudes between  $63^\circ < |\beta| < 70^\circ$ , the choice of the rotation angle around the mean line of sight is constrained by the geometry of the spacecraft. There is always a possible rotation angle that meets the duty cycle requirements (93% of time on-target), but some angles result in incompatible attitudes. For pointing directions with  $|\beta| > 70^\circ$  all choices of the rotation angle are compatible with the duty cycle requirements.
- *Rotation angle*: is there any technical or scientific advantage to choose a different rotation angle?
- *Synergies*: which field is the most interesting one for possible synergies with other facilities, in particular with regard to the radial-velocity follow-up process, considering the time frame of the mission?

In what follows we will discuss the impact of these three key ingredients on the final decision.

### 2.1. Duty cycle

As anticipated in Paper I, Section 2.4, the need of keeping the solar panels of PLATO at a nominal level of solar irradiation while constantly staring at the same LOP field for  $\geq 2$  years implies that the roll angle of the spacecraft must be moved at regular intervals throughout the year. Since the PLATO field, by design, shows a  $90^\circ$  symmetry, it is natural to perform  $90^\circ$  rotations each quarter, also known as quarterly rolls. A similar observing strategy was already devised for the original *Kepler* mission (Borucki et al. 2010). The ecliptic latitude  $\beta$  is the crucial parameter to be investigated, as it determines the incidence angle of the solar rays on the panels. There is a critical value of  $|\beta|$  above which an observing quarter can start at any moment, without any need of interruptions before the first roll.

Following a detailed assessment of the problem with the PLATO mission team, we concluded that the threshold must be set at  $|\beta| > 69^\circ.671$  for the geometrical center of the field, i.e., slightly more stringent than the formal requirement of  $|\beta| > 63^\circ$  previously applied in Paper I. While this is already fulfilled by LOPN1 ( $\beta \approx 75^\circ.85$ ; Table 2 of Paper I), LOPS1 is slightly below that value, being at  $\beta \approx -66^\circ.30$ . As a working hypothesis, we examined, within the “compliant” region of our HEALPix level-4 grid (Fig. 5 of Paper I), the grid point at  $\beta < -70^\circ$  and closest to LOPS1 (#2189 in our original HEALPix numbering scheme;  $\beta \approx -71^\circ.1$ ). We renamed this field LOPS2, and verified that:

- LOPS2 is centered at the same Galactic latitude as LOPS1 ( $b \approx -24^\circ.6$ ), but shifted by  $\sim 5^\circ.1$  westward along Galactic longitude, leaving the average stellar crowding (and hence the expected false positive ratio; Bray et al. 2023) essentially unchanged;

**Table 1.** Definitions of the main PLATO stellar samples.

sample	SpT	lum. class	mag. limit	noise
P1	F5-K7	dwarfs and subgiants	$V < 11$	$< 50$ ppm
P2	F5-K7	dwarfs and subgiants	$V < 8.5$	$< 50$ ppm
P4	M	dwarfs	$V < 16$	—
P5	F5-K7	dwarfs and subgiants	$V < 13$	—

**Notes.** The rows give: the name of the PLATO stellar sample, the spectral type, the luminosity class, the limiting magnitude in the  $V$  band, and the noise limit in ppm in one hour (see also Section 3.1).

- LOPS2 is centered at a slightly larger declination in modulus ( $\delta \simeq -47^\circ.9$  vs.  $-42^\circ.9$ ), with no significant impact on the follow-up strategy;
- the prioritization metric as defined in Paper I is 1% smaller (0.980 vs. 0.990), i.e., the difference is negligible;
- the number of P1 targets in LOPS2, defined as in Table 1 and evaluated with the most updated version of the PLATO Input Catalog (PIC) (v.2.0.0), is 0.4% lower, but still well within the margins of SciRD requirements.

In other words, LOPS2 appears as an optimal alternative, having properties very similar to LOPS1, but allowing us to be much more efficient during mission operations. For example, the in-orbit commissioning will take place before the start of the nominal science operations. In order to avoid constraints on the choice of the rotation angle for commissioning (and hence in the duty cycle), the pointing direction for the commissioning field must have  $|\beta| > 70^\circ$ , which was an incompatible constraint with LOPS1. We therefore consider LOPN1 (as defined in Paper I) and LOPS2 (as defined above; detailed coordinates in Table 2) as candidate LOP fields hereafter.

Although it has a negligible impact on the duty cycle, it is worth reminding that the dates of the quarterly rotations along the orbit are uniquely determined by the choice of the attitude. This is a consequence of the duty cycle requirement and the geometry of the spacecraft. For LOPS2 and LOPN1, the quarterly rotations will take place at the end of January, April, July, and October (the exact dates differ by few days in both hemispheres). For a scheduled launch end 2026 and considering that the commissioning shall take less than 90 days, it could very well be that the first quarter is significantly shorter than the nominal duration of approximately 90 days, similar to the situation experienced by *CoRoT* and *Kepler*.

## 2.2. Rotation angle

In paper I, both fields were presented at zero rotation angle, which, in our convention, implies that one side of the field is parallel to the Galactic plane. We investigated the impact of the rotation angle  $\varphi$  by generating nine simulated catalogs for both LOPN1 and LOPS2 by varying the angle by  $10^\circ$  intervals (from  $\varphi = 0^\circ$  to  $80^\circ$ ). For the resulting 18 catalogs, extracted from the PIC 2.0.0, we added a NSR column (calculated with PINE; Börner et al. 2024), in order to estimate the number of P1-P2-P4-P5 counts and to assess the visibility of our main targets of interest.

As expected, given the large size of the PLATO field and its fair degree of radial symmetry,  $\varphi$  has a mostly negligible impact on the number of targets. For both LOPN1 and LOPS2 the P1

counts are constant within  $\sim 1\%$ , with the highest number corresponding to the  $\varphi = 0^\circ$  case (Fig. B.1, left panel). On the other hand, P4 and P5 counts are virtually unaffected, showing just  $< 0.5\%$  variations, that is at the level of the predicted Poissonian noise (Fig. B.1, right panel). We can conclude that  $\varphi$  has no practical effects on the planet yield of PLATO.

It is worth considering whether there is any other reason to rotate the field, for instance due to specific astrophysical objects we would like to include, or avoid, in the LOP field. As for the former, we verified that 1) the number of known planetary systems is not significantly affected by  $\varphi$  for LOPN1, and is actually maximized at  $\varphi = 0^\circ$ - $10^\circ$  for LOPS2 due to an overdensity of TESS-discovered planets lying in the Galactic south-west corner of the field (as we will show in Section 3.4); and 2) no open cluster among the ones of potential interest for PLATO (i. e., nearby, sparse, and mature) slips in or out of the field for any rotation angle choice, as it will be shown in Section 3 for LOPS2. More in general, the range of Galactic latitudes probed is always  $0^\circ < |b| \lesssim 50^\circ$  regardless of  $\varphi$ , and therefore any property correlated with  $b$ , such as the amount of stellar crowding and the diversity of stellar populations probed (in terms of age, kinematics, metallicity, etc.) is approximately the same.

Finally, it makes sense to investigate whether there is any way to rotate the field in order to move any extremely bright star ( $V < 1$ ) off the silicon. Paper I identified Deneb and Vega as the brightest sources on LOPN1, and Sirius and Canopus for LOPS1. Moving from LOPS1 to LOPS2 also implies that Sirius is now left outside the focal plane for any choice of  $\varphi$ , while there is no consequence on the other three stars, that are unavoidable and always monitored with the same number of NCAMs (18-24 for Vega, 6 for Deneb, 24 for Canopus) for almost any possible rotation angle<sup>5</sup>. Fig. B.2 (but also Section 3.2 below) investigates this point a bit further, looking at how the number of bright stars (up to  $V < 3$ ) in LOPS2 changes as a function of  $\varphi$ , at  $10^\circ$  intervals from  $0^\circ$  to  $80^\circ$  (the symmetry of the PLATO field makes it invariant after  $90^\circ$  rotations). The nominal  $\varphi = 0^\circ$  case is the only one for which all the five  $1 < V < 2$  stars ( $\delta$  CMa,  $\epsilon$  CMa,  $\gamma_2$  Vel,  $\delta$  Vel,  $\epsilon$  Car) always land on 6 NCAMs regions, while for instance four of them fall on 12 NCAMs in the  $\varphi = 40$ - $50^\circ$  case. Finally, also the distribution of  $2 < V < 3$  stars does not change significantly as a function of  $\varphi$ .

In summary, we conclude that there is no reason to change the rotation angle of both LOPN1 and LOPS2 from its initial value of  $\varphi = 0^\circ$ . We will implicitly assume zero rotation (i.e., one side of the field almost tangent to the Galactic plane) hereafter, as plotted in the all-sky projection in Fig. 2.

## 2.3. Synergies and follow-up

The last possible criterion remaining to guide the choice between LOPN1 and LOPS2 are the synergies with other past, present and forthcoming observing facilities, including (and with a particular attention to) those to be involved with the PLATO follow-up process during and after the nominal scientific observations of the first field, approx. from mid-2027 with a minimum duration of two years.

As for the previous space-based transit surveys, we first remind that no overlap between a LOP field and K2 or CoRoT

<sup>5</sup> It could be possible in principle to fit Deneb within a  $\sim 30'$  CCD gap of the northern field at  $\varphi \simeq 11^\circ$ , but the technical feasibility of such a choice and its possible unintended consequences (see for instance Porterfield et al. 2016) need to be assessed. This will be done at a further stage, should LOPN1 be scheduled for observation.



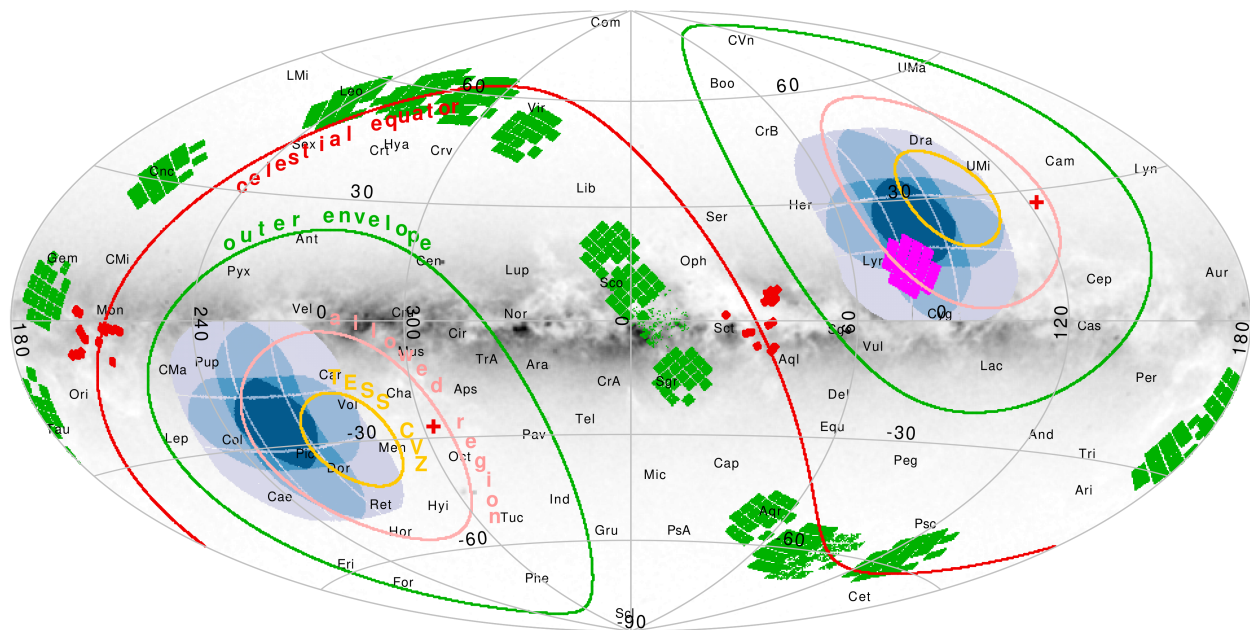


**Fig. 2.** All-sky Aitoff projection in Galactic coordinates of LOPS2 and LOPN1, showing the formal constraints for the selection of the PLATO LOP fields and the synergies with other missions. The two pink circles represent the  $|\beta| > 63^\circ$  technical requirement for the center of the LOP fields (“allowed region”), implying that the overall envelopes of every allowed field choice are two ecliptic caps at  $|\beta| \geq 38^\circ$  (green circles). LOPS2 (lower left) and LOPN1 (upper right) are plotted with blue shades according to the number of co-pointing cameras, as in Fig. 1. The footprints of CoRoT (red), *Kepler* (magenta), and K2 (green) are over-plotted together with the TESS continuous viewing zone at  $|\beta| \geq 78^\circ$  (yellow circle). The background gray layer is color-coded according to the areal density of  $G < 13.5$  stars from *Gaia* DR3. The celestial equator and poles are marked with a red line and crosses, respectively. This sky chart is also plotted in equatorial and Ecliptic coordinates in Fig. B.4-B.5.

(Howell et al. 2014; Auvergne et al. 2009) is possible at all, since the latter fields are all located close to the ecliptic by design, inaccessible during the LOP phase (Fig. 2). The TESS continuous viewing zone (CVZ) at  $|\beta| > 78^\circ$ , on the other hand, is monitored at 100% in LOPN1 and  $\geq 90\%$  in LOPS2, mostly in six- and 12-camera regions. Finally, the *Kepler* field is fully included in the LOPN1, almost entirely with at least 12 NCAMs and up to 24. While the scientific case of following-up the *Kepler* TTV systems with PLATO is very solid (Jontof-Hutter et al. 2021a,b), we emphasize that it should not be seen as a main driver of the mission, but rather as a potential source of interesting additional science<sup>6</sup>. Indeed, the last word is on the follow-up availability and timeliness, since the confirmation of the PLATO candidates and eventual mass determination is part of the mission products (and goals) through the Ground-based Observation Program (GOP) of the PLATO Consortium.

We already noted in Paper I that the range of declination spanned by any compliant LOP field (including LOPN1 and LOPS2) hinders the follow-up of a large fraction of the northern field with most southern facilities and vice versa, with the exception of a strip in the low- $|\delta|$  region of the fields, whose size depends on the maximum acceptable airmass  $X$  and the geographical latitude  $\psi$  of the observing site. Such a strip can be typically monitored from the opposite hemisphere only for 1-2 months per year at reasonably low airmass values ( $1.5 \lesssim X < 2.0$ ; see Paper I), making ultra-high precision ( $< 1$  m/s) RV measurements unfeasible or exceedingly difficult for the vast majority of P1 targets. A detailed analysis on how the visibility of LOPS2 and its sub-regions covered by six, 12, 18, 24 NCAMs is dependent on  $\psi$  and  $X$  is shown in Fig. B.3. As a reference value, we note that

<sup>6</sup> It is worth mentioning that the follow-up of the *Kepler* field is part of the science goals of the proposed Earth-2.0 mission (Ge et al. 2022).

at the Observatorio Roque de Los Muchachos (ORM) only 16% of LOPS2 is reachable at  $X < 2$  (and only in the 6-12 NCAMs region), while at Mauna Kea 36% of LOPS2 can be observed with the same requirement (but only 8% of the 24 NCAMs region can be reached).

A survey of the high-precision RV spectrographs available to the European community reveals that most of them are located in Chile: they include the already operational HARPS (Mayor et al. 2003) and ESPRESSO (Pepe et al. 2021); and the planned ANDES, whose first light at the ESO Extremely Large Telescope (ELT) is currently foreseen in 2031 (Marconi et al. 2022). More in general, large-scale facilities such as ELT will also host other instruments with a huge potential in the follow-up process, such as coronagraphs and infrared spectrographs. Conversely, no large telescope of the 30-m class is currently at the construction stage in any northern observatory.

It is worth mentioning two other important survey projects in the South that could have interesting implications for the PLATO preparation and/or follow-up: LSST (Ivezic et al. 2019) at the Vera C. Rubin Observatory, that will map the whole southern hemisphere (including LOPS2) beginning in 2025, and 4MOST at the VISTA telescope (de Jong et al. 2012), starting its consortium surveys also in 2024.

#### 2.4. LOPS2 as first LOP field

On the basis of what has been discussed in the previous Section, in June 2023 the SWT has formally approved LOPS2 (at  $\varphi = 0^\circ$ ) as the first LOP field. A full-sky map in Galactic coordinates including LOPS2 and LOPN1 is presented in Fig. 2; the same full-sky map is also plotted in equatorial and Ecliptic coordinates in Fig. B.4-B.5; a zoomed-in chart centered on LOPS2 is plotted in Fig. 3 in both Galactic and equatorial coordinates. All



**Table 2.** Some properties of the LOPS2 field.

parameter	value	notes
$\alpha$ [deg]	95.31043	ICRS
$\alpha$ [hms]	06:21:14.5	ICRS
$\delta$ [deg]	-47.88693	ICRS
$\delta$ [dms]	-47:53:13	ICRS
$l$ [deg]	255.9375	IAU 1958
$b$ [deg]	-24.62432	IAU 1958
$\lambda$ [deg]	101.05940	Ecliptic
$\beta$ [deg]	-71.12242	Ecliptic
P1 targets	8 235	SciRD req. 7 500
P2 targets	699	SciRD req. 500
P4 targets	12 415	SciRD req. 2 500
P5 targets	167 149	SciRD req. 122 500

**Notes.** The rows give: coordinates for the field center in equatorial, Galactic and ecliptic reference frames, and number of targets available in the P1-P2-P4-P5 samples. The latter are calculated from PIC 2.0.0 assuming the “EOL 22” scenario (see Section 2.4).

the relevant quantities for LOPS2 are listed in Table 2, including the number of targets for each PLATO sample. The latter are calculated by adopting PIC 2.0.0 as input catalog and conservatively assuming an end-of-life scenario with 22 surviving NCAMs (“EOL 22”). We refer the reader to Section A in the Appendix on how to check if a given object falls within the LOPS2 boundaries.

We mention that LOPS2 includes most of the TESS southern CVZ (as we will further discuss in Section 3.7), the Large Magellanic Cloud (LMC; but not the SMC), the southern Ecliptic pole (but not the celestial one), and one of its sides is a  $49^\circ$ -long strip parallel to the Galactic plane and reaching up to  $0^\circ.25$  from it; the opposite side goes as far as  $b \approx -49^\circ$ . The range of declination spanned by LOPS2 is  $-73^\circ.8 < \delta < -20^\circ.8$ , with 90% of its area lying within the  $-64^\circ.0 < \delta < -28^\circ.6$  range. Six constellations are covered entirely, or almost entirely by LOPS2: Pic, Col, Dor, Cae, Ret, Pup; smaller parts of CMa, Car, Vol, Men, Hor, Eri, Lep, Vel, Hyi are also overlapped.

The average interstellar extinction coefficient  $A_V$  and its spatial dependence is shown in Fig. 4 for both the P1+P2 and P5 samples of LOPS2. In the former case we always got  $A_V < 0.07$ ; in the latter sample, a clear structure with  $A_V \approx 0.3$  appears, corresponding to some parts of the Vela-Puppis region (Cantat-Gaudin et al. 2019). Clearly, the main reason for the larger extinction of the P5 sample is the much larger average distance of its stars, due to a much fainter magnitude limit ( $V < 13$  for the P5 sample,  $V < 11$  for P1). No significant excess of extinction can be seen on these maps in the LMC region, because even our faintest and intrinsically more luminous targets lie always within 3 kpc from the Sun: the LMC is just a background object for the PLATO planet-hunting survey. See also Section 3.1 for some details on the distance distribution.

### 3. Astrophysical content of LOPS2

#### 3.1. Main PLATO targets

Adopting PIC v. 2.0.0 as input catalog, and calculating the NSR through the PINE code (Börner et al. 2024), we can calculate the

counts for the four main samples of PLATO (defined according to the formal requirements of the SciRD):

- 8 235 P1 targets, i. e., FGK dwarfs and subgiants with  $\text{NSR} \leq 50$  ppm in one hour and  $V \leq 11$ ;
- 699 P2 targets, i. e., FGK dwarfs and subgiants with  $\text{NSR} \leq 50$  ppm in one hour and  $V \leq 8.5$ ;
- 12 415 P4 targets, i. e., M dwarfs with  $V \leq 16$ ;
- 167 149 P5 targets, i. e., FGK dwarfs and subgiants with  $V \leq 13$ .

The definitions listed above are also summarized in Table 1. When the samples are computed as disjoint sets (that is, P2 is excluded from P1, and P1+P2 is excluded from P5), in LOPS2 we have 699 P2 targets, 7 536 P1 targets and 158 914 P5 targets. The total sample of available targets in LOPS2 is therefore 179 564 FGKM stars. We note that, with some exceptions and unless otherwise stated, targets in LOPS2 that are not included in the PLATO samples will *not* be observed by default and should be proposed in the GO program. The detailed policy will be communicated in advance of the first GO call. According to the ESA Science Management Plan (available on the ESA website, but also summarized in Rauer et al. 2024, Section 10) the first public release of the PIC, which also includes flags for P1-P2-P4-P5, will be released to the community nine months before the launch, concurrently with the call for the GO proposals. According to the current mission schedule, this is expected to happen in spring 2026.

The distances of individual solar-type LOPS2 targets (i.e., samples P1+P2 and P5) are plotted in Fig. 5, while the statistical distribution in terms of distance, interstellar extinction  $A_V$  and magnitude is shown in the histograms of Fig. B.6-B.7, for both the whole PIC and for a few subsamples of interest. Unsurprisingly for a magnitude-limited sample, and as also shown in Paper I, late-type, main-sequence targets such as G/K dwarfs are on average much closer to us with respect to early-type stars and (sub-)giants, due to their fainter absolute magnitude. As a consequence, the former have also lower interstellar extinction values with respect to the latter (right panel of Fig. B.6).

The histograms of some other astrophysical properties of the P1+P2 and P5 samples are plotted in Fig. B.8-B.9. The spatial distributions of the P1, P2, P4, P5 samples are plotted in the four panels of Fig. B.10: P2 and P4 stars are almost perfectly homogeneously distributed, because they both lie relatively close to the Sun, and are purely magnitude-limited samples<sup>7</sup>. P5 is also magnitude-limited, but being on average much fainter is also farther from the Sun, and the consequent line-of-sight effects due to the Galactic disk are revealed by the significant density gradient along Galactic latitude. Finally, P1 is concentrated toward the inner region of LOPS2, observed with 18/24 NCAMs, where the noise requirement is easier to be met at equal magnitude.

#### 3.2. Bright stars

As part of the field selection process, and as anticipated in Section 2.2, we investigated the presence of very bright stars on LOPS2. We used the Yale Bright Star Catalogue version 5 revised (YBSC; Hoffleit & Warren 1995) as input, being a reasonably complete and accurate census of all the stars brighter than  $V \approx 6.5$ . The strategy of PLATO for moderately saturated stars imaged on the NCAMs (i.e., between magnitudes 4

<sup>7</sup> Formally, the P2 definition also includes a  $\text{NSR} \leq 50$  ppm requirement but with the current design it is always satisfied even at its  $V = 8.5$  faint limit.

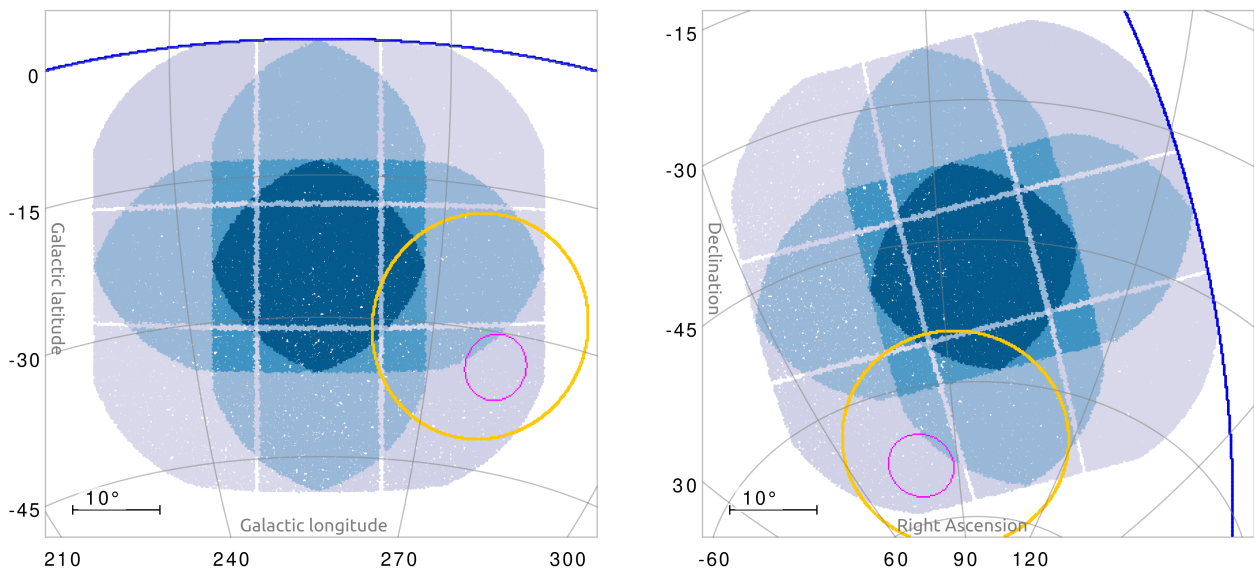


**Fig. 3.** LOPS2 footprint. *Left panel:* orthographic projection in Galactic coordinates centered on LOPS2. The field is color-coded according to the number of NCAMs as in Fig. 1. The yellow circle at  $\beta = -78^\circ$  approximates the southern TESS continuous viewing zone (CVZ), while the magenta circle is centered on the Large Magellanic cloud. *Right panel:* as in left panel, but in equatorial coordinates.

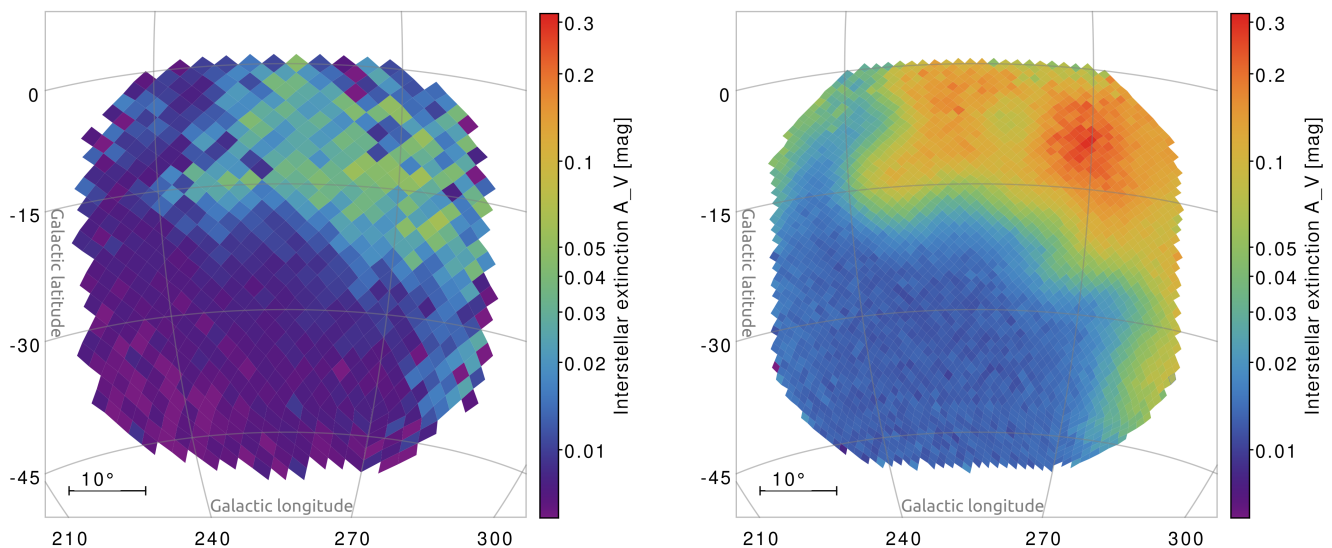


**Fig. 4.** Interstellar extinction properties of LOPS2. *Left panel:* Average V-band extinction  $A_V$  of the P1+P2 targets from PIC 2.0.0, calculated over HEALPix level-5 cells and represented in a color scale. *Right panel:* same, but for the P5 sample and over a finer level-6 grid. The high-extinction bump at  $A_V \approx 0.3$  is due to the closest parts of the Vela-Puppis region (Cantat-Gaudin et al. 2019).

and 8 in the PLATO Vegamag system, and approximately<sup>8</sup> also in the  $4 \lesssim V \lesssim 8$  range) is to use larger imagerettes (saturated star windows) that extend up to  $256 \times 6$  pixels in size to extract the photometry, if the additional telemetry cost needed to download more data is justified. For stars brighter than magnitude 4, a different strategy is being discussed. For example, smearing photometry is technically possible (White et al. 2017; Pope et al. 2019), but alternatives are being considered.

In any case, knowing the position of such bright sources could be of interest since their bright halos, bleeding columns and smearing trails can potentially contaminate any other fainter target in their neighborhood. A discussion on the technical

<sup>8</sup> The exact saturation limit is largely determined by factors other than the color term  $P - V$ , including the position on the FOV, the PSF shape, the actual in-orbit CCD gain and optical transmission, etc.

issues related to CCD saturation, blooming, non-linearity as well as optical ghosting is discussed in Verhoeve et al. (2016); Pertenais et al. (2022); Janssen et al. (2024) and will be better explored in the forthcoming papers of this series.

Among the 712 YBSC stars lying in the LOPS2, only 47 are brighter than  $V = 4$  (Fig. 6, left plot). With the only exception of Canopus =  $\alpha$  Car (also by far the brightest one;  $V = -0.72$ ), Phact =  $\alpha$  Col, and  $\tau$  Pup, all the 12 extremely bright stars at  $V < 3$  are located close to the Galactic plane at  $|b| < 15^\circ$ , where also the average stellar density increases very rapidly as the line of sight crosses the Galactic disk (Fig. 6, right plot). Not surprisingly, all of them are early-type and/or evolved giants, so none would fit the spectral type requirement to be included in the PLATO P2 sample.

Scrolling down the list,  $\zeta$  Dor A = HD 33262 at  $V = 4.68$  is the brightest star in LOPS2 to be included in the PIC: it

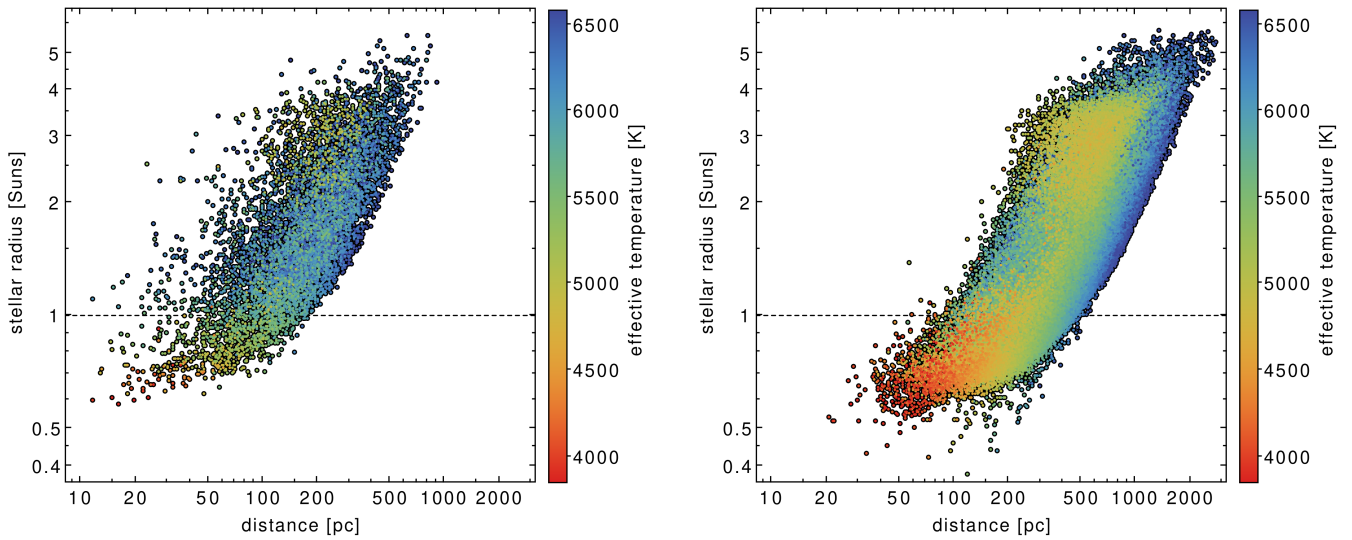


**Fig. 5.** Distance of the P1/P2 and P5 samples in LOPS2. *Left panel:* Distribution of the 8 235 P1+P2 stars in LOPS2 in the  $(R_*$ , distance) plane. The stellar effective temperature from the PIC v2.0.0 is color-coded. *Right panel:* same, but for the P5 sample (167 149 stars; P1/P2 not included). The distribution moves to larger distances due to the fainter magnitude limit of P5 ( $V < 13$  vs.  $V < 11$ ).

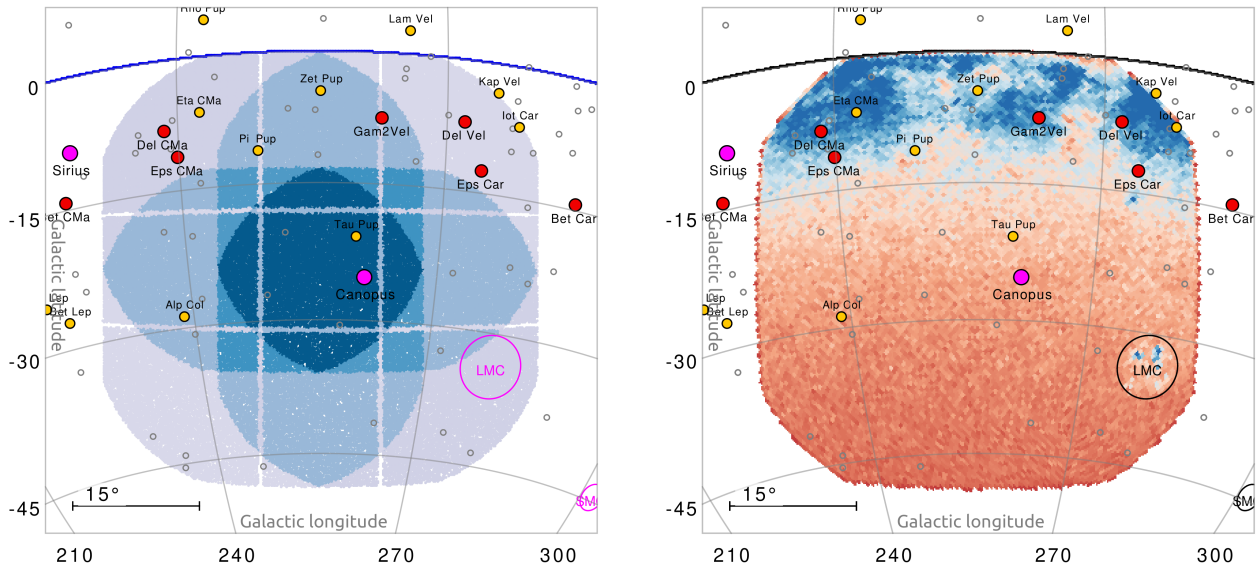


**Fig. 6.** Bright stars and stellar crowding in LOPS2. *Left panel:* orthographic projection in Galactic coordinates centered on LOPS2. The field is color-coded according to the number of NCAMs as in Fig. 1. The brightest stars from the Yale Bright Star Catalog are plotted as circles of different colors: magenta ( $V < 1$ ), red ( $1 < V < 2$ ), yellow ( $2 < V < 3$ ), gray ( $3 < V < 4$ ). *Right panel:* same, but the footprint of LOPS2 is color-coded according to the areal density of  $G < 13.5$  stars from *Gaia* DR3. The color scale increases proportionally to density from orange to blue with a transition at  $\sim 400$  targets per  $\text{deg}^2$ , at  $b \approx -15^\circ$ .

is the F7V component of a very wide visual binary. It is also known as a young and active star surrounded by a debris disk (Dodson-Robinson et al. 2011). B Car = HD 68456 = HR 3220 comes as a close second at  $V \approx 4.73$ ; it is a single-lined spectroscopic binary whose F7V primary was also identified as a field blue straggler by Fuhrmann et al. (2011), transferring mass to its low-mass white dwarf companion on a  $P = 899$  d orbit. 212 Pup = HD 64379, at  $V = 5.05$ , is the brightest binary system made of main-sequence stars (F7V+K5V) in our sample, with a narrow separation ( $3''$ ). Finally, the brightest single solar twin in the P2 sample is HD 59967 ( $V = 6.66$ ), a young G2V star (Lorenzo-Oliveira et al. 2018) with a debris disk (Pearce et al. 2022), showing evident high levels of stellar activity and with no

detected planetary companions from FEROS (Zakhohay et al. 2022) and HARPS (Grandjean et al. 2023).

### 3.3. Nearby stars

Among the 562 known stars within 10 pc from the Sun (Reylé et al. 2021, 2023-02-06 version), 14 are located within LOPS2. Only seven of them are bright enough ( $V \lesssim 16$ ) to be reliably monitored by PLATO<sup>9</sup>. Six of them are M dwarfs or sub-dwarfs, spanning spectral types from sdM1V to M4.5V; sorted by increasing  $G$  magnitude and spectral type: GJ 191, CD-44 3045 B and A, AP Columbae, L 230-188, SCR J0740-4257.

<sup>9</sup> The excluded targets are all at  $G \gtrsim 20$ , i.e., way too faint for PLATO to deliver reliable photometry.



The seventh one is LAWD 26 = GJ 293, a bright hydrogen-rich white dwarf (WD; DA;  $G \sim 13.7$ ,  $V \sim 14.1$ ), spectroscopically confirmed by Bell & Rodgers (1964) and recently identified by Sanderson et al. (2022) as one of the most promising white dwarf targets for the discovery of astrometric planets with *Gaia*.

Other nearby and reasonably bright WDs can be identified from the catalog by Gentile Fusillo et al. (2021): 86 targets with  $G < 15$  lie within the LOPS2 footprint<sup>10</sup>. Among these, and besides the already mentioned LAWD 26, four additional stars show a parallax  $\pi > 50$  mas, i.e., they are closer than 20 pc: two of them were also spectroscopically confirmed by O’Brien et al. (2023), both as DA spectral types.

It is worth mentioning that Kapteyn’s star = GJ 191 ( $V \sim 8.8$ ,  $K \sim 5.0$ ) is an old M1 sub-dwarf at only 3.9 pc from the Sun, and also the nearest known halo star (Kotoneva et al. 2005). It will be observed by PLATO through 12 cameras, and with an average NSR estimated around 18.4 ppm in 1 h according to the current noise budget calculations. Two planetary candidates were claimed to be discovered through RVs around GJ 191 by Anglada-Escude et al. (2014), but were later disproved as due to stellar activity by Robertson et al. (2015) and Bortle et al. (2021), who also noted that the star is photometrically very stable. As will be discussed in Section 3.4, a coordinated RV follow-up of this target could take advantage of the simultaneous PLATO coverage to disentangle the contributions of stellar activity and the Keplerian signal from planets, if any.

CD-44 3045 A and B, also known as GJ 257, represent an equal-mass visual binary (M3V + M3V) with an angular separation of 2.4” at 2016.0 according to *Gaia* DR3. Hence, they will fall on the same  $\sim 15$ ” pixel of PLATO, and observed as a single object in combined light within the P4 sample.

### 3.4. Known planetary systems

It is of primary interest to identify all the already known planets and planetary candidates within LOPS2, since 1) it makes the vetting and follow-up process much more efficient, 2) there are many science cases for which a long-term and/or extreme-precision follow-up of already known planets can yield compelling scientific results (see for instance Jontof-Hutter et al. 2021b), and 3) the unprecedented photometric accuracy of PLATO may allow us to discover additional transiting planets around planet-hosting stars and/or confirm low-SNR candidates and mono-transits (Magliano et al. 2024).

For the reasons mentioned above, it has been decided that the final PIC will include all confirmed and candidate exoplanets known at the compilation date, so all the planetary systems mentioned in the following sections, if technically feasible with PLATO, will be forced into the catalog regardless whether they meet the P1-P2-P4-P5 SciRD requirement or not. We mention that a preliminary review of the known planetary systems located in LOPS2 was also presented by Eschen et al. (2024), although limited to transiting planets only and with a particular focus on the PLATO vs. TESS synergy. We note that their overall numbers are roughly consistent with ours, but a direct comparison is

not possible because a combination of different catalogs and/or unreported catalog versions were employed in their match.

#### 3.4.1. Transiting planets

We retrieved the list of known planets from Exo-MerCat (Aleí et al. 2020, Aleí et al. 2024 in prep.), a meta-catalog built by comparing and merging with an automated process scanning three input catalogs: Exoplanet Encyclopedia<sup>11</sup>, the NASA Exoplanet Archive<sup>12</sup> and the Open Exoplanet Catalog<sup>13</sup>. In this Section we focus on the transiting sub-sample only, which is the most important one given the scientific opportunity they represent for PLATO.

Overall, 108 confirmed transiting planets are located in LOPS2 (Fig. 7, left panel and Table B.1); they belong to 84 distinct planetary systems. Among the 13 systems with multiple transiting planets there are five doublets (GJ 143, TOI-216, TOI-286, TOI-431, TOI-2525), six triplets (TOI-270, TOI-451, TOI-712, LHS 1678, L98-59<sup>14</sup> and HD 28109), and two high-multiplicity systems that look as perfect showcases for the photometric performances of PLATO:

- TOI-700, a four-planet system hosted by a relatively bright ( $V \simeq 13$ ) M2V star, including two super-Earths in or close to the habitable zone (Gilbert et al. 2020, 2023);
- HD 23472 = TOI-174, a packed five-planet system (Trifonov et al. 2019; Teske et al. 2021) orbiting around a  $V \simeq 9.7$  K dwarf, made of three confirmed super-Earths (with at least a suspected 5:3 mean-motion resonance) and two candidate high-density “super-Mercuries”, among the least massive planets to ever have been detected through RVs (Barros et al. 2022).

Among the mentioned multiple transiting systems we also identify three systems hosted by relatively young stars ( $< 10^9$  years): TOI-451, belonging to the Pisces Eridanus stream (120 Myr; Newton et al. 2021), and the field stars TOI-201 (870 Myr; Hobson et al. 2021) and TOI-712 (830 Myr; Vach et al. 2022).

There are also five additional entries in Exo-MerCat whose estimated masses fall within the brown dwarf (BD) regime (HIP 33609b, TOI-569b, TOI-811b, TOI-1496b) or across the planet/BD transition (HATS-70b; Zhou et al. 2019). They are plotted as yellow diamonds in Fig. 7.

A closer look to the planetary parameters of the 108 transiting planets (Fig. 8, left panel) reveals a vast diversity of planetary properties. Adopting some common definitions from the literature, we can split our sample into four main classes:

- 47 hot Jupiters (HJ;  $R_p > 6 R_\oplus$ ,  $P < 10$  d). This sub-sample is unlikely to increase significantly in the future, given the almost perfect sensitivity of TESS and the existing ground-based surveys in this region of the parameter space. Notably, there are three ultra-hot Jupiters (UHJs;  $T_{\text{eq}} > 2200$  K): WASP-121b (Delrez et al. 2016), KELT-25b (Rodríguez Martínez et al. 2020), and the already mentioned HATS-70b. WASP-121b is of particular interest since it spawned an impressively vast literature on its atmospheric characterization, including the study of its optical phase

<sup>10</sup> We emphasize that WDs will not be included in the main PIC sub-samples (P1-P2-P4-P5) due to the spectral class requirement (Section 3.1), unless they are flagged as planetary hosts or candidate hosts (See Section 3.4). Within the technical limits, though, they can be included as “scientific calibration and validation” targets (scvPIC; Zwintz 2024) or as GO targets.

<sup>11</sup> <https://exoplanet.eu/home/>

<sup>12</sup> <https://exoplanetarchive.ipac.caltech.edu/index.html>

<sup>13</sup> <https://www.openexoplanetcatalogue.com/>

<sup>14</sup> L98-59 and GJ 143 lie very close to a LOPS2 external border (Fig. 7, left plot), therefore their inclusion in the target list (and the delivered photometric precision) will depend on the actual pointing accuracy and system performance.

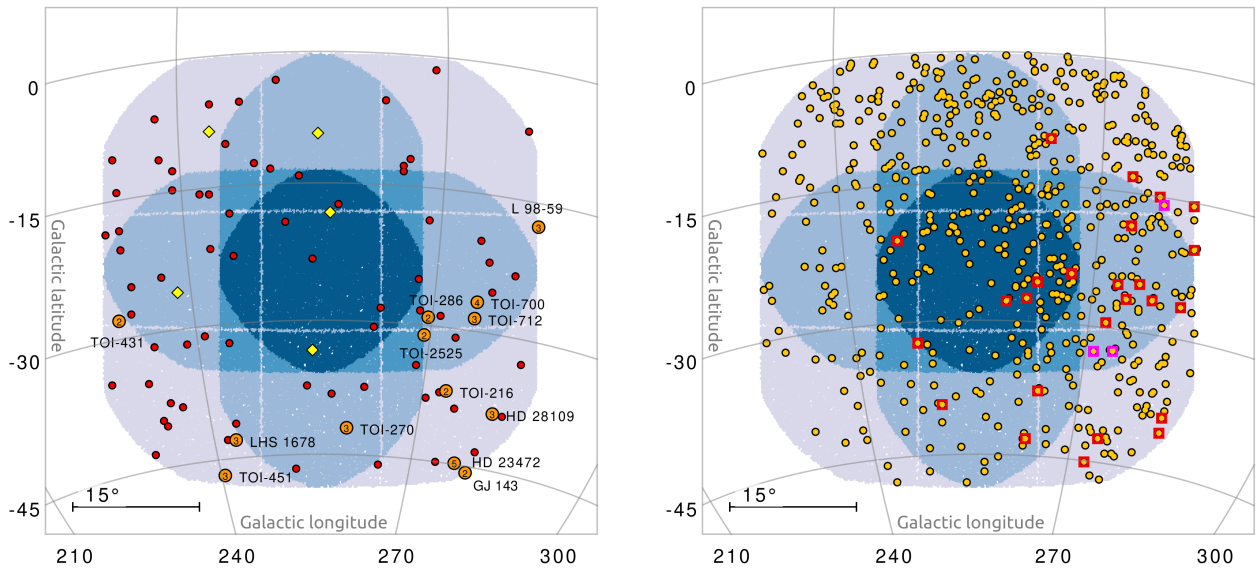


**Fig. 7.** Known planetary systems with at least one transiting planet in LOPS2 (orthographic projection in Galactic coordinates). *Left panel:* entries from the Exo-MerCat database (Section 3.4): single transiting planets (red circles), systems with multiple transiting planets (orange circles with labels; the number inside the circles is the multiplicity), transiting brown dwarfs (yellow diamonds). *Right panel:* same projection, but TESS candidates from the TOI database are plotted with yellow circles. Systems with multiple transiting candidates are marked with red squares (doublets) or magenta squares (triplets).

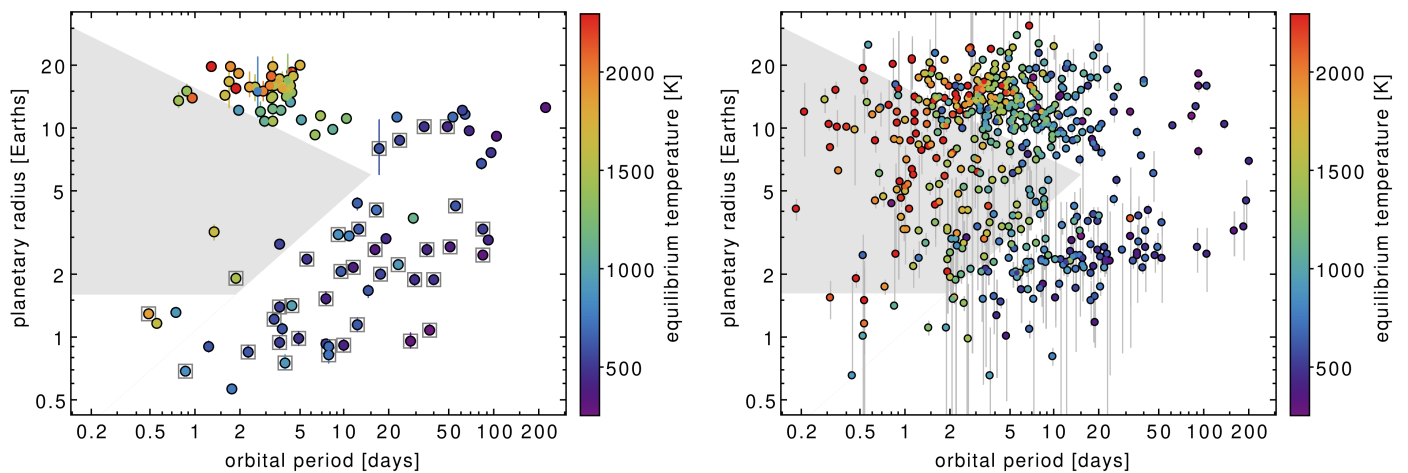


**Fig. 8.** Known planetary systems with at least one transiting planet in LOPS2. *Left panel:* Period-radius diagram with the 108 transiting planets identified from Exo-MerCat and plotted in the left panel of Fig. 7. The “Neptunian desert” region as identified by Mazeh et al. (2016) and with the modified lower boundary by Deeg et al. (2023) is plotted in light gray. Planets belonging to multiple systems are marked with a gray square. *Right panel:* Period-radius diagram with the 612 candidate transiting planets from the TESS TOI database and yet unpublished, plotted in the right panel of Fig. 7

curve (Bourrier et al. 2020; Daylan et al. 2021) and claims of temporal variability as well (Wilson et al. 2021);

- 14 warm or cool Jupiters (WJ/CJ);  $R_p > 6 R_\oplus$ ,  $P > 10$  d), eight of them on orbital periods longer than 50 d. The longest period planet of our whole LOPS2 sample belongs to this sample: TOI-4562b, a temperate Jupiter analog on a  $P \approx 225$  d orbit (Heitzmann et al. 2023) recently claimed to show TTVs by Fermiano et al. (2024);
- 24 Neptunians and mini-Neptunes ( $1.7 R_\oplus < R_p < 6 R_\oplus$ ), including at least one planet undoubtedly within the “hot Neptune” desert (Mazeh et al. 2016; gray area in Fig. 8): NGTS-4b (West et al. 2019) plus two other more marginally so (TOI-451b, TOI-269b);
- 23 rocky planets ( $R_p < 1.7 R_\oplus$ ), including four ultra short-period ones (USP;  $P \lesssim 1$  d): TOI-206b ( $P =$

0.74 d; Giacalone et al. 2022), LHS 1678b ( $P = 0.86$  d; Silverstein et al. 2024), TOI-431b ( $P = 0.49$  d; Osborn et al. 2021) and TOI-500b ( $P = 0.55$  d; Serrano et al. 2022). The latter will be observed close to the center of LOPS2 through 24 NCAMs, so PLATO will be able to gather at least  $\approx 1300$  full phase curves at  $\text{NSR} \approx 33$  ppm in one hour.

We calculated for each entry of the Exo-MerCat sample the so called *ephemeris drift*  $\sigma(T_0)$  at epoch 2027.0, i.e., the expected  $1\text{-}\sigma$  error on the transit prediction (according to the most accurate ephemeris available) at the approximated epoch when PLATO is supposed to start its scientific operations. The median is  $\sigma(T_0) \sim 7$  min. Only ten planets show a drift larger than two hours; not surprisingly, they are mostly small and/or long-period planets observed by TESS on a limited number of sectors and

not accessible by ground-based facilities. At  $\sigma(T_0) \simeq 1.8$  d, an extreme case is TOI-1338b = BEBOP-1b (the first circumbinary planet discovered by TESS, one of the only two known multiple planetary system of this kind; Kostov et al. 2020; Standing et al. 2023), virtually “lost” for the time being. For each of all these loose-ephemeris targets, the first two or three months of PLATO photometry will deliver a new, extremely accurate ephemeris, crucial for the community to setup any further follow-up observations.

### 3.4.2. Transiting candidate planets

Currently, TESS (Ricker et al. 2015) is by far the largest provider of candidate planets within LOPS2. It makes sense to quantify how many. In any case, they will be included into the PIC, not only because some fraction of them<sup>15</sup> will eventually turn out to be genuine planets, but also because PLATO itself (both through its light curves and its follow-up program) can play a fundamental role in their validation and confirmation (Mantovan et al. 2022).

From the 2024-08-20 release of the TESS Object of Interest database (TOI; Guerrero et al. 2021) we identified 824 entries in LOPS2 and matched them with the TESS Follow-up program (TFOP) data base, which includes a disposition flag (“TFOPWG”) reflecting the current status of each target according to the follow-up results. After selecting only successfully vetted planetary candidates (disposition keyword: PC, APC or CP, meaning “planetary candidate”, “ambiguous planetary candidate” and “confirmed planet”, respectively) not already published we are left with 544 candidates hosted by 513 stars<sup>16</sup> (Fig. 7, right panel). We emphasize that these numbers include candidates with a very wide range of FPR, and that a quick inspection at the “comment” column of the TOI database reveals that a considerable fraction of APC entries could likely turn out as false positives. Nevertheless, an individual vetting of each TOI is beyond the scope of this paper. Notably, 27 stars among the LOPS2 TOI host multiple candidates, a configuration which is known to significantly decrease the a-priori FPR. Three systems have multiplicity  $N = 3$ : TOI-699, TOI-790, and TOI-2392 currently under active follow-up by the TFOP working group.

It is worth mentioning that 27 among our list of TESS candidates are listed in the TOI table as having orbital periods longer than 100 d (they are visible at the right end of Fig. 8, right panel) or with no period at all. A closer inspection at the comment field reveals that almost all of them are so called “monotransits”, i.e., candidates detected through a single event whose orbital period is unconstrained. In fact, an even larger number of TOI candidates, especially in the long-period end, are flagged as having an ambiguous period due to an insufficient orbital phase coverage by TESS. The almost uninterrupted 2-year coverage of LOPS2 will easily break the ambiguity and detect the correct orbital period (Magliano et al. 2024).

### 3.4.3. Non transiting planets

As already mentioned, also non-transiting planets are worth observing with PLATO with the goal of better characterizing the

stellar host or to discover additional transiting companions (or both). By cross-matching Exo-MerCat with the sky footprint of LOPS2, after excluding the transiting planets already discussed in the previous sections, we retain a total of 77 planets in 53 systems discovered through three different instrumental techniques (Fig. 9, left plot):

- *Radial velocity*: 64 planets grouped in 41 planetary systems. Among the 15 multiple systems, HD 40307 (Mayor et al. 2009) stands out as that with the highest multiplicity: at least four planets confirmed by independent analyses, plus two more controversial candidates<sup>17</sup> (Tuomi et al. 2013; Díaz et al. 2016). A few RV systems are not counted here because they also host confirmed transiting planets, so they were included in the sample described in Section 3.4.1: they are TOI-500 and TOI-431 (both hosting a transiting super-Earth), L98-59 (with three transiting planets, Kostov et al. 2019; Demangeon et al. 2021), and TOI-1338A = BEBOP-1 (Standing et al. 2023);
- *Direct imaging*: 11 planets hosted by ten systems, among which  $\beta$  Pic b (Lagrange et al. 2010, 2019), AB Pic (Chauvin et al. 2005), HR 2562 (Konopacky et al. 2016), and WD 0806-661 b (Luhman et al. 2011) stand out as the best characterized. All of them are very massive planets, close to or across the planet-BD transition;
- *Eclipse Timing Variation (ETV)*: RR Cae ( $V = 14.4$ ), a post-common-envelope dM+WD eclipsing binary showing a  $P \simeq 16$  years timing modulation claimed as due to the light-travel time effect from an outer  $M_p = 3.4 \pm 0.2 M_{\text{jup}}$  giant planet (Qian et al. 2012; Rattanamala et al. 2023). PLATO will obviously be unable to sample the full phase of its signal, yet its uninterrupted series of  $\sim 2400$  eclipses will constitute the most precise photometric data set on this target;
- *Astrometry*: a sub-stellar candidate orbiting a L1.5 ultracool dwarf, DENIS-P J082303.1-491201 (Sahlmann et al. 2013). At  $V \sim 19$  this target is likely too faint to be included in the PLATO target list.

It is also worth mentioning WASP-126c, a non-transiting outer companion of the transiting hot Jupiter WASP-126b claimed by Pearson (2019) based on the Transit Timing Variation (TTV) analysis of TESS data, but unconfirmed by subsequent studies (Maciejewski 2020). If real, its  $P \simeq 23$  d, 1-min wide timing modulation would be very easy to confirm or disprove by PLATO, even after a single quarter of photometry.

As anticipated in Paper I, the synergy between PLATO and the thousands of astrometric planets that will be discovered by *Gaia* (Perryman et al. 2014; Sozzetti et al. 2014) is not to be missed. According to the early estimate by Perryman et al. (2014), 25-50 among those planets, mostly in the short orbital period tail ( $P = 2-3$  yr), are expected to transit; even for the most favorable cases, the ephemeris will be accurate enough to pinpoint the transit with an error of a few weeks at best (Sozzetti et al. 2023), implying that ground-based campaigns will be largely ineffective or even unfeasible. This opens an exciting opportunity with PLATO, especially for the LOP phase. On top of this, the discovery of additional transiting companions

<sup>15</sup> Quantifying the false positive ratio (FPR) of the TOI database is non-trivial because the vetting process is partially done in a manual fashion (Kunimoto et al. 2023). We note, however, that more than 6% of the TOI entries have already been flagged as FP so far, and likely much more will follow before the PLATO launch.

<sup>16</sup> The full list will be made available online on Zenodo.

<sup>17</sup> As a side note, the inclusion of HD 40307 and other bright RV systems in LOPS2 brings up the opportunity of planning a  $\geq 2$  yr observing campaign where ultra-high-precision RV measurements can be combined with a simultaneous and almost uninterrupted space-based light curve to disentangle the planetary signal from stellar activity effects, following the approach developed by Lanza et al. (2011); Aigrain et al. (2012); Haywood et al. (2014), among others.



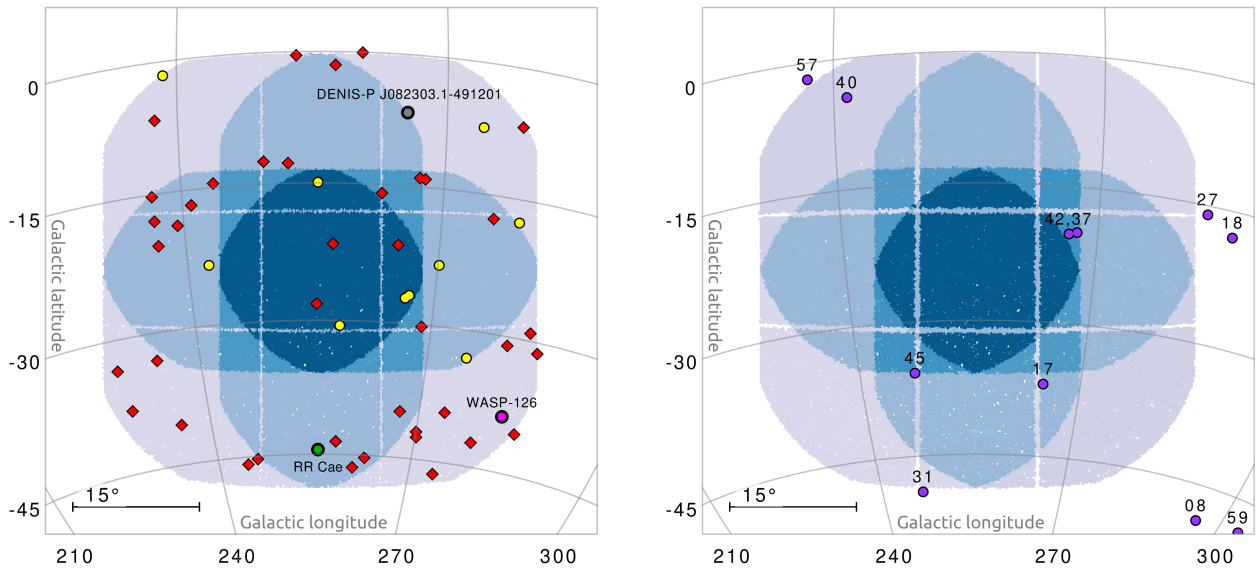


**Fig. 9.** Known non-transiting planetary systems in LOPS2 (orthographic projection in Galactic coordinates). *Left panel:* entries from the ExoMerCat database (Section 3.4): planets discovered through RVs (red diamonds), direct imaging (yellow circles), astrometry (gray circle), and ETV (green circle). The location of the candidate TTV system WASP-126 is also marked with a magenta point. *Right panel:* Candidate astrometric planets published by the *Gaia* collaboration (purple circles); each data point is labelled with its ASOI ID number.

on shorter orbits would be extremely interesting to investigate the architecture of such largely unexplored planetary systems.

The first official release of confirmed astrometric planets from *Gaia* will be included in DR4, expected not before mid-2026. A preliminary list of candidates has been released in DR3, in the non-single-star (NSS) part (Gaia Collaboration et al. 2023a). Five targets, all M dwarfs, *Gaia*-ASOI-017, -037, -040, -042, -045 will be monitored in LOPS2 (Fig. 9, right panel). Only *Gaia*-ASOI-037 ( $V \approx 13.7$ ), and -040 ( $V \approx 15.4$ ) are currently included in the PIC; the remaining three are fainter than the  $V = 16$  requirement set for the PLATO P4 sample. These will possibly be added on a special separate list if simulations will show that meaningful photometry can be extracted.

### 3.5. Star clusters and associations

It is well known that star clusters provide us with an ideal laboratory to study the formation and evolutionary processes shaping the architecture of planetary systems (Adibekyan et al. 2021). Not only does it provide the opportunity to compare the property of planets hosted in different dynamical environments, also the stellar parameters (including age and chemical composition) of stars belonging to clusters can be measured or derived with a much better accuracy than for field stars (Vejar et al. 2021).

We adopted the catalog by Hunt & Reffert (2023) as starting point for our search, being the most recent and complete census of Galactic star clusters and associations based on *Gaia* DR3 (Paper I was based on the work by Cantat-Gaudin et al. 2020 instead). Following their prescription, we restricted our input list to a sub-sample of 4 105 “high-quality” clusters detected at high confidence from their initial sample of 7 167, by imposing  $CST > 5.0$  and  $CMDC150 > 0.5$ . To identify clusters of possible interest for PLATO, we further selected just those having at least one  $V < 15$  member (the rough practical limit to detect transits around solar-type stars) in LOPS2. The positions of the resulting set of 367 clusters are plotted as red circles on the sky map of LOPS2 in the left panel of Fig. 10. As expected, there is a strong

gradient as a function of Galactic latitude, and the vast majority of clusters lie at  $|b| < 15^\circ$  from the plane.

As discussed in Rauer et al. (2024), the main focus of the PLATO planet-hunting survey is on main-sequence stars later than F5V. If we neglect interstellar extinction and assume for the F5V/G2V spectral types an absolute magnitude  $M(V) = 3.37$  and taking into account the best-fit extinction coefficient  $AV_{50}$  and distance  $dist_{50}$  from Hunt & Reffert (2023), we can set the requirement

$$V - AV_{50} + 5 - 5 \log(dist_{50}) < 3.37 \text{ AND } V < 15 \quad (1)$$

to get a final list of 3 506 targets of interest with spectral type later than F5V. Despite the large number of clusters in LOPS2, more than one third of those targets are hosted by just eight relatively nearby open clusters: NGC 2516, Alessi 34, UPK 545, Haffner 13, NGC 2546, NGC 2451B, IC 2391, NGC 2547, sorted by decreasing number of later than F5V,  $V < 15$  targets (from 543 to 77) and labelled in the left panel of Fig. 11. They are all located within 1000 pc from the Sun. Their average areal density within  $r_{50}$  (defined as the radius containing half of the cluster members) is much smaller than  $1 \text{ arcmin}^{-2}$  even for the densest ones, meaning none of them is critically crowded considering the  $15''$  pixel size of PLATO, with 90% of the flux within  $3 \times 3$  pixels, and the availability of sophisticated PSF or DIA techniques (Nardiello et al. 2020; Montalto et al. 2020) when a target has been allocated an imagette.

All the mentioned clusters are much younger than the Sun, having estimated ages in the range of 15-150 Myr. This is confirmed by independent spectroscopic studies in the literature, but also by their de-reddened color-magnitude diagrams, showing (with only one exception, see below) a straight main sequence with no hint of evolved members (Fig. 11, right panel). Two clusters in particular stand out because of their properties and deserve some more discussion:

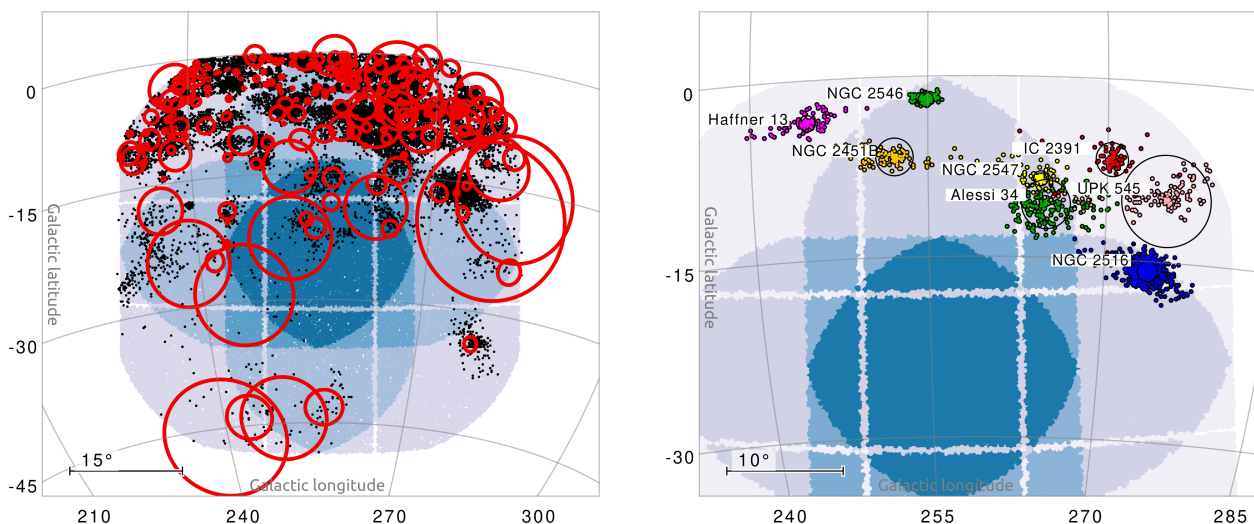


**Fig. 10.** Open clusters and associations in LOPS2. *Left panel:* sky map of the 367 clusters identified by [Hunt & Reffert \(2023\)](#) at high confidence and with at least one member in LOPS2, plotted as red circles with radius  $r_{50}$  (radius containing 50% of the members within the tidal radius). All the 10 682 members at  $V < 15$  are plotted as black points. *Right panel:* The eight clusters in our sample having the largest number of  $V < 15$  targets of spectral type F5V. Each target is color-coded with the same scheme as in [Fig. 11](#).

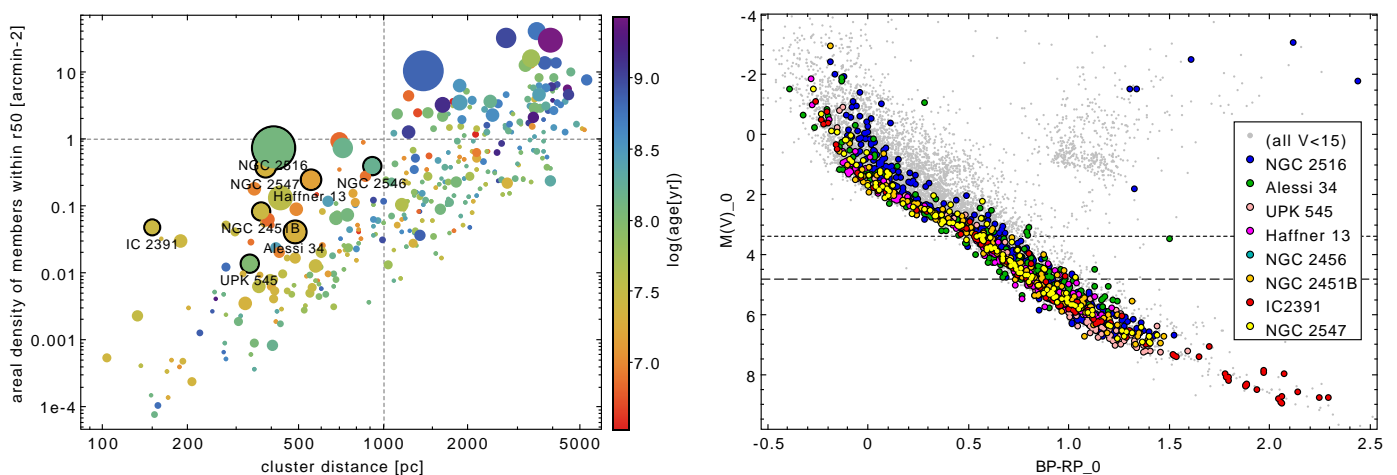


**Fig. 11.** Open clusters and associations in LOPS2. *Left panel:* the 367 clusters identified by [Hunt & Reffert \(2023\)](#) at high confidence and with at least one member in LOPS2, plotted as a function of their distance and areal density (as defined in the text). The logarithmic age of each cluster is color-coded, while the point area is proportional to the number of  $V < 15$  stars. The eight clusters having the largest number of  $V < 15$  targets of spectral type F5V and later are labelled. *Right panel:* absolute and de-reddened color-magnitude diagram (CMD) for all the 10 682  $V < 15$  stars in LOPS2 belonging to clusters (gray points). Members of the eight labeled clusters are plotted with larger circles and color-coded as in the legend.

- *IC 2391* is by far the closest object in our sample at a distance of 150 pc. It is a sparse, young ( $51 \pm 5$  Myr from the Li depletion boundary; [Randich et al. 2018](#)) solar-metallicity cluster ( $[\text{Fe}/\text{H}] = -0.04 \pm 0.03$ ; [De Silva et al. 2013](#)) with about 350 high-confidence members identified so far ([Nisak et al. 2022](#)). *IC 2391* is also the only cluster in our short list for which late-K stars will be accessible by PLATO. Stellar activity at such young ages could be a limiting factor. For instance, the solar analog *Gaia* DR3 5318186221414047104 ( $V = 10.9$ ,  $T_{\text{eff}} = 5720$  K,  $R_{\star} = 0.96 R_{\odot}$ ,  $\log g = 4.46$ ), which is a bona-fide member of *IC 2391*, shows (in TESS light curves) an obvious rotational modulation at  $P_{\text{rot}} \approx 4$  d and with a 3% semi-amplitude. The same star is also a moderately fast rotator, at  $v \sin i = 9$  km/s ([De Silva et al. 2013](#)) requiring an extra effort to get RV confirmation in the rocky planet regime.
- *NGC 2516*. The richest cluster of our sample ( $\sim 2000$  known members, of which 543 at  $V < 15$  later than F5V;  $d = 407$  pc), and the only one lying for the most part at  $|b| > 15^{\circ}$ . At an age of  $138 \pm 40$  Myr ([Franciosi et al. 2022](#)) it also is, together with *NGC 2546*, the oldest cluster of our sample. Metallicity is slightly super-solar,  $[\text{Fe}/\text{H}] = +0.08 \pm 0.01$  according to [Baratella et al. \(2020\)](#). Interestingly, *NGC 2516* has also been proven to possess an extended halo of stars spanning up to 500 pc, or  $20^{\circ}$  in the sky ([Bouma et al. 2021](#)). As a passing note, we also mention that the hot Jupiter TOI-1937A b ([Yee et al. 2023](#)) could possibly belong to this cluster, but the evidence about its membership has been inconclusive so far.

Being a particularly complex task, the selection, characterization and prioritization of the cluster stars to be included in the PIC as a special subset will constitute the main topic of a dedicated future paper.

Other stars in associations, especially young stellar objects (YSO) not yet on the main sequence, could be identified from specific catalogs, such as the Konkoly Optical YSO catalog (KYSO; Marton et al. 2023), a data base of bona-fide, mostly spectroscopically confirmed YSOs compiled by cross-matching *Gaia* DR3 with several existing catalogs. Among the 11 671 KYSO entries, 431 fall on LOPS2. If we further restrict our sample to  $V < 15$ , only 53 stars survive: 33 belong to the  $\gamma$  Velorum cluster (Franciosini et al. 2018), 12 to the Gum Nebula, 5 to different regions/branches of the Vela molecular ridge. Two more stars are field Herbig Ae/Be stars, and one is the brightest star of the open cluster NGC 2362 (Currie et al. 2009), the only one to make it through our magnitude threshold.

### 3.6. Variable and binary stars

Thanks to its very large area (2132 deg<sup>2</sup>, i.e., 5.2% of the whole sky) and to the wide range in Galactic latitude covered, LOPS2 will include a large number and variety of variable stars. A cross-match with the latest versions of the VSX (Variable Star index; Watson et al. 2006) and Gavras et al. (2023) catalogs yields 47 356 and 282 366 entries, respectively (with notable over-densities in the LMC and close to the Galactic plane). The numbers decrease to 31 211 and 15 932, respectively, when we limit our sample at  $V < 15$ . Among these we mention:

- 7 787 eclipsing binaries (including 3017/2155 with explicit detached/contact-type classification);
- 6 111 long-period variables (LPV);
- 268  $\gamma$  Cassiopeiae stars;
- 185 chemically-peculiar stars;
- 47 cataclysmic variables (CV);
- 700  $\delta$  Scuti pulsators;
- 651 Cepheids and 699 RR Lyr;
- 29 slowly-pulsating B stars (SPB);
- 17  $\beta$  Cephei stars (BCEP);
- seven  $\gamma$  Doradus stars (GDOR).

It should be emphasized that some of these classes are interesting not just for stellar science, but also to plan more focused planet-hunting surveys. For instance, circumbinary planets represent a rare laboratory to challenge our theories on planetary formation and migration through a disk, and can be discovered both by detecting their transits (Kostov et al. 2020)<sup>18</sup>, or by modeling their eclipse timing variations (ETV; Goldberg et al. 2023; Brown-Sevilla et al. 2021). Pulsators with intrinsically stable modes, such as  $\delta$  Scuti and  $\gamma$  Dor variables, may enable the detection of non-transiting planets on wide orbits through the pulsation timing technique, thanks to the unique combination of timing accuracy and temporal baseline of PLATO (Vaulato et al. 2022). Early-type stars with very specific chemical signatures such as  $\lambda$  Bootis stars have been predicted since long to host a much higher fraction of giant planets with respect to ordinary field stars, although this has been recently disputed (Saffe et al. 2021).

Some wide-orbit detached eclipsing binaries (DEBs) in LOPS2 can be considered as benchmarks for stellar evolution studies, since their absolute radii and masses can be measured with an extremely high precision ( $< 3\%$ ; Serenelli et al. 2021). From the comprehensive list of 273 benchmark DEBs by Southworth (2011), 36 are within LOPS2, and 12 are brighter than  $V = 15$ . Among them CV Velorum ( $V = 6.69$ ) a

B2.5V+B2.5V system (Albrecht et al. 2014) known to show a significant misalignment between the orbital spin and the rotation axis of its components (Marcussen & Albrecht 2022), stands out.

Cataclysmic Variables (CVs) are compact binary systems, typically containing a white dwarf which is accreting material from a low-mass star through Roche lobe overflow. Many CVs show outbursts where they brighten by  $\sim 2$ -5 mag on a recurrence time of a few weeks to many months, which is why setting a fixed magnitude limit as done above could be misleading. If we relax that constraint, there are 94 CVs in both VSX and Gavras et al. (2023) which lie in the LOPS2 field, many of which at quiescent are fainter than  $V = 18$  mag. However, VW Hya, which shows normal and superoutbursts, and IX Vel which shows Z Cam low states, are relatively bright ( $V = 12.5$  and  $V = 10.1$ , respectively). Other CVs in the LOPS2 field include UW Pic which is polar, where the white dwarf has a magnetic field strength of  $\sim 20$  MG. We expect that many CVs and other transients will be readily observable using PLATO during outbursts.

A census of all the SIMBAD objects in LOPS2 sorted by decreasing number of associated publications reveals, besides the objects already mentioned in the previous sections, other specific variable stars of interest:

- $\gamma$  Doradus ( $V \approx 4.2$ ), the prototype of the  $\gamma$  Dor class of variables (Kaye et al. 1999);
- AI Velorum ( $V \approx 6.70$ ), one of the most studied high-amplitude, double-mode  $\delta$  Scuti pulsator;
- AB Doradus, a pre-main-sequence quadruple system (Guirado et al. 2011) known for the super-flaring activity of its primary component (Schmitt et al. 2019), and also the eponymous and brightest member of the AB Dor moving group (Zuckerman et al. 2004);
- $\gamma^2$  Velorum ( $V \approx 1.83$ ), a binary made of the closest and brightest known Wolf-Rayet (WR; De Marco et al. 2000) star and a blue supergiant, belonging to the Vela OB2 association (Jeffries et al. 2014). Another bright WR star is HR 2583 = HD 50896 ( $V = 6.91$ ), a suspected binary system showing brightness variations still of unknown origin (Flores et al. 2023);
- $\epsilon$  Canis Majoris, a binary with a very bright B2II component ( $V \approx 1.50$ ), the strongest EUV source in the whole sky;
- R Doradus, an asymptotic giant branch (AGB) star with a  $300 R_{\odot}$  radius, probably the star with the largest apparent diameter as seen from the Sun.

Aside from these few very bright variables and the cross-match with the catalog by Gavras et al. (2023), we have also searched for confirmed non-radial pulsators in LOPS2. This was done from a combined *Gaia*-TESS approach. Hey & Aerts (2024) distilled about 60 000 variables using light curves from the first year of the TESS mission, starting from the original *Gaia* DR3 catalog of candidate main-sequence pulsators by Gaia Collaboration et al. (2023b) relying on their stellar properties derived by Aerts et al. (2023). Hey & Aerts (2024) reclassified all the stars whose dominant frequency in the totally independent sparsely sampled *Gaia* DR3 light curves and the 30-min sampled TESS light curves are equal. All these stars have a dominant amplitude above 4 mmag in the *Gaia* *G* band. Among the 6430 stars from Hey & Aerts (2024) occurring in LOPS2, about 5000 are now classified as confirmed multi-periodic pulsators, while the others are rotational variables or eclipsing binaries. These non-radial pulsators in LOPS2 are split up into 1455 gravity-mode pulsators (of  $\gamma$  Dor or SPB type), 2079  $\delta$  Sct pulsators, and 1449 hybrid pressure- and gravity mode pulsators.

<sup>18</sup> The first (and so far only) circumbinary planet detected by TESS, TOI-1338 (Kostov et al. 2020), is by chance in LOPS2.



Mombarg et al. (2024) provide estimates of the (convective core) masses, radii, and relative ages for more than 10 000 of the  $\gamma$  Dor, SPB, and hybrid pulsators classified by Hey & Aerts (2024). They did so by subjecting the pulsators' *Gaia* data to grid-based modelling based on rotating stellar models. These models were constructed such as to be compliant with the asteroseismology of rotating *Kepler* pulsators in the mass range from  $1.3 M_{\odot}$  and  $9 M_{\odot}$  from Li et al. (2020); Pedersen et al. (2021). Some 3000 of the stars treated by Mombarg et al. (2024) occur in LOPS2. For about 300 among them Aerts et al. (2024) distilled the near-core rotation frequency from their identified dominant dipole prograde gravito-inertial mode as found consistently in both the *Gaia* DR3 and TESS light curves. Ongoing work on the full 5-year TESS light curves will increase the number of new pulsators with a measurement of the internal rotation frequency and this estimate will become more precise. Moreover, simulations with PLATOSIM (Janssen et al. 2024) reveal that detections of a dense spectrum of oscillation modes suitable for asteroseismology are expected for all these  $\gamma$  Dor and hybrid pulsators brighter than  $V < 14$  (Janssen et al., *in prep.*), making them ideal calibration stars for the stellar science program of the mission.

### 3.7. Synergy with TESS

It is worth investigating the synergy with TESS not only in terms of known planets and planetary candidates, but also because the availability of long ( $\geq 28$  d) and precise light curves can enable a useful characterization of the target stars in advance, including parameters which can play a role at the prioritization stage, such as rotational periods, activity levels, variability and/or binarity.

Among the 519 704 unique TESS targets (Stassun et al. 2018, 2019) observed at the regular 2-min cadence up to Sector 82 included (i.e., August 2024, end of Cycle 6), 37 910 lie within the approximate footprint of LOPS2 with an average areal density spanning the 5-20 stars per  $\text{deg}^2$  range (Fig. 12, left panel; the two most evident over-densities are centered on the LMC and NGC 2516). Among these, 55% were observed for at least three TESS sectors (not always contiguous) and 15% for at least 13 sectors, or one year cumulated (mostly within the  $\beta \lesssim -78^{\circ}$  cap). Slightly more than 40% of the available TESS short-cadence targets are not included in the current version of the PIC<sup>19</sup>, mostly because their stellar parameters fall outside our ( $T_{\text{eff}}, R_{\star}$ ) parameter space (M21), or, to a lesser extent, because they do not meet our magnitude requirements. All those remaining targets of scientific interest left out can be requested by the community through the PLATO GO program, if they are technically feasible.

If we focus on the general sector coverage of the TESS FFIs instead (Fig. 12, right panel) we find that 25% of the LOPS2 sky area has been already surveyed through at least 12 TESS sectors, 55% through at least five sectors, and 88% by three.

### 3.8. Synergy with CHEOPS

CHEOPS (Benz et al. 2021) is an ESA S-class mission launched in 2019, equipped with a 30-cm reflecting telescope designed for ultra-high-precision photometry of individual targets in a single optical band (Fortier et al. 2024). Its main goal is the follow-up and characterization of known transiting planets, articulated over a wide range of science cases; see Benz et al. (2021) for

a summary of the CHEOPS GTO program. Its 3.5-year primary mission ended in 2023, and currently CHEOPS is running its first mission extension until 2026, with a possible second extension foreseen until 2029. Given the scientific (and possibly temporal) overlap with the PLATO observations, it is worth investigating how much of LOPS2 can be accessed by CHEOPS.

CHEOPS is not subject to a rigid scanning law such as TESS. Rather, it works on a flexible schedule, and its pointing ability is limited only by three avoidance angles to minimize scattered light from the Sun, the Moon and the Earth limb. The Sun Exclusion Angle (SEA) is currently set to  $120^{\circ}$  (as throughout the whole nominal mission), and is the most limiting factor to reach large ecliptic latitudes such as those spanned by LOPS2. It is easy to see that a SEA of  $120^{\circ}$  implies that the whole  $\beta < -60^{\circ}$  cap (the magenta area plotted in Fig. 13, left panel) is inaccessible to CHEOPS. In other words, only 33% of the LOPS2 footprint can currently be pointed by CHEOPS, mostly in the six- and 12-camera regions and in any case for a very limited amount of days per year, because of the SEA limitation. The 24-NCAM region is completely inaccessible. Moreover, the fraction of accessible P1 targets (black dots in Fig. 13) is even lower (23%), since P1 targets are more densely located in the inner regions (18 and 24 telescope) of LOPS. Should the CHEOPS observing strategy and/or the value of the avoidance angles be changed during the extended mission, the geometric overlap could increase by a significant amount; a relaxation of the SEA of a few degrees, for instance, would make part of the PLATO 24-camera region and its dense population of P1 targets accessible to CHEOPS.

### 3.9. Synergy with Ariel

Ariel is an ESA M-class mission currently in development, with a planned launch to L2 in 2029 (Tinetti et al. 2018, 2021), i. e., with a significant temporal overlap with the PLATO nominal mission. Based on a 1-m class telescope equipped with two near-to-mid infrared low-resolution spectrographs (covering the 1.1-7.8  $\mu\text{m}$  range) and three photometric channels also employed as fine guidance system (FGS; 0.5-1.1  $\mu\text{m}$ ), Ariel will monitor transiting planets through emission spectroscopy, transmission spectroscopy and phase curves, with repeated observations to gather the required SNR. Ariel targets will be observed through a four-“Tier” approach: Tier 1 targets will undergo an extensive low-resolution reconnaissance survey, Tier 2 targets will be selected for a deeper survey at higher resolution, and Tier 3 is made of a relatively small number of benchmark planets to be explored for variability (Edwards & Tinetti 2022). Tier 4 will be dedicated to phase curves and bespoke observations of targets of special interest, which are expected to be identified e.g. in Tier 1 or by space-based missions and ground-based surveys prior to Ariel.

The current Ariel target list, called Mission Reference Sample (MRS) is a living catalog, started by Edwards & Tinetti (2022) and regularly updated<sup>20</sup>. The latest version (2024-07-09) contains 722 confirmed transiting planets, and 2025 candidates from the TESS TOI/ExoFOP database (Guerrero et al. 2021). The majority of MRS targets (58%) are hot Jupiters. Also, nearly 90% of the “confirmed planets” sub-sample have transits deeper than 1 mmag, i. e., are easily detectable by TESS at high SNR (or in most cases, even from ground-based facilities). A cross-match with the LOPS2 footprint reveals that PLATO will observe 60 confirmed planets from the MRS (22 in Tier-1, 29 in Tier-2, nine in Tier-3) belonging to 49 host stars (Fig. 13, right panel).

<sup>19</sup> Being included in the PIC does not automatically imply being scheduled for observations or being included in the P1-P2-P4-P5 sample, even though the vast majority of them will do (Montalto et al. 2021).

<sup>20</sup> [https://github.com/arielmision-space/Mission\\_Candidate\\_Sample](https://github.com/arielmision-space/Mission_Candidate_Sample)

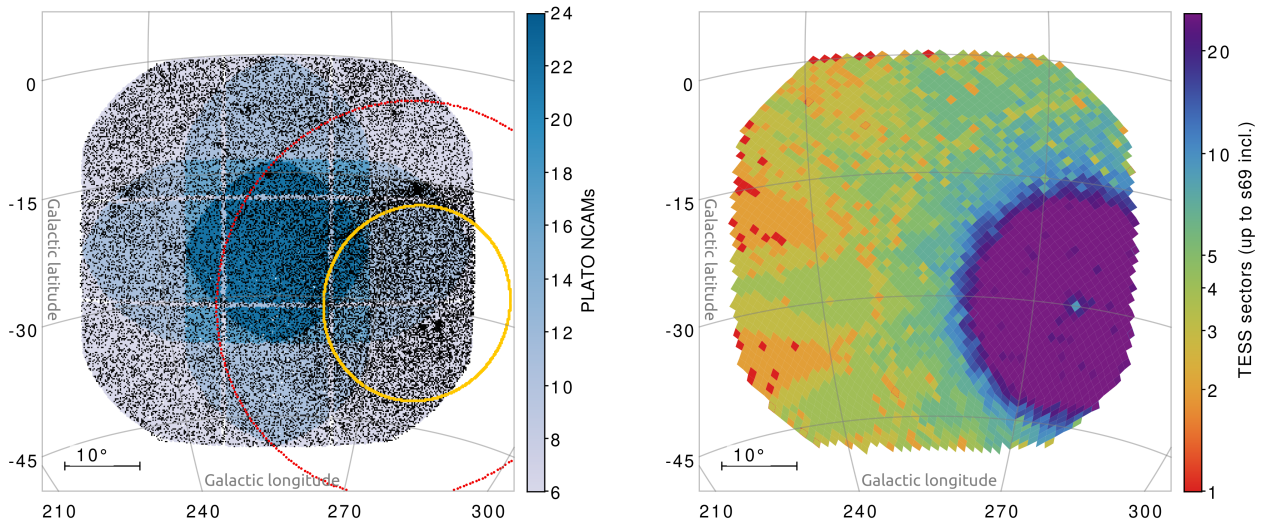


**Fig. 12.** Distribution of observed TESS targets in LOPS2, orthographic projection in Galactic coordinates. *Left panel:* all 37 910 CTL targets within LOPS2 observed in short cadence by TESS from sector 1 to 82 included (black points), superimposed on the LOPS2 field. The yellow circle is the TESS southern CVZ (up to 35 sectors), the red circle is roughly the northern boundary of Camera 4, i.e., the sky region where at least 4 TESS sectors are available. *Right panel:* same, but the TESS FFI coverage in terms of TESS sectors is color-coded over an HEALPix level-6 grid.

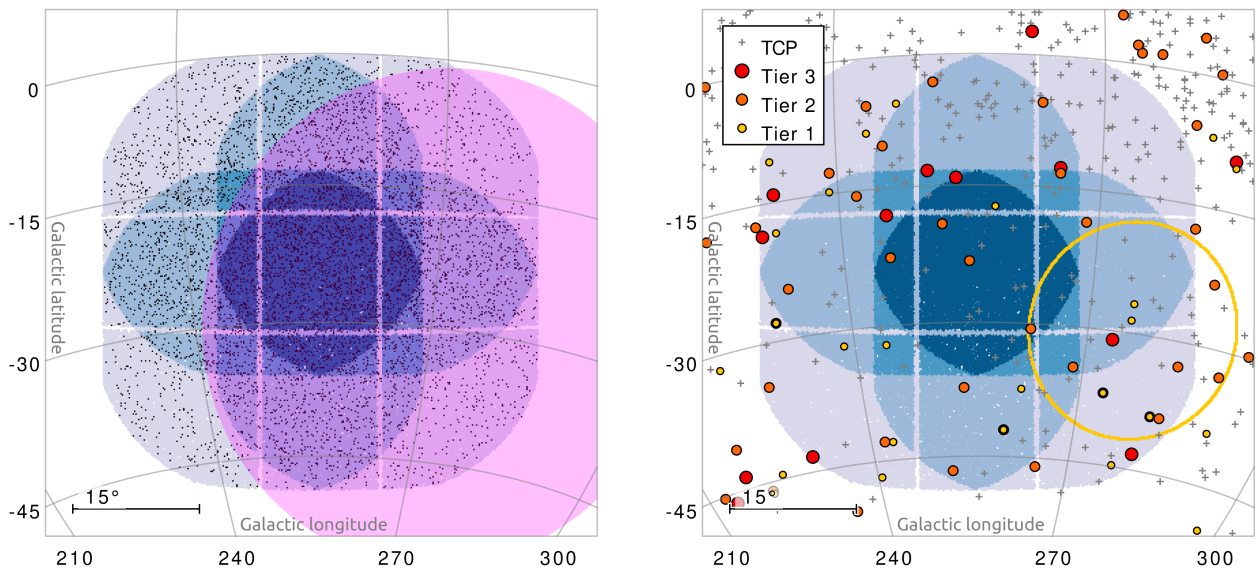


**Fig. 13.** Overlap between CHEOPS/Ariel and LOPS2 (orthographic projection in Galactic coordinates). *Left panel:* in magenta, sky area forbidden to CHEOPS due to the Sun Exclusion Angle currently set at  $120^\circ$  (corresponding to  $\beta < -60^\circ$  for the southern ecliptic cap). P1 targets are plotted as black dots. *Right panel:* Ariel targets from the current MRS. Confirmed targets belonging to the Ariel Tier 1/2/3 (see text for details) are plotted as yellow, orange and red dots, respectively, while the TESS candidate planets are plotted as gray crosses (see text for details). The yellow circle is the TESS CVZ.

Given the selection criteria of the MRS, PLATO will be a provider of new, additional targets for Ariel, mainly of a small (but scientifically very interesting) population of long-period transiting giants not (yet) discovered by TESS, or discovered as mono-transit events only (Magliano et al. 2024). Moreover, the PLATO vs. Ariel synergy will be strong, for the already known and future targets, on the extremely accurate stellar parameters delivered by PLATO through asteroseismological analysis (and in particular, ages; Goupil et al. 2024), the in-depth characterization of stellar activity and rotational periods (Breton et al. 2024), the refinement of the planetary ephemeris for targets difficult to be followed up from the ground, the extension of the temporal baseline for TTV studies (Borsato et al. 2022), and the accurate planetary masses obtained by the PLATO follow-up program

(Rauer et al. 2024). On the hot Jupiters belonging to the brighter tail of the MRS, PLATO will also be able to detect the planetary albedo and/or heat redistribution behavior through phase curves (Shporer 2017; Singh et al. 2019), in a few cases possibly with color information thanks to the FCAM coverage.

### 3.10. Synergy with JWST

On a closing note, we also mention that the JWST southern CVZ at  $\beta < -85^\circ$  (Gardner et al. 2006) is fully enclosed in the LOPS2 footprint, unfolding another synergy with a space-based mission that is and will be crucial in the investigation of exoplanetary atmospheres. Further, JWST is able to monitor continuously for



at least 200 days every southern source at  $\beta < -45^\circ$ , and this includes the whole LOPS2.

#### 4. Conclusions

In this work we presented the first field to be observed by PLATO during its LOP phase, and illustrated some of its astrophysical content relevant for planetary and stellar science. While the position of LOPS2 on the sky is now fixed, the PIC will continue to evolve and improve. The release of *Gaia* DR4 will deliver much more accurate stellar parameters for all of our targets of interest, including all non-single star (NSS) solutions, individual epoch measurements, variability metrics, metallicities/abundances etc. based on the first 66 months of observations, and a large catalog of planets and planetary candidates discovered by *Gaia* astrometry. As presented in this paper, LOPS2 also contains numerous highly relevant targets to address complementary science topics. In this context, the general community will be invited to propose observations in response to ESA announcements of opportunity for a Guest Observer program. The first open call is planned to be issued nine months prior to launch.

Meanwhile, effort will be spent on building the more effective target lists and defining criteria on how to allocate the PLATO telemetry resources (images, centroids, light curves) among the selected targets. The selected field meets the mission scientific requirements on samples P1-P2-P4-P5 as defined by SciRD. In the near future, the PSWT will implement a *prioritization metric* able to define a subset of most valuable stars for the ground-based follow-up, called *prime sample*. For planets hosted by this sample, the PLATO mission will eventually provide planet candidate confirmation and high-resolution spectroscopy, with planetary mass measurements. The prioritization process will also allow prioritization of tPIC targets for images acquisition, sampling timing, etc. This process, to be documented in a third paper of this series, does not separately consider the different samples. The prioritization metric is evaluated regardless of whether a star belongs to the P1, P2 or P5 sample. For instance, a K3 subgiant at  $V \lesssim 11$  and  $R_\star \approx 3 R_\odot$  can be included in P1 with a similar NSR  $\approx 45$  ppm with respect to a K3V star at  $V \gtrsim 11$  and  $R_\star \approx 0.8 R_\odot$  belonging to P5, due to the magnitude constraint. However, detecting a true Earth analog during LOPS would be impossible in the former case, while perfectly within the reach<sup>21</sup> of PLATO in the latter, so that this observation will be given higher priority.

In synthesis, the prioritization scheme will lead to the selection of the PLATO *prime sample*, a PIC subset of up to 20 000 stars to be observed during the LOP for which the PLATO Consortium is committed to do and deliver the follow-up observations. For that purpose, additional constraints (also to be documented in Paper III) other than the prioritization metric will be added to ensure that the targets are feasible with the available ground-based facilities and within the timeline of the PLATO operations.

*Acknowledgements.* We thank the referee for his valuable comments and suggestion. We thank Hans Deeg for his useful comments.

This work presents results from the European Space Agency (ESA) space mission PLATO. The PLATO payload, the PLATO Ground Segment and PLATO data processing are joint developments of ESA and the PLATO mission consortium (PMC). Funding for the PMC is provided at national levels, in particular by countries participating in the PLATO Multilateral Agreement (Austria, Belgium, Czech Republic, Denmark, France, Germany, Italy, Netherlands,

Portugal, Spain, Sweden, Switzerland, Norway, and United Kingdom) and institutions from Brazil. Members of the PLATO Consortium can be found at <https://platomission.com/>. The ESA PLATO mission website is <https://www.cosmos.esa.int/plato>. We thank the teams working for PLATO for all their work.

CA and AT acknowledge support from the long-term structural Methusalem funding program by means of the project SOUL: Stellar evolution in full glory, KU Leuven grant METH/24/012. JMMH is funded by Spanish MCIU/AEI/10.13039/501100011033 grant PID2019-107061GB-C61. VN, GP, MM, SB, SD, VG, DM, LM, IP, LP, RR acknowledge support from PLATO ASI-INAF agreements n. 2022-28-HH.0

This research has made use of the SIMBAD database (operated at CDS, Strasbourg, France; [Wenger et al. 2000](#)), TOPCAT and STILTS ([Taylor 2005, 2006](#)). This research has made use of the Exoplanet Follow-up Observation Program (ExoFOP; DOI:10.26134/ExoFOP5) website, which is operated by the California Institute of Technology, under contract with the National Aeronautics and Space Administration under the Exoplanet Exploration Program.

#### References

- Adibekyan, V., Santos, N. C., Demangeon, O. D. S., et al. 2021, A&A, 649, A111
- Aerts, C., Molenberghs, G., & De Ridder, J. 2023, A&A, 672, A183
- Aerts, C., Van Reeth, T., Mombarg, J. S. G., & Hey, D. 2024, A&A, submitted
- Aigrain, S., Pont, F., & Zucker, S. 2012, MNRAS, 419, 3147
- Albrecht, S., Winn, J. N., Torres, G., et al. 2014, ApJ, 785, 83
- Alei, E., Claudi, R., Bignamini, A., & Molinaro, M. 2020, Astronomy and Computing, 31, 100370
- Anglada-Escudé, G., Arriagada, P., Tuomi, M., et al. 2014, MNRAS, 443, L89
- Auvergne, M., Bodin, P., Boissard, L., et al. 2009, A&A, 506, 411
- Baratella, M., D’Orazi, V., Carraro, G., et al. 2020, A&A, 634, A34
- Barros, S. C. C., Demangeon, O. D. S., Alibert, Y., et al. 2022, A&A, 665, A154
- Bell, R. A. & Rodgers, A. W. 1964, The Observatory, 84, 29
- Benz, W., Broeg, C., Fortier, A., et al. 2021, Experimental Astronomy, 51, 109
- Bétrissey, J., Buldgen, G., Reese, D. R., et al. 2023, A&A, 676, A10
- Börner, A., Paproth, C., Cabrera, J., et al. 2024, Experimental Astronomy, 58, 1
- Borsato, L., Nascimbeni, V., Piotta, G., & Szabó, G. 2022, Experimental Astronomy, 53, 635
- Bortle, A., Fauser, H., Ji, J., et al. 2021, AJ, 161, 230
- Borucki, W. J., Koch, D., Basri, G., et al. 2010, Science, 327, 977
- Bouma, L. G., Curtis, J. L., Hartman, J. D., Winn, J. N., & Bakos, G. Á. 2021, AJ, 162, 197
- Bourrier, V., Kitzmann, D., Kuntzer, T., et al. 2020, A&A, 637, A36
- Bray, J. C., Kolb, U., Rowden, P., et al. 2023, MNRAS, 518, 3637
- Breton, S. N., Lanza, A. F., Messina, S., et al. 2024, A&A, 689, A229
- Brown-Sevilla, S. B., Nascimbeni, V., Borsato, L., et al. 2021, MNRAS, 506, 2122
- Cantat-Gaudin, T., Anders, F., Castro-Ginard, A., et al. 2020, A&A, 640, A1
- Cantat-Gaudin, T., Jordi, C., Wright, N. J., et al. 2019, A&A, 626, A17
- Chauvin, G., Lagrange, A. M., Zuckerman, B., et al. 2020, A&A, 438, L29
- Cunha, M. S., Roxburgh, I. W., Aguirre Børsen-Koch, V., et al. 2021, MNRAS, 508, 5864
- Currie, T., Lada, C. J., Plavchan, P., et al. 2009, ApJ, 698, 1
- Daylan, T., Günther, M. N., Mikal-Evans, T., et al. 2021, AJ, 161, 131
- de Jong, R. S., Bellido-Tirado, O., Chiappini, C., et al. 2012, in Society of Photo-Optical Instrumentation Engineers (SPIE) Conference Series, Vol. 8446, Ground-based and Airborne Instrumentation for Astronomy IV, ed. I. S. McLean, S. K. Ramsay, & H. Takami, 84460T
- De Marco, O., Schmutz, W., Crowther, P. A., et al. 2000, A&A, 358, 187
- De Silva, G. M., D’Orazi, V., Melo, C., et al. 2013, MNRAS, 431, 1005
- Deeg, H. J., Georgieva, I. Y., Nowak, G., et al. 2023, A&A, 677, A12
- Delrez, L., Santerne, A., Almenara, J. M., et al. 2016, MNRAS, 458, 4025
- Demangeon, O. D. S., Zapatero Osorio, M. R., Alibert, Y., et al. 2021, A&A, 653, A41
- Díaz, R. F., Ségransan, D., Udry, S., et al. 2016, A&A, 585, A134
- Dodson-Robinson, S. E., Beichman, C. A., Carpenter, J. M., & Bryden, G. 2011, AJ, 141, 11
- Edwards, B. & Tinetti, G. 2022, AJ, 164, 15
- Eschen, Y. N. E., Bayliss, D., Wilson, T. G., et al. 2024, MNRAS, 535, 1778
- Fermiano, V., Saito, R. K., Ivanov, V. D., et al. 2024, A&A, 690, L7
- Fernique, P., Boch, T., Donaldson, T., et al. 2014, MOC - HEALPix Multi-Order Coverage map Version 1.0, IVOA Recommendation 02 June 2014
- Flores, B. L., Hillier, D. J., & Dessart, L. 2023, MNRAS, 518, 5001
- Fortier, A., Simon, A. E., Broeg, C., et al. 2024, A&A, 687, A302
- Franciosini, E., Sacco, G. G., Jeffries, R. D., et al. 2018, A&A, 616, L12
- Franciosini, E., Tognelli, E., Degl’Innocenti, S., et al. 2022, A&A, 659, A85
- Fuhrmann, K., Chini, R., Hoffmeister, V. H., & Stahl, O. 2011, MNRAS, 416, 391
- Gaia Collaboration, Arenou, F., Babusiaux, C., et al. 2023a, A&A, 674, A34

<sup>21</sup> As a figure of reference, a photometric precision of 80 ppm in one hour enables the robust detection of a true Earth analog around a quiet Sun twin with three transits ([Rauer et al. 2024](#)).



- Gaia Collaboration, De Ridder, J., Ripepi, V., et al. 2023b, *A&A*, 674, A36
- Gardner, J. P., Mather, J. C., Clampin, M., et al. 2006, *Space Sci. Rev.*, 123, 485
- Gavras, P., Rimoldini, L., Nienartowicz, K., et al. 2023, *A&A*, 674, A22
- Ge, J., Zhang, H., Zang, W., et al. 2022, arXiv e-prints, arXiv:2206.06693
- Gentile Fusillo, N. P., Tremblay, P. E., Cukanovaite, E., et al. 2021, *MNRAS*, 508, 3877
- Giacalone, S., Dressing, C. D., Hedges, C., et al. 2022, *AJ*, 163, 99
- Gilbert, E. A., Barclay, T., Schlieder, J. E., et al. 2020, *AJ*, 160, 116
- Gilbert, E. A., Vanderburg, A., Rodriguez, J. E., et al. 2023, *ApJ*, 944, L35
- Goldberg, M., Fabrycky, D., Martin, D. V., et al. 2023, *MNRAS*, 525, 4628
- Goupil, M. J., Catala, C., Samadi, R., et al. 2024, *A&A*, 683, A78
- Grandjean, A., Lagrange, A. M., Meunier, N., et al. 2023, *A&A*, 669, A12
- Guerrero, N. M., Seager, S., Huang, C. X., et al. 2021, *ApJS*, 254, 39
- Guirado, J. C., Marcaide, J. M., Martí-Vidal, I., et al. 2011, *A&A*, 533, A106
- Haywood, R. D., Collier Cameron, A., Queloz, D., et al. 2014, *MNRAS*, 443, 2517
- Heitzmann, A., Zhou, G., Quinn, S. N., et al. 2023, *AJ*, 165, 121
- Heller, R., Harre, J.-V., & Samadi, R. 2022, *A&A*, 665, A11
- Hey, D. & Aerts, C. 2024, *A&A*, 688, A93
- Hobson, M. J., Brahm, R., Jordán, A., et al. 2021, *AJ*, 161, 235
- Hoffleit, D. & Warren, W. H., J. 1995, *VizieR Online Data Catalog*, V/50
- Howell, S. B., Sobek, C., Haas, M., et al. 2014, *PASP*, 126, 398
- Hunt, E. L. & Reffert, S. 2023, *A&A*, 673, A114
- Ivezić, Z., Kahn, S. M., Tyson, J. A., et al. 2019, *ApJ*, 873, 111
- Jannsen, N., De Ridder, J., Seynaeve, D., et al. 2024, *A&A*, 681, A18
- Jeffries, R. D., Jackson, R. J., Cottaar, M., et al. 2014, *A&A*, 563, A94
- Jontof-Hutter, D., Lissauer, J., & Rowe, J. 2021a, in *Plato Mission Conference 2021. Presentations and posters of the online PLATO Mission Conference 2021*, 11
- Jontof-Hutter, D., Wolfgang, A., Ford, E. B., et al. 2021b, *AJ*, 161, 246
- Kasting, J. F., Whitmire, D. P., & Reynolds, R. T. 1993, *Icarus*, 101, 108
- Kaye, A. B., Handler, G., Krisciunas, K., Poretti, E., & Zerbi, F. M. 1999, *PASP*, 111, 840
- Konopacky, Q. M., Rameau, J., Duchêne, G., et al. 2016, *ApJ*, 829, L4
- Kostov, V. B., Orosz, J. A., Feinstein, A. D., et al. 2020, *AJ*, 159, 253
- Kostov, V. B., Schlieder, J. E., Barclay, T., et al. 2019, *AJ*, 158, 32
- Kotoneva, E., Innanen, K., Dawson, P. C., Wood, P. R., & De Robertis, M. M. 2005, *A&A*, 438, 957
- Kunimoto, M., Bryson, S., Daylan, T., et al. 2023, *Research Notes of the American Astronomical Society*, 7, 7
- Lagrange, A. M., Bonnefoy, M., Chauvin, G., et al. 2010, *Science*, 329, 57
- Lagrange, A. M., Meunier, N., Rubini, P., et al. 2019, *Nature Astronomy*, 3, 1135
- Lanza, A. F., Boisse, I., Bouchy, F., Bonomo, A. S., & Moutou, C. 2011, *A&A*, 533, A44
- Li, G., Van Reeth, T., Bedding, T. R., et al. 2020, *MNRAS*, 491, 3586
- Lorenzo-Oliveira, D., Freitas, F. C., Meléndez, J., et al. 2018, *A&A*, 619, A73
- Luhman, K. L., Burgasser, A. J., & Bochanski, J. J. 2011, *ApJ*, 730, L9
- Maciejewski, G. 2020, *Acta Astron.*, 70, 181
- Magliano, C., Covone, G., Nascimbeni, V., et al. 2024, *MNRAS*, 528, 2851
- Mantovan, G., Montalto, M., Piotto, G., et al. 2022, *MNRAS*, 516, 4432
- Marconi, A., Abreu, M., Adibekyan, V., et al. 2022, in *Society of Photo-Optical Instrumentation Engineers (SPIE) Conference Series*, Vol. 12184, *Ground-based and Airborne Instrumentation for Astronomy IX*, ed. C. J. Evans, J. J. Bryant, & K. Motohara, 1218424
- Marcussen, M. L. & Albrecht, S. H. 2022, *ApJ*, 933, 227
- Marton, G., Abraham, P., Rimoldini, L., et al. 2023, *A&A*, 674, A21
- Matuszewski, F., Nettelmann, N., Cabrera, J., Börner, A., & Rauer, H. 2023, *A&A*, 677, A133
- Mayor, M., Pepe, F., Queloz, D., et al. 2003, *The Messenger*, 114, 20
- Mayor, M., Udry, S., Lovis, C., et al. 2009, *A&A*, 493, 639
- Mazeh, T., Holczer, T., & Faigler, S. 2016, *A&A*, 589, A75
- Mombarg, J. S. G., Aerts, C., Van Reeth, T., & Hey, D. 2024, *A&A*, submitted
- Montalto, M., Borsato, L., Granata, V., et al. 2020, *MNRAS*, 498, 1726
- Montalto, M., Piotto, G., Marrese, P. M., et al. 2021, *A&A*, 653, A98
- Nardiello, D., Piotto, G., Deleuil, M., et al. 2020, *MNRAS*, 495, 4924
- Nascimbeni, V., Piotto, G., Börner, A., et al. 2022, *A&A*, 658, A31
- Newton, E. R., Mann, A. W., Kraus, A. L., et al. 2021, *AJ*, 161, 65
- Nisak, A. H., White, R. J., Yep, A., et al. 2022, *AJ*, 163, 278
- O'Brien, M. W., Tremblay, P. E., Gentile Fusillo, N. P., et al. 2023, *MNRAS*, 518, 3055
- Osborn, A., Armstrong, D. J., Cale, B., et al. 2021, *MNRAS*, 507, 2782
- Pearce, T. D., Launhardt, R., Ostermann, R., et al. 2022, *A&A*, 659, A135
- Pearson, K. A. 2019, *AJ*, 158, 243
- Pecaut, M. J. & Mamajek, E. E. 2013, *ApJS*, 208, 9
- Pedersen, M. G., Aerts, C., Pápics, P. I., et al. 2021, *Nature Astronomy*, 5, 715
- Pepe, F., Cristiani, S., Rebolo, R., et al. 2021, *A&A*, 645, A96
- Perryman, M., Hartman, J., Bakos, G. Á., & Lindgren, L. 2014, *ApJ*, 797, 14
- Pertenais, M., Ammler-von Eiff, M., Burreli, M., et al. 2022, in *Society of Photo-Optical Instrumentation Engineers (SPIE) Conference Series*, Vol. 12180, *Space Telescopes and Instrumentation 2022: Optical, Infrared, and Millimeter Wave*, ed. L. E. Coyle, S. Matsuura, & M. D. Perrin, 121804M
- Pertenais, M., Cabrera, J., Paproth, C., et al. 2021, in *Society of Photo-Optical Instrumentation Engineers (SPIE) Conference Series*, Vol. 11852, *Society of Photo-Optical Instrumentation Engineers (SPIE) Conference Series*, 118524Y
- Pope, B. J. S., White, T. R., Farr, W. M., et al. 2019, *ApJS*, 245, 8
- Porterfield, B., Coe, D., Gonzaga, S., Anderson, J., & Grogan, N. 2016, *Here Be Dragons: Characterization of ACS/WFC Scattered Light Anomalies*, *Instrument Science Report ACS 2016-6*, 16 pages
- Qian, S. B., Liu, L., Zhu, L. Y., et al. 2012, *MNRAS*, 422, L24
- Randich, S., Tognelli, E., Jackson, R., et al. 2018, *A&A*, 612, A99
- Rattanamala, R., Awiphan, S., Komonjinda, S., et al. 2023, *MNRAS*, 523, 5086
- Rauer, H., Aerts, C., Cabrera, J., et al. 2024, arXiv e-prints, arXiv:2406.05447
- Reylé, C., Jardine, K., Fouqué, P., et al. 2021, *A&A*, 650, A201
- Ricker, G. R., Winn, J. N., Vanderspek, R., et al. 2015, *Journal of Astronomical Telescopes, Instruments, and Systems*, 1, 014003
- Robertson, P., Roy, A., & Mahadevan, S. 2015, *ApJ*, 805, L22
- Rodríguez Martínez, R., Gaudi, B. S., Rodríguez, J. E., et al. 2020, *AJ*, 160, 111
- Saffe, C., Miquelarena, P., Alacoria, J., et al. 2021, *A&A*, 647, A49
- Sahlmann, J., Lazorenko, P. F., Ségransan, D., et al. 2013, *A&A*, 556, A133
- Sanderson, H., Bonsor, A., & Mustill, A. 2022, *MNRAS*, 517, 5835
- Schmitt, J. H. M. M., Ioannidis, P., Robrade, J., Czesla, S., & Schneider, P. C. 2019, *A&A*, 628, A79
- Serenelli, A., Weiss, A., Aerts, C., et al. 2021, *A&A Rev.*, 29, 4
- Serrano, L. M., Gandolfi, D., Mustill, A. J., et al. 2022, *Nature Astronomy*, 6, 736
- Shporer, A. 2017, *PASP*, 129, 072001
- Silverstein, M. L., Barclay, T., Schlieder, J. E., et al. 2024, *AJ*, 167, 255
- Singh, V., Scandariato, G., & Pagano, I. 2019, *MNRAS*, 486, 5867
- Southworth, J. 2011, *MNRAS*, 417, 2166
- Sozzetti, A., Giacobbe, P., Lattanzi, M. G., et al. 2014, *MNRAS*, 437, 497
- Sozzetti, A., Giacobbe, P., Lattanzi, M. G., & Pinamonti, M. 2023, *MNRAS*, 520, 1748
- Standing, M. R., Sairam, L., Martin, D. V., et al. 2023, *Nature Astronomy*, 7, 702
- Stassun, K. G., Oelkers, R. J., Paegert, M., et al. 2019, *AJ*, 158, 138
- Stassun, K. G., Oelkers, R. J., Pepper, J., et al. 2018, *AJ*, 156, 102
- Taylor, M. B. 2005, in *Astronomical Society of the Pacific Conference Series*, Vol. 347, *Astronomical Data Analysis Software and Systems XIV*, ed. P. Shopbell, M. Britton, & R. Ebert, 29
- Taylor, M. B. 2006, in *Astronomical Society of the Pacific Conference Series*, Vol. 351, *Astronomical Data Analysis Software and Systems XV*, ed. C. Gabriel, C. Arviset, D. Ponz, & S. Enrique, 666
- Teske, J., Wang, S. X., Wolfgang, A., et al. 2021, *ApJS*, 256, 33
- Tinetti, G., Drossart, P., Eccleston, P., et al. 2018, *Experimental Astronomy*, 46, 135
- Tinetti, G., Eccleston, P., Haswell, C., et al. 2021, arXiv e-prints, arXiv:2104.04824
- Trifonov, T., Rybizki, J., & Kürster, M. 2019, *A&A*, 622, L7
- Tuomi, M., Anglada-Escudé, G., Gerlach, E., et al. 2013, *A&A*, 549, A48
- Vach, S., Quinn, S. N., Vanderburg, A., et al. 2022, *AJ*, 164, 71
- Vaulato, V., Nascimbeni, V., & Piotto, G. 2022, *A&A*, 668, A110
- Vejar, G., Schuler, S. C., & Stassun, K. G. 2021, *ApJ*, 919, 100
- Verhoeff, P., Prod'homme, T., Oosterbroek, T., et al. 2016, in *Society of Photo-Optical Instrumentation Engineers (SPIE) Conference Series*, Vol. 9915, *High Energy, Optical, and Infrared Detectors for Astronomy VII*, ed. A. D. Holland & J. Beletic, 99150Z
- Watson, C. L., Henden, A. A., & Price, A. 2006, *Society for Astronomical Sciences Annual Symposium*, 25, 47
- Wenger, M., Ochsenein, F., Egret, D., et al. 2000, *A&AS*, 143, 9
- West, R. G., Gillen, E., Bayliss, D., et al. 2019, *MNRAS*, 486, 5094
- White, T. R., Pope, B. J. S., Antoci, V., et al. 2017, *MNRAS*, 471, 2882
- Wilson, J., Gibson, N. P., Lothringer, J. D., et al. 2021, *MNRAS*, 503, 4787
- Yee, S. W., Winn, J. N., Hartman, J. D., et al. 2023, *ApJS*, 265, 1
- Zakhzhay, O. V., Launhardt, R., Müller, A., et al. 2022, *A&A*, 667, A63
- Zhou, G., Bakos, G. Á., Bayliss, D., et al. 2019, *AJ*, 157, 31
- Zuckerman, B., Song, I., & Bessell, M. S. 2004, *ApJ*, 613, L65
- Zwintz, K. 2024, in *EAS2024*, 1836

- 
- <sup>1</sup> INAF – Osservatorio Astronomico di Padova, vicolo dell’Osservatorio 5, 35122 Padova, Italy
  - <sup>2</sup> Dipartimento di Fisica e Astronomia “Galileo Galilei”, Università degli Studi di Padova, Vicolo dell’Osservatorio 3, 35122 Padova, Italy
  - <sup>3</sup> Deutsches Zentrum für Luft- und Raumfahrt (DLR), Institut für Planetenforschung, Rutherfordstraße 2, 12489 Berlin-Adlershof, Germany
  - <sup>4</sup> INAF – Osservatorio Astrofisico di Catania, Via S. Sofia 78, 95123, Catania, Italy
  - <sup>5</sup> INAF – Osservatorio Astronomico di Roma, Via Frascati, 33, 00078 Monte Porzio Catone (RM), Italy
  - <sup>6</sup> SSDC-ASI, Via del Politecnico, snc, 00133 Roma, Italy
  - <sup>7</sup> Institute of Astronomy, KU Leuven, Celestijnenlaan 200D, 3001, Leuven, Belgium
  - <sup>8</sup> INAF-Osservatorio Astronomico di Palermo, Piazza del Parlamento, 1, I-90129, Palermo, Italy
  - <sup>9</sup> Deutsches Zentrum für Luft- und Raumfahrt (DLR), Institut für Optische Sensorsysteme, Rutherfordstraße 2, 12489 Berlin-Adlershof, Germany
  - <sup>10</sup> Aix-Marseille Université, CNRS, CNES, Laboratoire d’Astrophysique de Marseille, Technopôle de Marseille-Etoile, 38, rue Frédéric Joliot-Curie, 13388 Marseille cedex 13, France
  - <sup>11</sup> Max-Planck-Institut für Sonnensystemforschung, Justus-von-Liebig-Weg 3, 37077 Göttingen, Germany
  - <sup>12</sup> LESIA, CNRS UMR 8109, Université Pierre et Marie Curie, Université Denis Diderot, Observatoire de Paris, 92195 Meudon, France
  - <sup>13</sup> European Space Agency (ESA), European Space Research and Technology Centre (ESTEC), Keplerlaan 1, 2201 AZ Noordwijk, The Netherlands
  - <sup>14</sup> Centro de Astrobiología (CSIC–INTA), Depto. de Astrofísica, 28692 Villanueva de la Cañada, Madrid, Spain
  - <sup>15</sup> Center for Space and Habitability, University of Bern, Bern, Switzerland.
  - <sup>16</sup> Department of Physics, University of Warwick, Gibbet Hill Road, Coventry CV4 7AL, UK
  - <sup>17</sup> Armagh Observatory & Planetarium, College Hill, Armagh, BT61 9DG, UK
  - <sup>18</sup> Institute of Geological Sciences, Freie Universität Berlin, Malteserstraße 74-100, 12249 Berlin, Germany
  - <sup>19</sup> Institute of Astronomy, KU Leuven, Celestijnenlaan 200D, 3001 Leuven, Belgium
  - <sup>20</sup> Observatoire de Genève, Université de Genève, Chemin Pegasi 51, 1290 Sauverny, Switzerland

**Appendix A: Is my favorite target within the LOPS2?**

A software tool to check whether a given line of sight passes through the PLATO fields will be made available in the near future by ESA with support from the PLATO Consortium. Meanwhile, for any non-critical purpose, the footprint of LOPS2 can be reasonably approximated by the intersection between a spherical circle with  $r = 28.1^\circ$  and a “square” made with arcs of great circles (cf. Fig. 1). The corresponding TOPCAT expression is:

$$\text{inSkyEllipse}(l,b,255.9375,-24.62432,28.1, \\ 28.1,0) \ \&\& \ \text{inSkyPolygon}(l,b,288.6075,-44.1, \quad (\text{A.1}) \\ 223.2675,-44.1,233.1675,-0.25,278.7075,-0.25)$$

where  $(l, b)$  are the Galactic coordinates of the target. This expression can be translated into any other language of choice since it contains the coordinates of the five pivot points involved (the center of the circles plus the four vertexes of the square).

A more accurate representation of LOPS2, also including the NCAM sub-regions, can be built by approximating the field on a level-9 HEALPix grid, and then converting the footprints into IVOA<sup>22</sup>-compliant Multi-Order Coverage (MOC) regions (Fernique et al. 2014), through the mocpy code<sup>23</sup>. The MOC regions for 6, 12, 18, 24 NCAMs and the underlying HEALPix grid will be made available as online supplementary material. We emphasize that the actual sky coverage could be slightly different due to several factors (the in-orbit optical performances, the relative co-alignment of the cameras, the pointing accuracy, etc.) so all these regions should be used with some caution especially when a target of interest is close to the external boundaries or to the inner gaps.

**Appendix B: Additional tables and figures****Table B.1.** Glossary of acronyms used throughout this article.

Acronym	Description
asPIC	All-sky PLATO Input Catalog (M21)
CVZ	Continuous Viewing Zone
DEB	Detached Eclipsing Binary
DIA	Difference Image Analysis
EB	Eclipsing Binary
FPR	False Positive Rate
FCAM	PLATO Fast camera
FOV	Field Of View
GC	Globular Cluster
GO	PLATO Guest Observing program
HJ	hot Jupiter
HZ	Habitable Zone
LMC	Large Magellanic Cloud
LOP	Long-duration Observation Phase
LOPN	LOP field North
LOPN1	Current LOPN proposal (this work)
LOPS	LOP field South
LOPS1	Current LOPS proposal (this work)
M21	Montalto et al. (2021)
N22	Nascimbeni et al. (2022)
NCAM	PLATO Normal camera
NSR	Noise-to-Signal ratio
ORM	Observatorio Roque de Los Muchachos
OC	Open Cluster
P/L	PLATO Payload
PF	PLATO field
PIC	PLATO Input Catalog (M21)
PLATO	PLANetary Transits and Oscillations of stars (Rauer et al. 2024)
PPT	PLATO Performance Team
PSF	Point Spread Function
RV	Radial velocity
SNR	Signal-to-Noise ratio
SOP	Step and stare Observation Phase
SciRD	PLATO Scientific Requirements Document
SRJD	PLATO Scientific Requirements Justification Document
SWT	ESA PLATO Science Working Team
TCP	TESS candidate planets
TTV	Transit timing variations
WJ	warm Jupiter

<sup>22</sup> International Virtual Observatory Alliance, <https://ivoa.net/>

<sup>23</sup> <https://cds-astro.github.io/mocpy/>



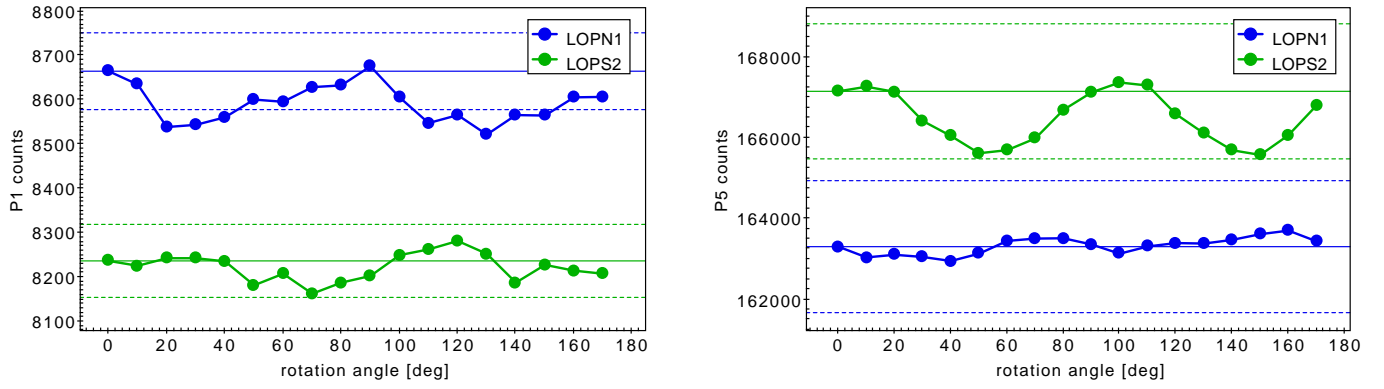


**Fig. B.1.** Optimization of the PLATO field rotation angle: number of P1 (left panel) and P5 (right panel) targets as a function of the rotation angle, for hypothetical PLATO fields centered at the LOPN1 (blue points and lines) or LOPS2 (green points and lines) coordinates. The continuous and dashed horizontal lines mark, for reference, the value of P1/P5 counts at  $\varphi = 0^\circ$  and a  $\pm 1\%$  deviation from it, respectively. See Section 2.2 for more details.

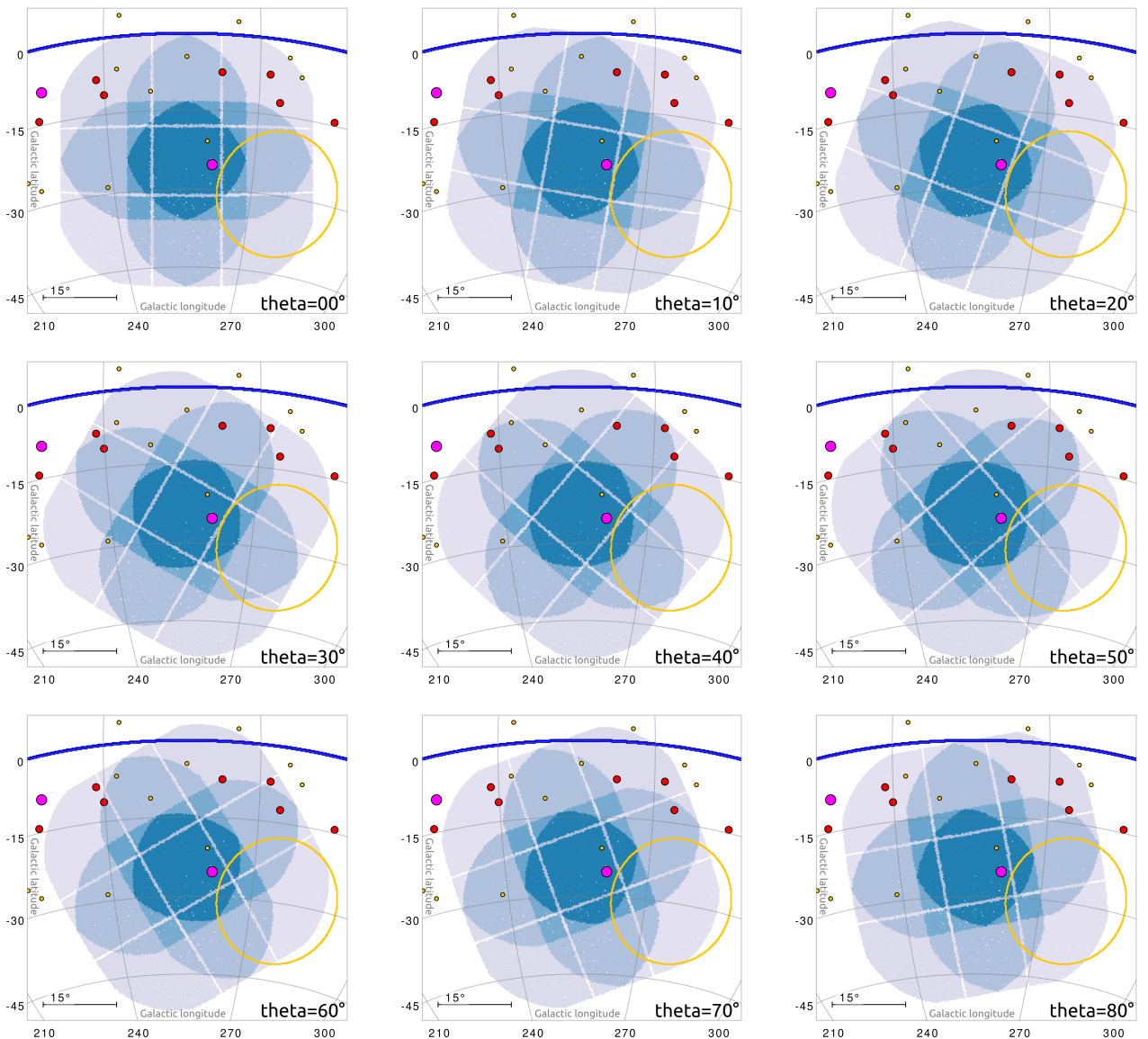


**Fig. B.2.** Optimization of the PLATO field rotation angle: PLATO test fields centered at the LOPS2 coordinates (Table 2) but rotated by  $0^\circ$ ,  $10^\circ$ ,  $20^\circ$ ,  $30^\circ$ ,  $40^\circ$ ,  $50^\circ$ ,  $60^\circ$ ,  $70^\circ$ ,  $80^\circ$  (in reading order); projection is Galactic. The  $\varphi = 0^\circ$  rotation angle corresponds to the nominal LOPS2 geometry. As in Fig. 6, the brightest stars from the Yale Bright Star Catalog are plotted as circles of different colors: magenta ( $V < 1$ ), red ( $1 < V < 2$ ), yellow ( $2 < V < 3$ ). The TESS southern CVZ is marked with a yellow circle. See Section 2.2 for more details.

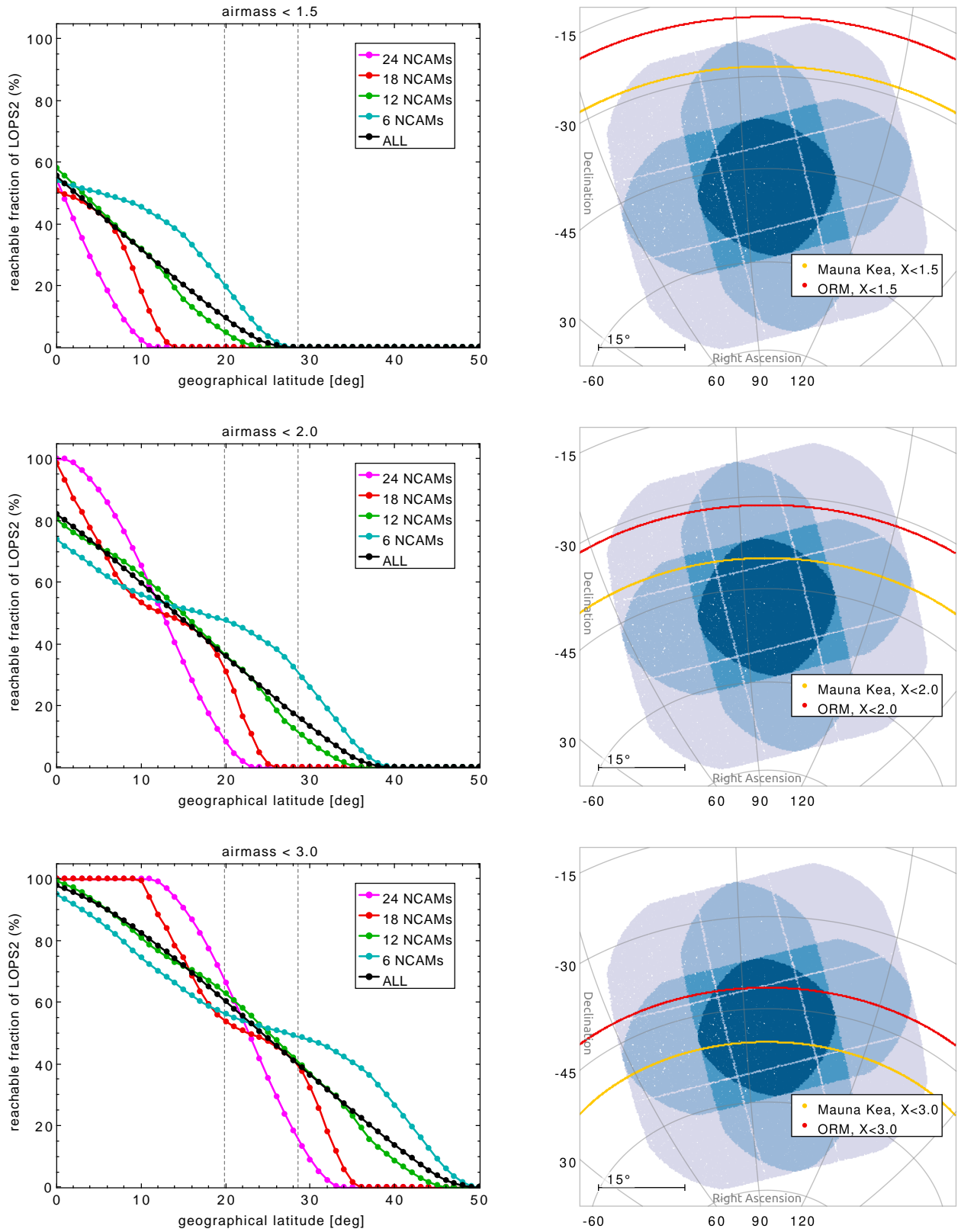


**Fig. B.3.** Visibility of LOPS2 from the Northern hemisphere. *Left panels:* reachable fraction of LOPS2 area (both for the whole field, and for its sub-regions observed by  $N$  NCAMs) as a function of the geographical latitude of the observatory, at limiting airmass of 1.5 (upper plot), 2.0 (middle plot), 3.0 (lower plot). The latitude of Mauna Kea ( $\psi \approx 19^\circ.8$ ) and ORM ( $\psi \approx 28^\circ.7$ ) observatories is marked with two vertical dashed lines. *Right panels:* Sky chart of LOPS2 (orthographic projection in equatorial coordinates) showing the minimum declination reachable from Mauna Kea (yellow circle) or ORM (red circle) at limiting airmass of 1.5 (upper plot), 2.0 (middle plot), 3.0 (lower plot). See also Section 2.3 for a discussion.

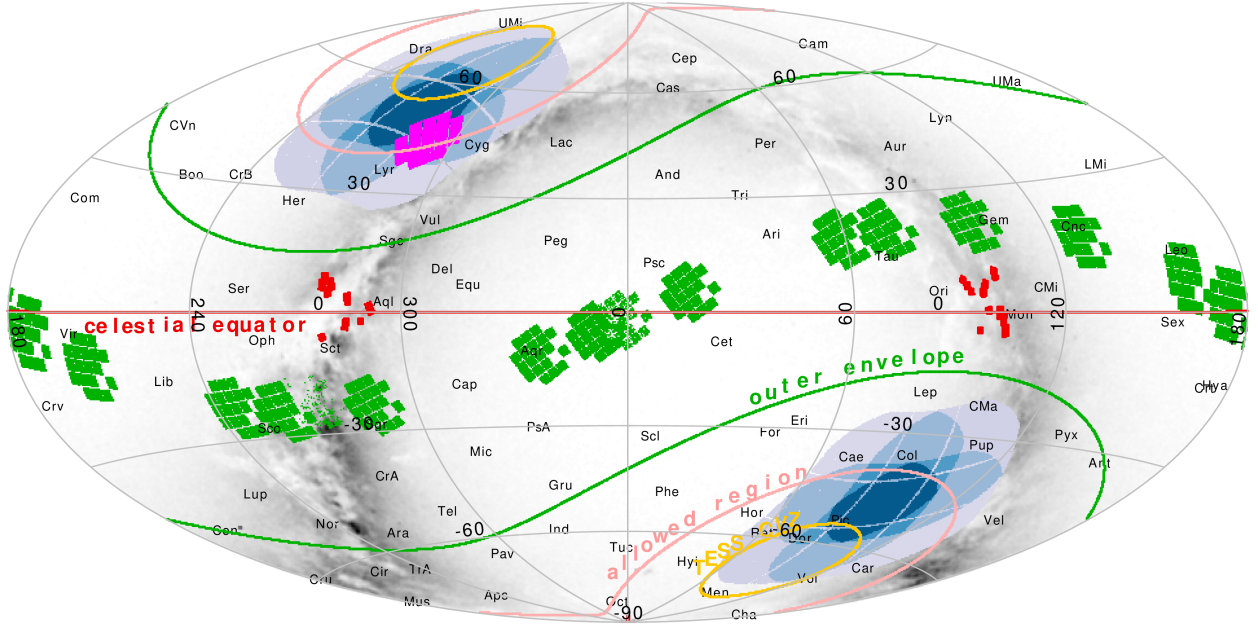


**Fig. B.4.** All-sky Aitoff projection in Equatorial coordinates of LOPS2 and LOPN1, showing the formal constraints for the selection of the PLATO LOP fields and the synergies with other missions. The two pink circles represent the  $|\beta| > 63^\circ$  technical requirement for the center of the LOP fields (“allowed region”), implying that the overall envelopes of every allowed field choice are two ecliptic caps at  $|\beta| \gtrsim 38^\circ$  (green circles). LOPS2 (lower left) and LOPN1 (upper right) are plotted with blue shades according to the number of co-pointing cameras, as in Fig. 1. The footprints of CoRoT (red), *Kepler* (magenta), and K2 (green) are over-plotted together with the TESS continuous viewing zone at  $|\beta| \gtrsim 78^\circ$  (yellow circle). The background gray layer is color-coded according to the areal density of  $G < 13.5$  stars from *Gaia* DR3. The celestial equator and poles are marked with a red line and crosses, respectively.

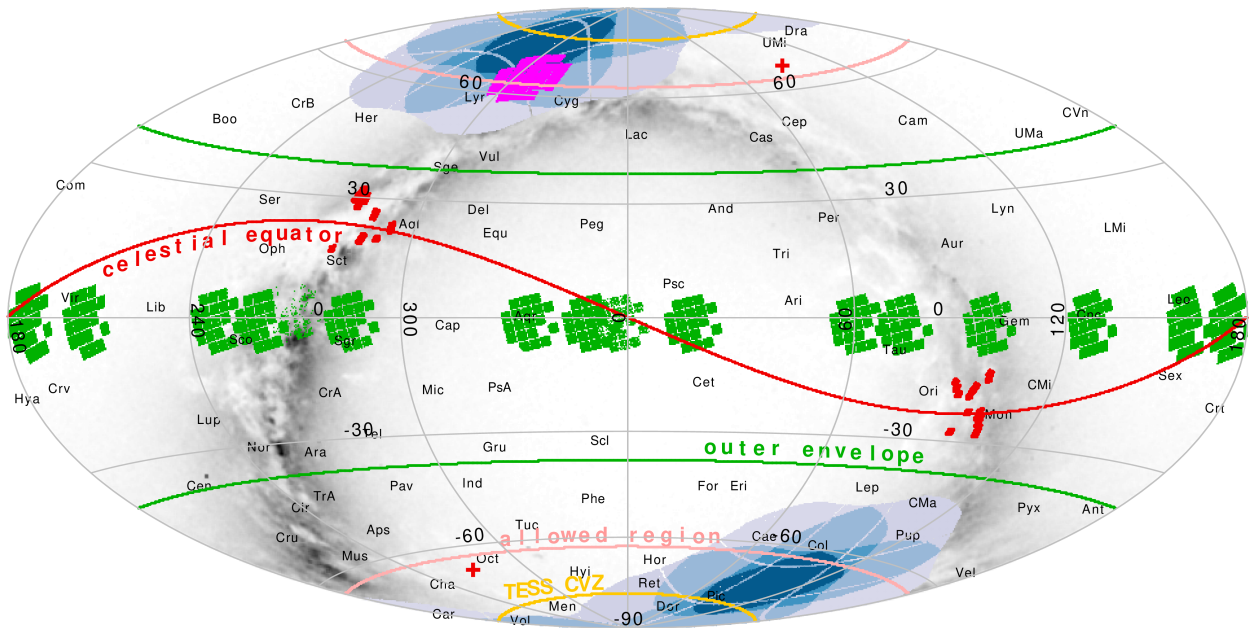


**Fig. B.5.** All-sky Aitoff projection in Ecliptic coordinates of LOPS2 and LOPN1, showing the formal constraints for the selection of the PLATO LOP fields and the synergies with other missions. The two pink circles represent the  $|\beta| > 63^\circ$  technical requirement for the center of the LOP fields (“allowed region”), implying that the overall envelopes of every allowed field choice are two ecliptic caps at  $|\beta| \gtrsim 38^\circ$  (green circles). LOPS2 (lower left) and LOPN1 (upper right) are plotted with blue shades according to the number of co-pointing cameras, as in Fig. 1. The footprints of CoRoT (red), *Kepler* (magenta), and K2 (green) are over-plotted together with the TESS continuous viewing zone at  $|\beta| \gtrsim 78^\circ$  (yellow circle). The background gray layer is color-coded according to the areal density of  $G < 13.5$  stars from *Gaia* DR3. The celestial equator and poles are marked with a red line and crosses, respectively.



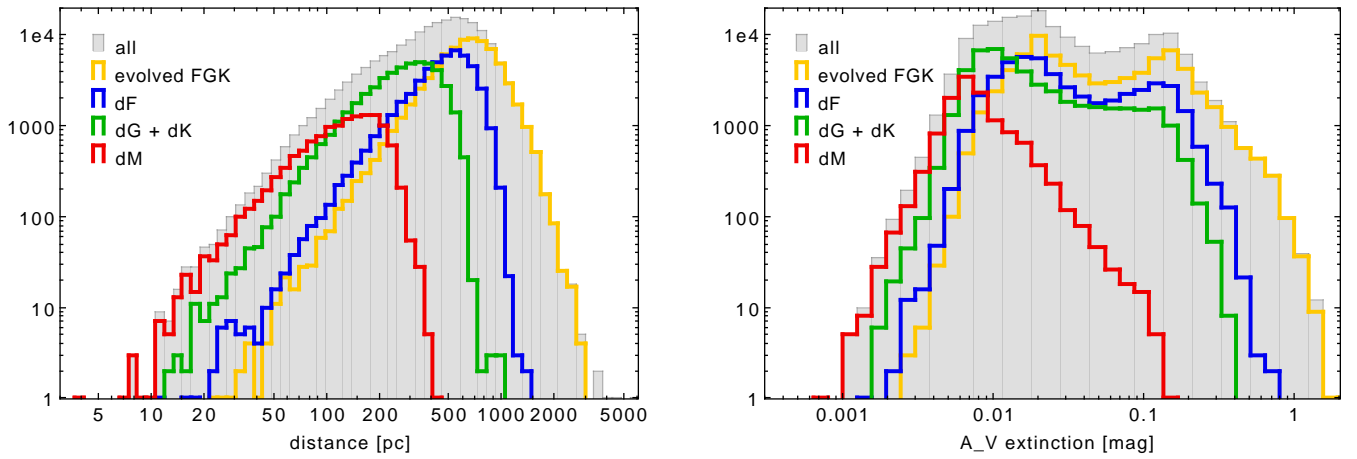


**Fig. B.6.** Distribution in distance and interstellar extinction of LOPS2 targets, from the PIC. Both the distribution of the whole sample (in gray) and for a few subsamples of interest is shown: M dwarfs, i. e., P4 (in red), main-sequence F stars (blue), main-sequence G and K stars (green) and FGK subgiants (orange). The definition of these sub-samples in terms of  $T_{\text{eff}}$  and  $R_{\star}$  can be found in [N22](#), Section 6.3. *Left panel*: logarithmic histogram of distance. *Right panel*: logarithmic histogram of the interstellar extinction in the Bessel V band.

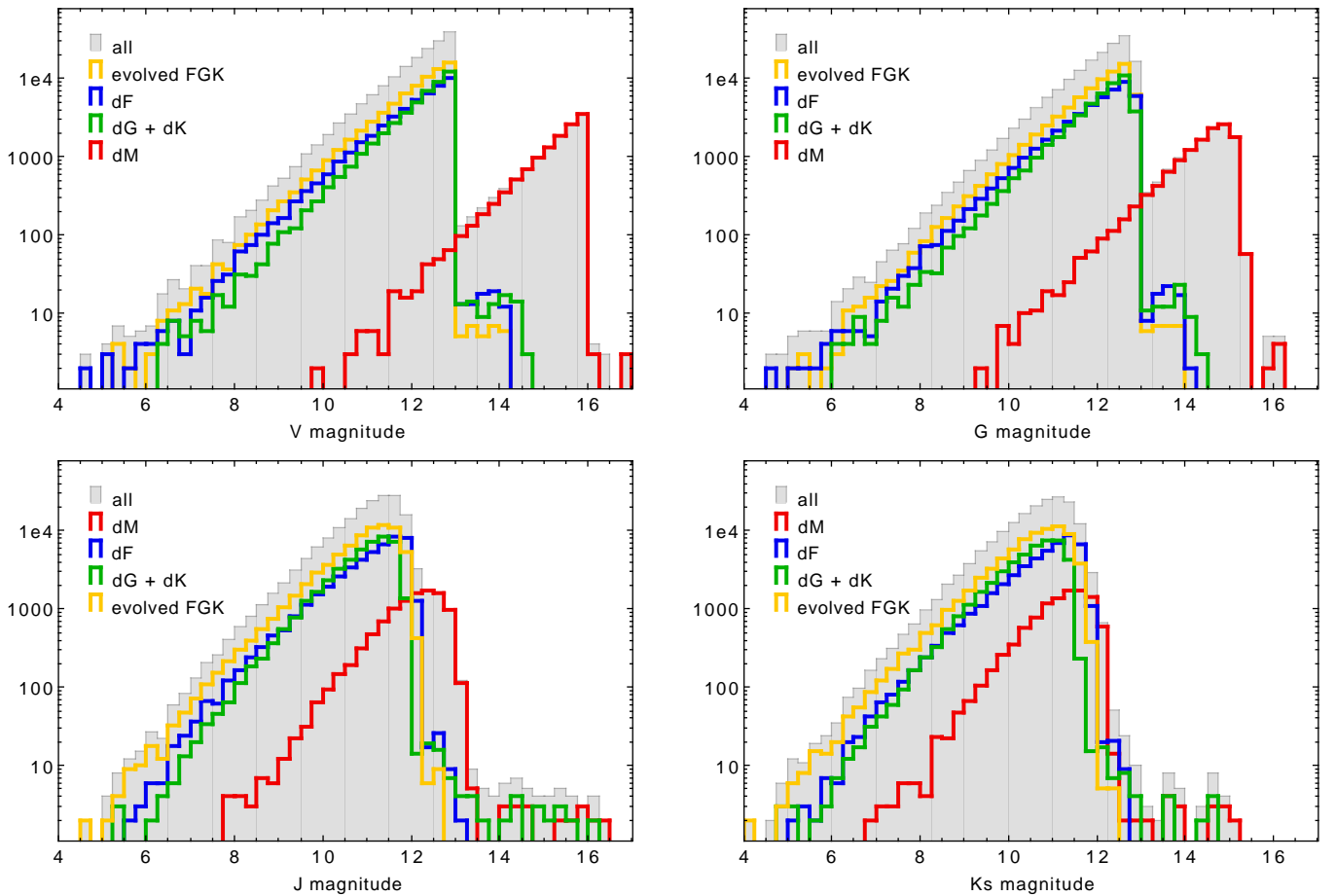


**Fig. B.7.** Distribution in V, Gaia G, 2MASS J, 2MASS K<sub>s</sub> magnitude (panels from upper left to lower right) of LOPS2 targets, from the PIC. Both the distribution of the whole sample (in gray) and for a few subsamples of interest is shown: M dwarfs, i. e., P4 (in red), main-sequence F stars (blue), main-sequence G and K stars (green) and FGK subgiants (orange).

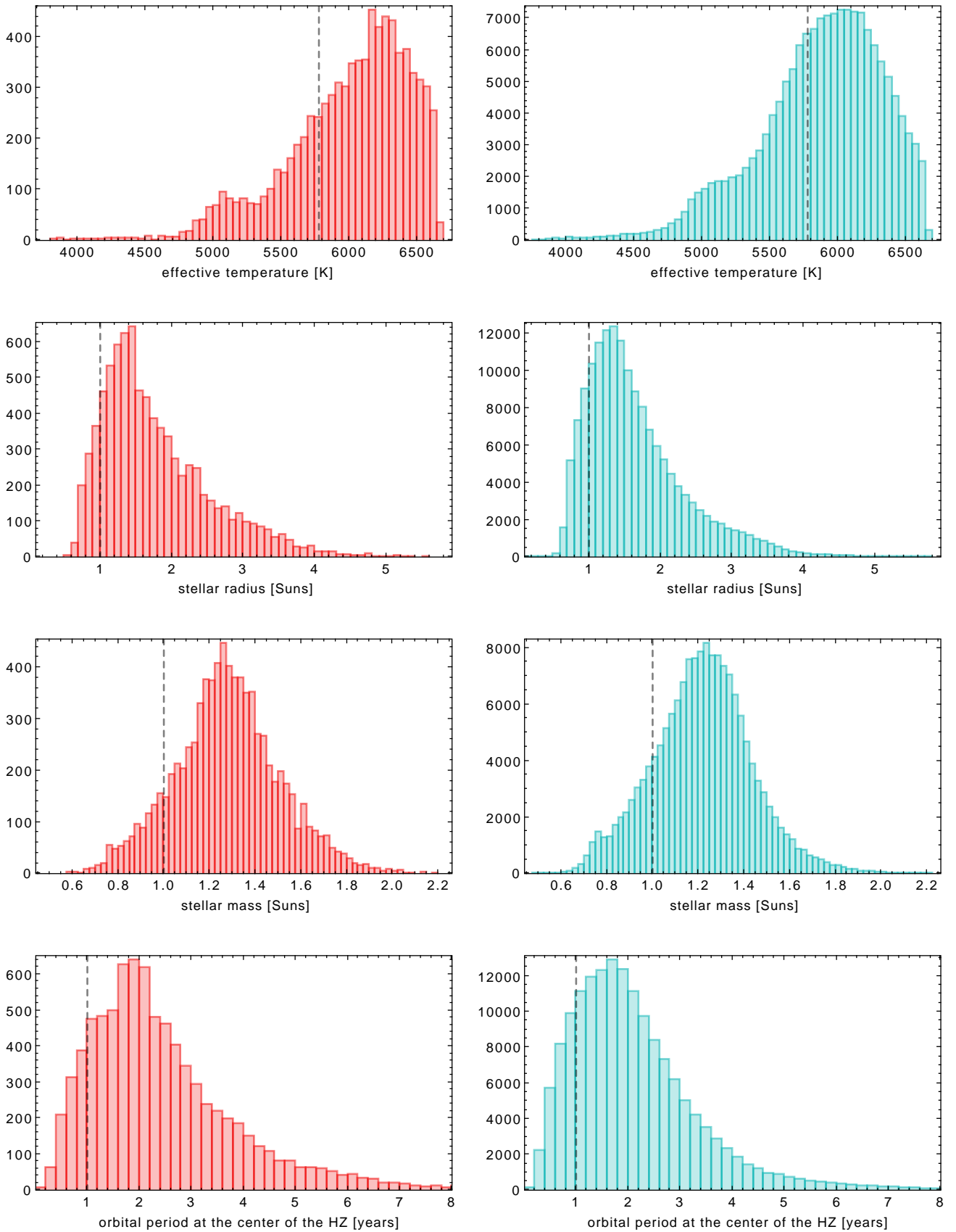


**Fig. B.8.** Histograms of some astrophysical quantities of the P1+P2 (red histograms, left side) and P5 (blue histograms, right side) samples within the LOPS2 field (see Section 3.1 for details). From top to bottom: effective temperature  $T_{\text{eff}}$  in K, stellar radius  $R_*$  and mass  $M_*$  in solar units, and orbital period  $P_{\text{HZ}}$  corresponding to the center of the habitable zone according to the [Kasting et al. \(1993\)](#) definition ( $a_{\text{HZ}} [\text{au}] = \sqrt{L_*/L_{\odot}}$ ) and the Kepler's laws. The Sun/Earth values are marked with dashed vertical line as reference.

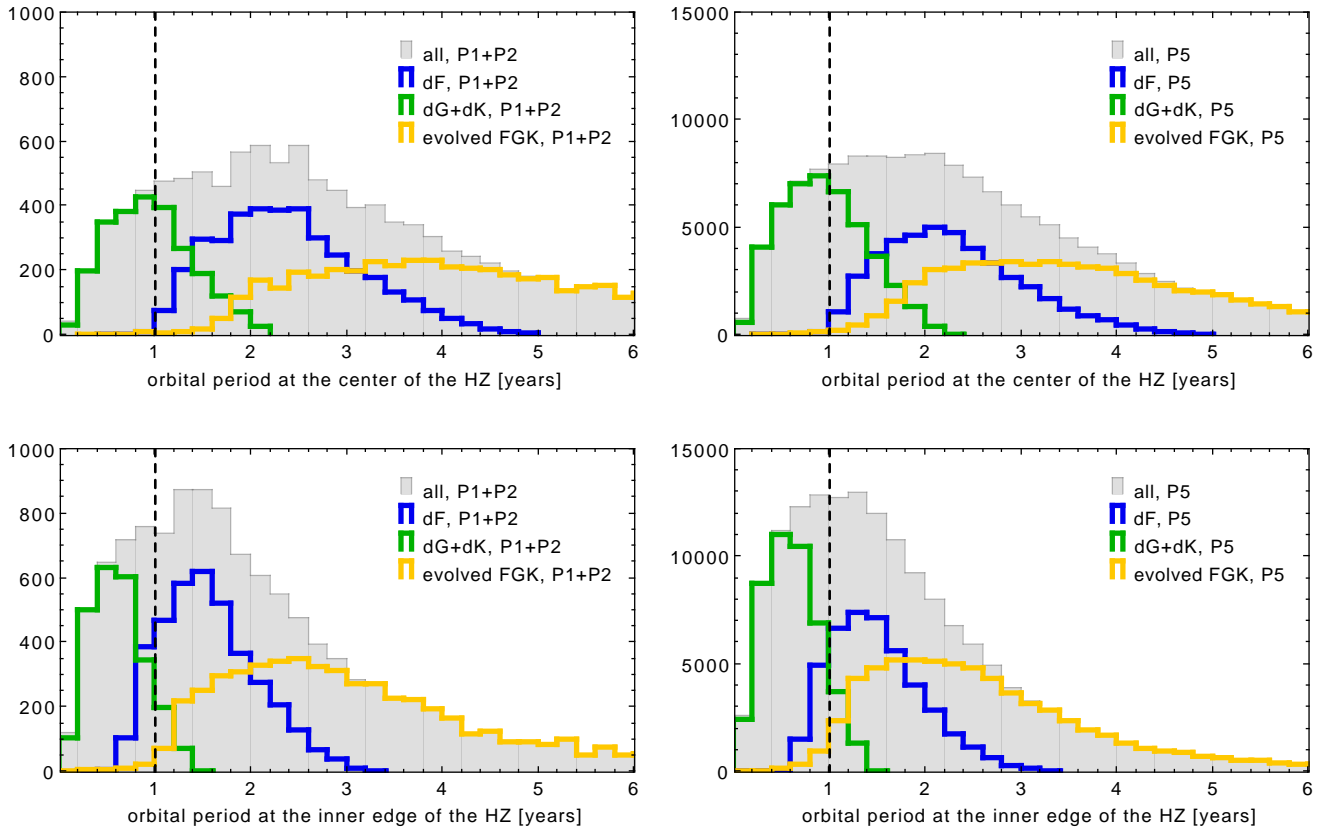


**Fig. B.9.** *Upper panels:* histograms of the expected orbital period of a planet at the center of the habitable zone according to the the [Kasting et al. \(1993\)](#) definition ( $a_{\text{hz}} [\text{au}] = \sqrt{L_{\star}/L_{\odot}}$ ) and Kepler's laws, for the P1+P2 (left side) and P5 (right side) samples within the LOPS2 field (see Section 3.1 for details). The Sun/Earth value (1 yr) is marked with dashed vertical line as reference. Both the distribution of the whole sample (in gray) and for a few subsamples of interest is shown: main-sequence F stars (blue), main-sequence G and K stars (green) and FGK subgiants (orange). The definition of these sub-samples in terms of  $T_{\text{eff}}$  and  $R_{\star}$  can be found in [N22](#), Section 6.3. *Lower panels:* same, but for a planet located at the inner edge of the habitable zone according to the the [Kasting et al. \(1993\)](#) definition ( $a_{\text{hz}} [\text{au}] = 0.77 \times \sqrt{L_{\star}/L_{\odot}}$ ).



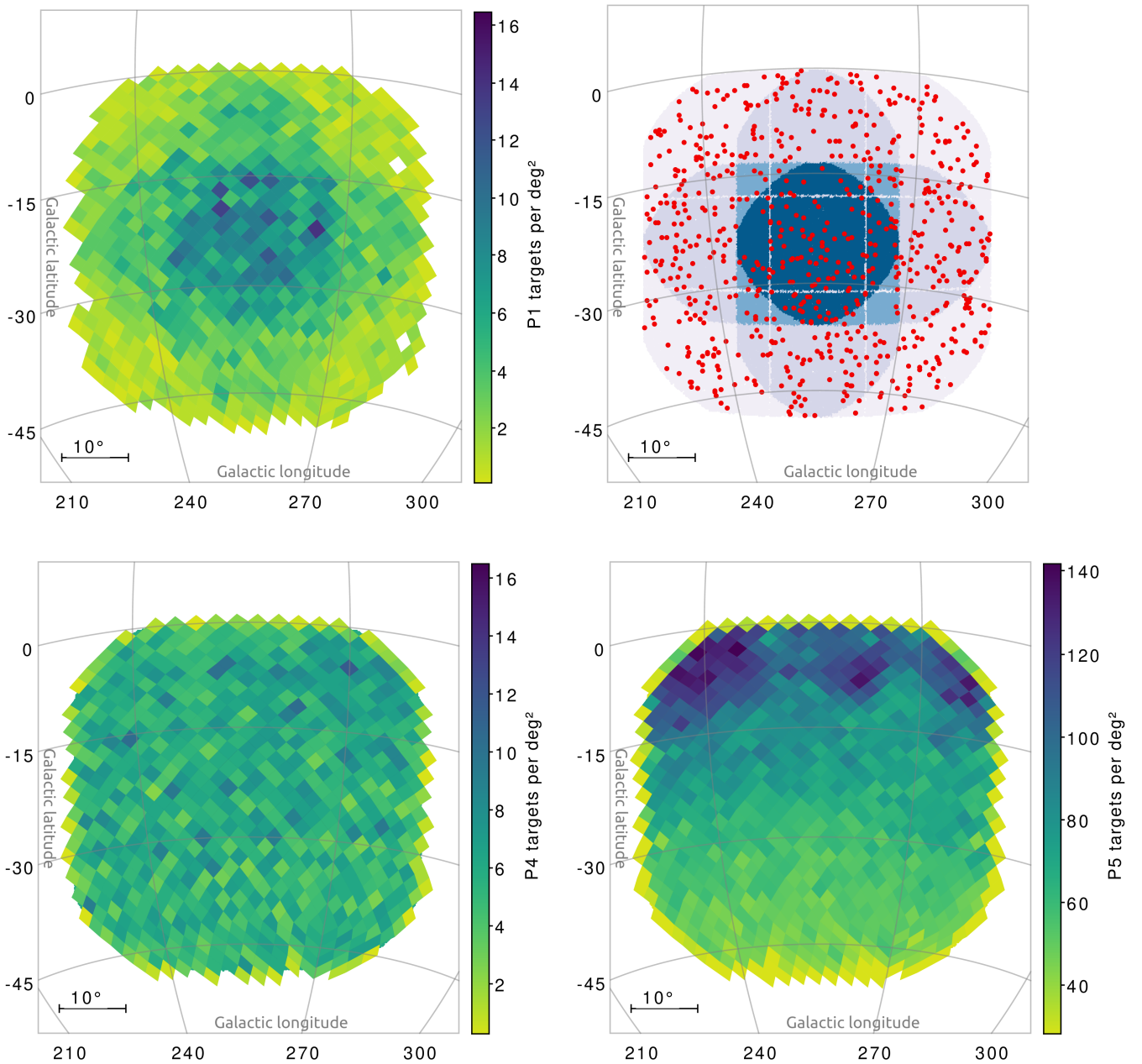


**Fig. B.10.** Spatial distribution of the P1-P2-P4-P5 targets (in reading order) over the LOPS2 field. P1, P4 and P5 targets are represented as color-coded density maps based on an HEALPix level-5, while the sparse and almost perfectly isotropic distribution of the P2 sample is plotted with individual red points. See also Section 3.1 for a discussion of the sample properties.

**Table B.1.** List of confirmed transiting exoplanets in LOPS2 (see Section 3.4.1 for details).

planet name	$N_p$	$P$ [days]	$R_p/R_\oplus$	$M_p/M_\oplus$	$T_{\text{eq}}$ [K]	$V$ [mag]	edge?	$N_{\text{cam}}$	FCAM?	comment
GJ 238 b	1	1.74	0.6	—	750	11.57	no	24	yes	
GJ 341 b	1	7.58	0.9	—	532	9.46	yes	6	no	
HATS-39 b	1	4.58	17.6	200.2	1635	12.74	no	6	no	
HATS-40 b	1	3.26	17.7	505.3	2085	13.48	no	12	no	
HATS-41 b	1	4.19	14.9	3083.0	1683	12.68	no	6	no	
HATS-42 b	1	2.29	15.7	597.5	1842	13.68	no	12	no	
HATS-43 b	1	4.39	13.2	83.0	993	13.56	no	12	no	
HATS-44 b	1	2.74	12.0	178.0	1164	14.4	no	12	no	
HATS-45 b	1	4.19	14.4	222.5	1508	13.32	no	6	no	
HATS-51 b	1	3.35	15.8	244.1	1540	12.52	no	6	no	
HATS-55 b	1	4.2	14.0	292.7	1359	13.52	no	6	no	
HATS-66 b	1	3.14	15.8	1694.0	1984	14.28	no	12	yes	
HATS-70 b	1	1.89	15.5	4100.0	2723	12.23	no	6	no	UHJ
HATS-76 b	1	1.94	12.1	835.6	935	16.68	no	6	no	very faint
HD 21749 b	2	35.61	2.6	22.7	421	8.08	yes	6	no	=GJ143 b
HD 21749 c	2	7.79	0.9	3.7	698	8.08	yes	6	no	=GJ143 c
HD 23472 b	5	17.67	2.0	8.3	547	9.73	no	6	no	
HD 23472 c	5	29.8	1.9	3.4	465	9.73	no	6	no	
HD 23472 d	5	3.98	0.8	0.6	908	9.73	no	6	no	
HD 23472 e	5	7.91	0.8	0.7	722	9.73	no	6	no	
HD 23472 f	5	12.16	1.1	0.8	627	9.73	no	6	no	
HD 28109 b	3	22.89	2.2	18.5	917	9.42	no	6	no	
HD 28109 c	3	56.01	4.2	7.9	609	9.42	no	6	no	
HD 28109 d	3	84.26	3.2	5.7	527	9.42	no	6	no	
HD 56414 b	1	29.05	3.7	—	1126	9.22	no	12	no	
KELT-14 b	1	1.71	19.5	408.1	1953	11.0	no	24	no	
KELT-15 b	1	3.33	19.5	416.4	1775	11.39	no	12	no	
KELT-25 b	1	4.4	18.4	—	2265	9.84	no	6	no	UHJ
L 98-59 b	3	2.25	0.8	0.4	614	11.68	yes	6	no	
L 98-59 c	3	3.69	1.4	2.2	532	11.68	yes	6	no	
L 98-59 d	3	7.45	1.5	1.9	410	11.68	yes	6	no	
LHS 1678 b	3	0.86	0.7	—	857	12.6	no	6	no	USP
LHS 1678 c	3	3.69	0.9	—	528	12.6	no	6	no	
LHS 1678 d	3	4.97	1.0	—	477	12.6	no	6	no	
LHS 1815 b	1	3.81	1.1	1.6	610	12.17	no	12	yes	
NGTS-1 b	1	2.65	14.9	258.1	785	15.67	no	12	no	very faint
NGTS-10 b	1	0.77	13.5	687.1	1432	14.51	no	12	no	USP
NGTS-15 b	1	3.28	12.3	238.7	1192	14.67	no	6	no	
NGTS-17 b	1	3.24	13.9	242.8	1516	14.41	no	6	no	
NGTS-23 b	1	4.08	14.2	194.8	1379	14.13	no	12	no	
NGTS-29 b	1	69.34	9.6	124.9	439	10.51	no	6	no	
NGTS-3 A b	1	1.68	16.6	756.4	1695	14.67	no	12	yes	
NGTS-4 b	1	1.34	3.2	20.6	1639	13.14	no	12	no	
NGTS-6 b	1	0.88	14.9	425.6	1395	14.24	no	6	no	USP
TOI-1221 b	1	91.68	2.9	1112.4	437	10.49	no	12	no	
TOI-1338 b	1	95.4	7.7	11.3	487	11.72	no	18	yes	
TOI-163 b	1	4.23	16.7	387.8	1659	11.47	no	6	no	
TOI-1937 A b	1	0.95	14.0	638.8	2083	13.18	no	18	no	USP
TOI-199 b	1	104.85	9.1	54.0	347	10.7	no	18	no	TTV
TOI-201 b	1	52.98	11.3	133.5	699	9.07	no	24	yes	
TOI-206 b	1	0.74	1.3	—	905	14.94	no	6	no	USP
TOI-216.01	2	34.53	10.1	178.0	476	12.32	no	6	no	
TOI-216.02	2	17.16	8.0	18.8	603	12.32	no	6	no	
TOI-2184 b	1	6.91	11.4	206.6	1429	12.25	no	12	no	
TOI-220 b	1	10.7	3.0	13.8	794	10.47	no	12	yes	
TOI-2338 b	1	22.65	11.2	1900.6	742	12.48	no	12	no	

Table B.1. Continued.

planet name	$N_p$	$P$ [days]	$R_p/R_\oplus$	$M_p/M_\oplus$	$T_{\text{eq}}$ [K]	$V$ [mag]	edge?	$N_{\text{cam}}$	F-CAM?	comment
TOI-2368 b	1	5.18	10.8	206.6	995	12.49	no	6	no	
TOI-2416 b	1	8.28	9.9	953.5	1074	13.02	no	6	no	
TOI-2459 b	1	19.1	3.0	—	445	10.77	no	18	no	
TOI-2525 b	2	23.29	8.7	26.7	555	14.22	no	12	yes	
TOI-2525 c	2	49.25	10.1	208.8	432	14.22	no	12	yes	
TOI-2529 b	1	64.59	11.6	743.0	633	11.53	no	12	no	
TOI-2589 b	1	61.63	12.1	1112.4	547	11.42	no	12	no	
TOI-269 b	1	3.7	2.8	8.8	550	14.37	no	12	no	
TOI-270 b	3	3.36	1.2	1.6	578	12.6	no	12	no	
TOI-270 c	3	5.66	2.4	6.2	486	12.6	no	12	no	
TOI-270 d	3	11.38	2.1	4.8	385	12.6	no	12	no	
TOI-2803 A b	1	1.96	18.1	309.9	1883	12.54	yes	6	no	
TOI-2818 b	1	4.04	15.3	225.7	1368	11.94	no	12	no	
TOI-286 b	2	4.45	1.4	4.6	972	9.87	no	12	yes	
TOI-286 c	2	39.39	1.9	3.7	472	9.87	no	12	yes	
TOI-431 b	2	0.49	1.3	3.1	1859	9.12	no	6	no	USP
TOI-431 d	2	12.46	3.3	9.9	632	9.12	no	6	no	
TOI-451 b	3	1.86	1.9	—	1482	10.94	no	6	no	
TOI-451 c	3	9.19	3.1	—	869	10.94	no	6	no	
TOI-451 d	3	16.36	4.1	—	718	10.94	no	6	no	
TOI-4562 b	1	225.12	12.5	732.0	337	12.14	no	12	no	very long P
TOI-470 b	1	12.19	4.3	—	656	11.17	no	12	no	
TOI-481 b	1	10.33	11.1	486.3	1250	9.97	no	12	no	
TOI-500 b	1	0.55	1.2	1.4	1608	10.54	no	24	yes	USP
TOI-540 b	1	1.24	0.9	—	607	14.82	no	12	yes	
TOI-622 b	1	6.4	9.2	96.3	1376	9.0	no	12	no	
TOI-640 b	1	5.0	19.9	279.7	1737	10.51	no	18	yes	
TOI-700 b	4	9.98	0.9	—	410	13.15	no	12	yes	
TOI-700 c	4	16.05	2.6	—	350	13.15	no	12	yes	
TOI-700 d	4	37.42	1.1	—	264	13.15	no	12	yes	HZ
TOI-700 e	4	27.81	1.0	—	292	13.15	no	12	yes	HZ
TOI-712 b	3	9.53	2.0	—	645	10.84	no	12	yes	
TOI-712 c	3	51.7	2.7	—	367	10.84	no	12	yes	
TOI-712 d	3	84.84	2.5	—	311	10.84	no	12	yes	HZ
TOI-813 b	1	83.89	6.7	—	606	10.36	no	6	no	
TOI-858 B b	1	3.28	14.1	349.6	1520	11.18	yes	6	no	
TOI-871 b	1	14.36	1.7	—	617	10.57	no	12	no	
WASP-100 b	1	2.85	14.9	400.5	1985	10.8	no	6	no	
WASP-101 b	1	3.59	16.0	162.1	1545	10.34	no	6	no	
WASP-119 b	1	2.5	15.7	390.9	1573	12.31	no	6	no	
WASP-120 b	1	3.61	16.5	1541.5	1866	10.96	no	12	no	
WASP-121 b	1	1.27	19.6	367.7	2306	10.51	no	12	no	UHJ
WASP-126 b	1	3.29	10.8	90.3	1468	10.99	no	6	no	TTV claim
WASP-159 b	1	3.84	15.5	174.8	1837	12.84	no	6	no	
WASP-160 B b	1	3.77	12.2	88.4	1113	13.04	no	12	no	
WASP-168 b	1	4.15	16.8	133.5	1333	12.12	no	24	yes	
WASP-23 b	1	2.94	10.8	281.0	1109	12.54	no	24	yes	
WASP-61 b	1	3.86	15.8	851.8	1623	12.49	no	6	no	
WASP-62 b	1	4.41	14.8	165.3	1381	10.21	no	12	yes	
WASP-63 b	1	4.38	15.8	117.6	1504	11.16	no	24	yes	
WASP-64 b	1	1.57	14.2	403.9	1658	12.7	no	12	yes	
WASP-79 b	1	3.66	17.2	270.2	1705	10.04	yes	6	no	

**Notes.** The columns give: the name of the planet, the multiplicity of the system, the orbital period  $P$  in days, the planetary radius  $R_p$  and mass  $M_p$  in Earth units (when known), the planetary equilibrium temperature in K, the  $V$  magnitude of the host star, a flag if the target is close to the LOPS2 outer edge, the number of NCAMs, a flag if the target is also observed with the FCAMs, and a comment field.



**Table B.2.** List of TESS candidates in LOPS2, from the TOI/ExoFOP database (see Section 3.4.2 for details).

TOI ID	$N_p$	$T$ [mag]	$P$ [days]	$R_p/R_\oplus$	$\delta$ [ppm]	$T_{\text{eq}}$ [K]	comment
119.01	2	9.23	5.541	2.04	633	1117	Potential multi; slight depth aperture correlation with no offset
119.02	2	9.23	10.692	1.8	535	710	outer candidate in potential multi; variable host
124.01	1	11.04	1.843	21.27	1950	1785	TFOP SB1/APC; v-shaped
153.01	1	11.69	7.632	12.44	4580	0	
163.01	1	10.87	4.231	14.63	7261	1584	TOI-163 b
167.01	1	11.57	4.453	0.0	5910	1027	no stellar radius; Gaia DR2 Teff + plx indicate sun-like star
171.01	1	11.54	1.239	13.58	13300	1461	
174.01	5	8.7	17.667	1.87	854	462	HD 23472 b / TOI 174.01
174.02	5	8.7	29.798	1.61	671	374	HD 23472 c; multi
174.03	5	8.7	12.162	1.16	317	638	HD 23472 f / TOI 174.03
174.04	5	8.7	3.977	0.76	142	855	HD 23472 d / TOI 174.04
174.05	5	8.7	7.908	0.97	217	720	HD 23472 e / TOI 174.05
187.01	1	9.09	0.513	19.23	5691	3118	v-shaped; very likely EB; TFOP APC previously retired as BEB due to chromaticity; possible odd-even
189.01	1	10.22	2.194	8.01	5980	1332	TFOP APC/BEB; v-shaped
199.01	1	10.0	104.873	10.22	12183	358	TOI-199 b ( <a href="https://arxiv.org/pdf/2309.14915.pdf">https://arxiv.org/pdf/2309.14915.pdf</a> )
201.01	2	8.57	52.978	11.45	6347	598	TOI 201 b
201.02	2	8.57	5.849	1.19	109	1237	TOI 201.02; interior to TOI-201 b
206.01	1	12.47	0.736	1.53	1323	840	TOI-206 b
211.01	1	9.45	6.564	7.63	2132	1003	TFOPWG APC/BEB
214.01	2	8.01	18.554	1.58	448	623	L1 candidate; possible multi
214.02	2	8.01	9.696	0.81	122	794	inner candidate in possible multi
216.01	2	11.5	34.506	10.46	17388	449	TOI-216.01/TOI-216 c; clear TTVs in spoc-s1-s39 multisector
216.02	2	11.5	17.389	6.48	2972	564	TOI-216.02 / TOI-216b. Apparent TTVs. Possible additional single around 2046P
218.01	2	13.55	0.438	0.65	486	901	Bad transit shape; likely SV
218.02	2	13.55	8.352	1.8	3925	337	eruptive variable host; TOI 218.01 (P~0.48 d) may be SV
220.01	1	9.66	10.695	2.85	920	796	TOI 220 b (Hoyer et al 2021)
252.01	1	11.62	1.002	5.02	2320	1563	TFOP APC; synchronized to variability
268.01	1	9.6	5.066	7.69	1350	1071	TICID 219253008 is a phantom from split (TICID 685340264 and 685340263)
269.01	1	12.27	3.698	2.94	4756	534	TOI-269 b
270.01	3	10.42	5.661	2.41	3856	453	TOI-270 c / TOI 270.01
270.02	3	10.42	11.38	2.25	3147	359	TOI-270 d / TOI-270.02
270.03	3	10.42	3.36	1.18	973	539	TOI-270 b / TOI 270.03
271.01	1	8.41	2.476	2.81	387	1606	follow up in progress
275.01	1	10.98	0.92	8.7	9180	1913	TFOP APC/BEB; v-shaped
281.01	1	10.48	5.577	4.56	642	1293	L1 candidate
282.01	3	8.93	56.005	4.61	768	597	HD 28109 c
282.03	3	8.93	84.261	3.44	440	521	HD 28109 d / TOI 282.03
282.04	3	8.93	22.891	2.56	253	804	HD 28109 b; multi
283.01	1	9.65	17.617	2.01	722	610	
285.01	1	12.11	32.333	3.03	2426	329	possible single transit
286.01	2	9.08	4.512	1.4	313	850	potential L1 planet; potential multi
286.02	2	9.08	39.362	1.85	552	606	potential multi; L1 candidate
322.01	1	10.71	3.991	16.08	3306	1382	
386.01	1	10.01	5.112	10.67	1415	1521	v-shaped; two stars about 1" separation in same pixel; slight depth aperture correlation
407.01	1	12.7	2.165	13.56	4990	1970	TFOP SB1/APC
429.01	1	10.17	0.0	9.33	7526	958	single transit with unknown period; still a single transit as of Sector 69
431.01	2	8.17	12.461	3.28	2078	589	TOI-431 d / TOI 431.01
431.02	2	8.17	0.49	1.47	291	1731	TOI-431 b / TOI 431.02
445.01	1	9.14	0.765	12.95	1900	2971	
446.01	1	11.88	3.502	22.1	16196	1648	TFOP APC; retired as SB1
447.01	1	8.88	5.529	23.55	17914	1235	big;
448.01	1	13.17	0.882	8.39	11755	1428	NGTS-6 b
450.01	1	12.38	10.715	14.04	56326	340	TFOP APC; retired as SB2
451.01	3	10.27	16.365	3.92	2075	634	TOI-451 d / TOI-451.01
451.02	3	10.27	1.859	1.93	498	1310	TOI-451 b
451.03	3	10.27	9.191	2.73	941	769	TOI-451 c
459.01	1	9.54	4.429	6.34	700	1728	TFOP APC/SB1; synchronized to variability

Table B.2. Continued.

TOI ID	$N_p$	$T$ [mag]	$P$ [days]	$R_p/R_\oplus$	depth [ppm]	$T_{\text{eq}}$ [K]	comment
470.01	1	10.65	12.191	4.61	2625	660	TOI-470 b
472.01	1	12.29	0.568	24.85	42540	954	no GAIA radius with Teff 3869K; large planet around an M star if real
475.01	1	10.77	8.262	2.34	1418	531	
476.01	1	8.85	3.063	14.75	6160	1930	pulsating host
481.01	1	9.37	10.331	11.94	4577	1111	TOI-481 b
486.01	1	9.34	1.745	0.59	160	896	high proper motion star
499.01	1	10.1	8.533	4.15	1756	941	v-shaped; possible secondary; possible centroid offset towards TIC 769340768
500.01	1	9.32	0.548	1.36	227	1577	TOI-500 b
502.01	1	10.33	2.941	8.83	2421	1431	odd-even; V-shaped; possible EB
510.01	1	8.44	1.352	2.83	371	1110	TFOP RV0/APC; variable host; offset not consistent with nearby stars
512.01	2	8.95	7.189	1.53	285	831	first candidate in potential multi
512.02	2	8.95	20.275	1.74	410	764	potential multi
520.01	1	9.37	0.524	1.49	83	3256	
527.01	1	8.24	18.089	22.2	5527	984	planet radius greater than 20 $R_e$ which is large for orbital period; v-shaped
533.01	1	10.89	19.572	3.61	1677	540	
539.01	1	10.54	0.31	1.55	258	2138	$a/R_s \sim 2$ ; possibly evaporating
540.01	1	11.48	1.239	0.97	2319	550	TOI-540 b
541.01	1	14.6	1.353	18.11	18071	1618	low SNR
542.01	1	14.74	1.632	11.56	14067	1359	
553.02	2	10.02	11.923	2.29	681	695	TOI 553.02; active TFOP PC; potential multi
553.03	2	10.02	40.891	2.71	945	461	period updated to 40.89 days with spoc multisector; period could be half; potential multi
555.01	1	14.92	1.942	11.76	32945	857	HATS-76 b
569.01	1	9.43	6.556	8.4	2970	879	crowded field; confirmed BD
570.01	1	9.98	1.469	5.2	1475	1455	V-shaped; crowded field
579.01	1	9.67	1.684	14.07	912	1220	multi year spoc shows no centroid offset but hint of odd-even; host is evolved
580.01	1	9.55	1.55	13.39	3594	5565	variable host; possible secondary not at half phase; multiple stars in pixel; v-shaped
583.01	1	9.38	6.56	11.2	4049	1081	v-shaped
588.01	1	7.31	39.472	16.35	7758	1015	likely too large; possible secondary not at half phase
601.01	1	9.92	3.478	11.33	1177	1229	evolved host
602.01	1	10.05	11.1	28.12	4990	2010	TFOP APC; retired as SB1
609.01	1	9.84	4.97	21.41	12601	908	TFOP APC/SB2
612.01	1	10.19	0.914	5.58	1368	2409	centroid offset not on a particular star; v-shaped
616.01	1	9.98	2.806	0.0	3350	0	transiting object might be too big; no stellar radius; Gaia $R_s = 4.24 R_{\text{sun}}$ would make $R_p \sim 20 R_e$
618.01	1	10.13	7.761	7.86	3110	1250	
622.01	1	8.54	6.403	9.3	3815	1274	TOI-622 b
626.01	1	9.51	4.401	19.74	6903	2177	KELT-25 b (Rodriguez Martinez et al; <a href="https://arxiv.org/abs/1912.01017">arXiv:1912.01017.pdf</a> )
637.01	1	8.82	2.858	0.0	529	1284	v-shaped; no stellar parameters but possible G/K dwarf host; possible offset to E
640.01	1	10.04	5.004	19.78	7390	1622	TOI-640 b
641.01	1	9.9	1.893	3.12	630	1333	
666.01	1	8.79	7.476	14.54	1519	1629	v-shaped; TFOP APC/VPC?/SM
678.01	1	10.87	11.33	3.41	821	808	crowded field
681.01	1	10.66	15.778	18.29	6806	1097	Likely EB; likely too large to be a planet at this irradiation
686.01	1	9.92	3.514	3.34	334	1635	
695.01	1	10.73	21.376	2.68	786	563	Was previously designated as EB/AFA; reinstated as PC
696.01	3	10.51	0.86	0.97	720	830	LHS 1678 b
696.02	3	10.51	3.694	1.04	833	511	LHS 1678 c
696.03	3	10.51	4.965	0.86	633	463	LHS 1678 d
697.01	1	9.3	8.608	2.62	555	840	potential L1 planet
699.01	3	9.8	14.801	2.45	345	761	potential L1 planet; possible multi; TOI 699.01
699.02	3	9.8	33.634	2.31	384	636	potential L1 planet; possible multi; TOI 699.02
699.03	3	9.8	672.637	2.97	423	257	could be variability; low SNR; potential multi; only two transits with maximum period of $\sim 672$ days; actual period likely shorter
700.01	4	10.88	16.051	2.59	2769	328	TOI-700 c / TOI-700.01
700.02	4	10.88	37.424	1.33	738	247	TOI-700 d / TOI-700.02

**Table B.2.** Continued.

TOI ID	$N_p$	$T$ [mag]	$P$ [days]	$R_p/R_\oplus$	depth [ppm]	$T_{\text{eq}}$ [K]	comment
700.03	4	10.88	9.977	0.96	460	384	TOI-700 b / TOI-700.03
700.04	4	10.88	27.81	0.95	407	273	TOI-700 e / TOI-700.04
702.01	1	11.75	3.568	2.05	907	676	L1 candidate
703.01	2	10.18	8.673	2.28	725	834	potential L1 candidate in multi-planet system; Gaia Rs=0.91+/-0.04
703.02	2	10.18	22.568	2.48	870	606	possible multi
704.01	1	10.09	3.814	1.11	458	578	LHS 1815 b
706.01	1	8.34	719.038	16.63	4851	245	Likely too large to be a planet at allowed insolarations. Two transits two years apart. Actual period is likely shorter.
707.01	2	10.06	52.799	2.4	541	464	potential multi; close to 3:1 resonance
707.02	2	10.06	17.476	1.49	163	671	close to 3:1 resonance; low SNR
709.01	2	14.22	32.377	3.68	52580	2129	TFOP work in progress.
709.02	2	14.22	777.052	1.34	7212	738	1.3 Re candidate around a white dwarf; potential multi-planet system; period likely shorter than maximum period of ~777 days
711.01	2	11.68	18.384	2.15	1010	458	possible multi; potential L1 candidate
711.02	2	11.68	35.943	2.74	1179	366	low SNR; possible multi
712.01	3	9.84	9.531	2.25	916	584	TOI-712 b
712.02	3	9.84	51.699	2.46	1339	357	TOI-712 c
712.04	3	9.84	84.839	2.04	1020	292	TOI-712 d
713.01	2	10.64	35.999	2.23	1087	356	potential L1 planet; possible multi
713.02	2	10.64	1.872	1.06	256	953	potential multi
714.01	2	11.5	4.324	1.5	977	563	potential multi planet system
714.02	2	11.5	10.178	1.57	943	423	possible multi
721.01	1	10.16	12.288	2.09	315	935	
722.01	1	11.94	15.3	2.4	1265	519	potential L1 planet; stellar radius is from SPOC Y1 multisector; TIC 38509907 has been joined with TIC 684936227; possible additional candidate at ~83.78 days
723.01	1	10.01	1.418	1.11	204	1284	potential L1 planet; variable host
724.01	1	9.73	3.213	2.06	510	1085	slightly v-shaped; variable host
738.01	1	12.68	3.441	8.9	8647	1089	
739.01	1	11.54	9.015	12.23	4800	945	V-shaped
746.01	1	11.38	10.98	10.18	8276	781	
785.01	1	11.47	18.626	1.18	425	367	bad transit shape; consistent centroid offset
786.01	2	9.8	12.669	2.31	321	1356	possible multi
786.02	2	9.8	38.554	2.14	329	596	potential multi; centroids scattered between sectors but majority on target
787.01	1	9.47	2.126	1.54	150	1774	centroid variation between sectors; slight depth aperture correlation
788.01	1	8.96	6.487	3.26	113	1048	low S/N; crowded field; possible offset toward faint neighbor TIC 765721735; some odd-even clearer in SPOC TEC plots
790.01	3	8.98	199.578	6.99	1767	423	potential multi
790.02	3	8.98	41.018	2.4	229	717	possible multi near 5:1 resonance
790.03	3	8.98	0.0	6.44	1628	411	single transit exterior to 2 TOIs
794.01	1	9.98	52.407	3.31	372	645	
795.01	1	10.22	8.761	2.93	480	1051	centroid variation among sectors; L1 candidate
798.01	1	11.91	95.239	0.0	5934	399	Gaia Teff + astrometry seem to indicate host is an M dwarf; no stellar radius
799.01	1	10.54	5.545	1.94	439	959	L1 candidate
800.01	1	12.25	0.966	3.27	997	1844	blue supergiant host
802.01	1	7.48	3.694	0.65	75	943	Centroid variation among sectors
804.01	1	10.71	2.838	0.0	190	1622	Crowded field. Low SNR. Some depth aperture correlation. Asymmetric transit shape. No stellar radius.
805.01	1	13.16	4.118	1.28	1948	441	
807.01	1	11.22	5.27	1.68	512	739	SPOC Y1+Y3 indicates 5-sigma centroid offset; very crowded field
809.01	1	10.27	183.459	3.38	645	416	low S/N
810.01	2	10.47	28.306	2.75	357	696	potential multi
810.02	2	10.47	90.848	2.62	314	472	outer candidate in possible multi planet system
811.01	1	10.93	25.176	14.2	12570	617	could be on companion 100757804; confirmed BD (Carmichael+21)
812.01	1	10.96	13.867	14.39	7930	1131	could be on 363914760
813.01	1	9.82	83.896	7.22	1218	595	TOI-813 b; CTOI from Planet Hunters TESS

Table B.2. Continued.

TOI ID	$N_p$	$T$ [mag]	$P$ [days]	$R_p/R_\oplus$	depth [ppm]	$T_{\text{eq}}$ [K]	comment
841.01	1	12.48	3.493	11.47	14230	914	
842.01	1	12.54	2.786	12.0	11629	1196	
858.01	1	10.64	3.28	13.81	11048	1402	may also be on 198008002
859.01	1	11.96	5.154	4.6	2522	816	
862.01	1	8.99	3.31	0.0	5092	1223	variable host; visual binary separated by $\sim 1$ arc sec; no stellar radius; Gaia DR2 $R_{\text{star}} \sim 2.7$ and $R_p/R_{\text{star}} \sim 0.07$ consistent with possible inflated hot Jupiter
863.01	1	9.92	0.525	1.44	277	2038	low SNR; some scatter in centroids between sectors
864.01	1	11.47	0.521	1.0	627	1006	
867.01	1	10.4	15.404	2.29	282	808	
870.01	1	10.88	22.038	2.34	1208	362	weak secondary
871.01	1	9.7	14.363	1.69	542	565	some odd-even
872.01	2	11.76	2.24	2.75	1153	1062	L1 candidate
872.02	2	11.76	4.973	2.61	826	814	candidate 2 in potential multi-planet system
873.01	1	12.06	5.931	1.8	1022	518	
874.01	1	8.75	5.905	2.01	225	1413	potential L1 planet; possible unrelated transit near TBJD 1512
875.01	1	11.29	11.02	2.34	1077	563	
877.01	1	10.58	6.016	13.63	5342	1526	TFOP APC
899.01	1	11.53	12.846	11.89	8527	822	
919.01	1	11.18	20.027	23.65	17516	689	large; v-shaped; likely EB; TFOP APC; formerly FP/EB; large radius for orbital period
921.01	1	11.26	5.129	3.38	809	951	
924.01	1	11.36	12.127	20.32	19172	776	v-shaped transit and large $R_p$ for given period; Gaia DR2 error 5.51 km/s; likely EB
932.01	2	10.74	19.311	2.75	1223	475	possible multi
932.02	2	10.74	7.986	1.71	460	675	inner candidate in potential multi
933.01	1	10.64	88.935	12.65	4026	526	possible odd-even
934.01	1	12.62	3.782	12.44	18871	952	
945.01	1	11.12	0.93	4.6	720	2234	
970.01	1	10.52	4.986	3.35	970	1252	some centroid offset not centered on another star
1009.01	1	8.43	1.96	0.0	1708	1456	no stellar radius; Simbad lists as B3III/IV; planet likely larger; odd-even; hot star with extremely rapid rotation
1011.01	1	8.24	2.47	1.45	250	1364	
1019.01	1	10.64	5.234	24.29	20797	1575	Large for its insolation
1085.01	1	11.6	3.254	14.95	13620	0	TFOP APC/SB2; 1000pm secondary; phased
1207.01	1	9.22	2.628	0.98	75	1418	centroid offsets scattered around target; sub-Earth $R_p$
1209.01	1	9.59	40.72	3.24	356	668	Crowded field. Slight depth aperture correlation without offset in difference image. Scattered light in some sectors likely affecting centroid. Asymmetric transit shape.
1212.01	1	10.35	105.585	2.5	463	430	low SNR; close to momentum dumps
1218.01	1	10.34	13.774	1.9	338	730	Crowded field
1219.01	1	10.1	1.914	2.04	248	2462	many fainter stars nearby; v-shaped; slight depth aperture correlation; possible secondary and phase modulations
1221.01	1	10.02	91.683	3.24	713	399	TOI-1221 b
1222.01	1	10.27	10.194	2.74	317	994	TFOP work in progress; epoch is from qlp-s39-tois
1225.01	2	11.7	13.896	2.46	749	686	L1 candidate
1225.02	2	11.7	8.121	2.32	595	821	potential multi; low MES
1226.01	1	11.49	3.929	2.33	486	1123	L1 candidate
1228.01	1	9.08	29.05	2.85	318	1115	HD 56414 b
1232.01	1	11.71	14.255	10.7	7900	786	
1338.01	1	11.45	95.174	7.85	2600	255	period confirmed 95.2 days (Veselin B. Kostov et al 2020); TOI-1338 b; circumbinary planet
1406.01	1	11.43	10.574	9.44	5460	1007	Confirmed brown dwarf; paper led by Theron Carmichael
1881.01	1	10.28	1.12	5.96	1901	2267	V-shaped; some odd-even; crowded field; CTOI from Luke Bouma
1937.01	1	12.49	0.947	14.67	16490	1646	TOI-1937 A b
2001.01	1	8.91	2.743	24.42	1518	3128	evolved host
2184.01	1	11.34	6.907	9.36	900	1491	TOI-2184 b
2200.01	1	12.24	2.936	7.19	6790	1147	TFOP work in progress
2205.01	1	15.08	0.889	14.25	41422	1044	near neighbor TIC 737476974; V-shaped; large PC
2208.01	1	15.74	0.674	12.47	103652	804	V-shaped; some odd-even
2218.01	1	11.47	0.346	10.19	2800	3243	V-shaped; small $a/R_s$ ; possibly EB



Table B.2. Continued.

TOI ID	$N_p$	$T$ [mag]	$P$ [days]	$R_p/R_\oplus$	depth [ppm]	$T_{\text{eq}}$ [K]	comment
2220.01	1	11.56	1.393	13.36	7098	1793	consistent very small odd-even; possible synchronization in early Y1; V-shaped; large
2222.01	1	12.68	2.246	17.51	12600	1943	
2238.01	1	10.72	3.39	2.41	260	1464	Low-SNR candidate. Poor transit shape but good BLS signal. Slight depth aperture correlation.
2248.01	1	10.46	62.162	10.34	3710	500	Gaia DR2 RV error 6.6 km/s; some phased scatter
2310.01	1	12.71	2.943	13.65	12560	1186	good transit shape; 0.6874 arcsec companion
2329.01	1	11.74	6.535	10.78	6370	925	ephemeris match to nearby neighbor 238920875; this is the brighter star; CTOI from Marco Montalto
2333.01	1	12.35	14.22	8.79	2390	1067	Depth-aperture but no bright stars nearby; CTOI from Marco Montalto
2338.01	1	11.7	22.654	12.28	11530	537	TOI-2338 b; CTOI from Marco Montalto
2339.01	1	11.95	9.773	12.02	2280	1298	CTOI from Marco Montalto
2352.01	1	11.09	1.68	5.37	2020	1496	v-shaped; CTOI from Marco Montalto
2353.01	1	11.9	5.752	6.23	702	1534	low SNR; CTOI from Marco Montalto
2356.01	1	11.71	3.663	3.53	970	1473	Potential L1 candidate; small depth aperture correlation; CTOI from Marco Montalto
2363.01	1	12.1	5.544	13.57	5400	1434	Crowded field; CTOI from Marco Montalto
2368.01	1	11.7	5.175	10.77	13300	810	Slight odd-even and inconsistent transit shapes which can be due to few transits available; CTOI from Marco Montalto
2388.01	1	8.12	1.344	0.0	44	1652	multiple star system; no gaia information; likely SV based on sinusoidal shape in spoc-s1-s65 and multiple signals found at similar period
2392.01	3	10.36	5.912	3.29	416	1431	potential multi
2392.02	3	10.36	3.407	2.96	315	2021	potential multi
2392.03	3	10.36	9.17	2.46	186	1210	low SNR; potential multi
2416.01	1	12.4	8.275	11.55	6510	942	
2441.01	2	12.83	12.89	2.97	3521	363	
2441.02	2	12.83	5.551	2.03	1282	481	low SNR; interior to TOI 2441.01
2447.01	1	10.01	0.0	10.22	8735	719	Single transit. Orbital period is likely > 30 days.
2448.02	1	10.0	19.758	3.81	483	1035	some depth aperture correlation and possible offset
2449.01	1	9.9	16.654	11.91	10168	1215	single transit
2459.01	1	9.4	19.105	2.94	1906	436	potential L1 candidate; deep transit around ~2200 TBJD in SPOC multisector that may be another planet
2463.01	1	9.03	10.608	11.66	1234	1592	evolved and variable star
2479.01	1	9.31	36.838	3.79	965	566	TFOP work in progress.
2490.01	1	11.28	0.0	7.89	4408	770	CTOI from Rafael Brahm; single at TBJD ~2181
2496.01	1	14.2	1.575	22.96	77504	742	deep transit but $R_p < 25 R_\oplus$ ; possibly synchronized; likely EB
2501.01	1	11.68	5.326	2.64	1502	642	found in faint-star QLP search; crowded field
2506.01	1	9.93	14.97	3.05	430	0	weak BLS; some variability in raw LC
2507.01	1	9.5	17.305	2.77	657	677	slight odd-even may be from detrending
2518.01	1	10.23	6.898	2.19	550	1095	potential L1 planet; possible centroid offset; slight depth aperture correlation
2519.01	1	10.28	6.955	2.29	770	691	
2525.01	2	13.4	23.342	9.73	6474	513	CTOI from Planet Hunters; TOI-2525 b/.01
2525.02	2	13.4	49.245	10.37	15606	400	CTOI from Planet Hunters; TOI-2525 c/.02
2527.01	1	11.17	2.302	12.15	1260	2270	possibly synchronized with variability; CTOI from Samuel Grunblatt
2529.01	1	10.67	0.0	10.97	4240	808	single transit; very slight depth-aperture; CTOI from Rafael Brahm
2531.01	1	12.43	8.148	10.14	13498	790	CTOI from Rafael Brahm; also found in faint-star QLP search
2536.01	1	12.7	31.992	0.0	13054	574	Gaia EDR3 parallax is .92 mas; CTOI from Rafael Brahm; no stellar radius
2539.01	1	11.48	0.986	5.2	1343	2119	SG1 should clear two neighbors
2540.01	2	8.27	12.719	2.59	1144	477	CTOI from George Zhou; inner candidate in potential multi; likely multi
2540.02	2	8.27	22.082	2.29	1019	435	CTOI from George Zhou; outer candidate in potential multi
2541.01	1	9.88	1.412	8.15	520	2858	Weak odd-even difference. Apparent secondary eclipse potentially due to stellar variability.
2544.01	1	10.69	21.069	15.36	3393	953	Eccentric EB with secondaries at 0.54 phase; originally alerted on secondaries at period of 10.5 days; retired as TFOP FP/EB
2549.01	1	11.73	4.858	0.0	11067	1546	no radius; found in faint-star QLP search
2553.01	1	11.78	8.385	11.33	12010	1066	

Table B.2. Continued.

TOI ID	$N_p$	$T$ [mag]	$P$ [days]	$R_p/R_\oplus$	depth [ppm]	$T_{\text{eq}}$ [K]	comment
2557.01	1	11.18	9.831	24.45	4990	1595	large Rp
2577.01	1	11.6	3.749	13.25	4860	1635	CTOI from Olmschenk (2021)
2588.01	1	10.64	3.587	10.01	3120	1016	v-shaped
2589.01	1	10.67	61.628	11.74	8878	601	TOI-2589 b
2606.01	1	11.78	1.451	20.54	7270	1944	V-shaped; Potential synchronisation in variability; hint of secondary in multiyear report
2612.01	1	13.23	13.357	19.3	29950	988	found in faint-star QLP search
2617.01	1	13.11	6.319	16.87	28370	958	found in faint-star QLP search
2618.01	1	12.05	8.25	11.87	2250	1764	found in faint-star QLP search; slight odd-even
2622.01	1	13.51	1.221	17.47	25580	1915	found in faint-star QLP search
2624.01	1	13.44	3.024	13.18	26980	1052	found in faint-star QLP search
2625.01	1	13.23	2.148	0.0	22125	1413	found in faint-star QLP search; no stellar radius; phase modulations and secondary in SPOC s1-s69
2626.01	1	12.61	3.456	10.56	20449	847	found in faint-star QLP search
2628.01	1	13.3	0.872	10.55	6610	2291	found in faint-star QLP search
2630.01	1	11.7	9.713	12.32	3540	1027	found in faint-star QLP search; Rp with tic8 almost half of previous Rp (~22 Re -> ~12 Re)
2637.01	1	15.84	0.152	0.0	105147	2710	Host is hot subdwarf; no stellar radius; period likely too short for companion to be planetary; period updated to ~0.15 d with clear additional events at half period in recent SPOC sectors
2645.01	1	12.4	1.444	20.67	43370	1552	found in faint-star QLP search
2646.01	1	13.19	0.313	8.1	4540	2247	found in faint-star QLP search; short period; possible SV
2650.01	1	13.44	2.23	12.78	6708	1652	found in faint-star QLP search
2652.01	1	13.31	2.485	0.0	7950	1583	no radius; found in faint-star QLP search
2653.01	1	12.14	0.927	0.0	1640	1663	no stellar radius; found in faint-star QLP search
2660.01	1	12.08	5.018	10.76	2500	1030	found in faint-star QLP search
2661.01	1	13.05	3.626	12.21	10450	1228	found in faint-star QLP search
2678.01	1	13.44	3.452	10.27	13260	957	found in faint-star QLP search
2683.01	1	12.44	1.529	12.69	2800	1392	slightly V-shaped; found in faint-star QLP search
2684.01	1	13.3	2.476	5.26	4370	1179	found in faint-star QLP search
2685.01	1	13.32	3.471	11.18	10070	972	found in faint-star QLP search
2695.01	1	13.05	0.557	13.24	3250	1398	V-shaped; found in faint-star QLP search
2698.01	1	13.37	3.271	0.0	9670	929	no radius; found in faint-star QLP search
2699.01	1	13.06	5.826	14.02	12800	809	found in faint-star QLP search
2704.01	1	12.71	3.636	16.43	16700	1557	found in faint-star QLP search; CTOI from Olmschenk et al. (2021)
2721.01	1	12.85	4.163	11.11	12870	1265	found in faint-star QLP search; CTOI from Olmschenk et al. (2021)
2722.01	1	11.15	0.709	4.67	800	1612	V-shaped; found in faint-star QLP search
2723.01	1	13.32	3.384	16.22	10730	1533	found in faint-star QLP search
2724.01	1	13.19	1.488	18.31	44400	1349	found in faint-star QLP search
2725.01	1	12.06	0.185	4.11	1390	2554	found in faint-star QLP search
2726.01	1	13.4	3.947	18.75	16080	1250	found in faint-star QLP search; correct host star for ephemeris match on 100589632/TOI 2342
2727.01	1	13.05	0.671	12.24	2330	1904	found in faint-star QLP search
2734.01	1	12.68	4.588	5.59	2040	1299	found in faint-star QLP search
2735.01	1	12.95	1.966	13.23	29670	1033	found in faint-star QLP search
2739.01	1	11.9	3.147	12.75	5640	940	V-shaped; found in faint-star QLP search; variable host
2752.01	1	13.16	4.92	12.64	10380	1134	found in faint-star QLP search
2755.01	1	13.29	3.319	9.77	6490	1121	found in faint-star QLP search
2761.01	1	13.22	6.121	17.63	17560	1445	found in faint-star QLP search
2763.01	1	12.0	3.998	0.0	5420	0	no radius; found in faint-star QLP search; CTOI from Olmschenk et al. (2021)
2764.01	1	12.69	2.277	10.86	3620	1479	found in faint-star QLP search
2765.01	1	12.13	1.019	7.1	2230	1955	found in faint-star QLP search
2766.01	1	11.66	7.275	17.43	15010	0	found in faint-star QLP search
2785.01	1	13.1	11.505	0.0	15910	665	no radius; found in faint-star QLP search
2787.01	1	13.42	4.322	12.73	2640	1557	found in faint-star QLP search
2788.01	1	13.42	4.065	8.31	7700	1173	found in faint-star QLP search
2791.01	1	12.76	3.748	14.01	5010	1864	found in faint-star QLP search; CTOI from Olmschenk et al. (2021)
2792.01	1	12.33	7.119	12.54	3920	749	found in faint-star QLP search
2793.01	1	13.29	0.356	6.23	2320	1977	V-shaped; found in faint-star QLP search

Table B.2. Continued.

TOI ID	$N_p$	$T$ [mag]	$P$ [days]	$R_p/R_\oplus$	depth [ppm]	$T_{\text{eq}}$ [K]	comment
2795.01	1	13.48	3.634	11.46	15330	927	found in faint-star QLP search
2798.01	1	12.8	3.994	19.0	14090	1524	found in faint-star QLP search
2799.01	1	13.18	1.437	16.93	23180	1742	found in faint-star QLP search
2800.01	1	12.18	7.754	9.78	6560	937	found in faint-star QLP search
2801.01	1	13.42	5.414	15.52	8400	1020	found in faint-star QLP search
2803.01	1	12.08	1.962	17.45	20910	1882	found in faint-star QLP search
2813.01	1	12.48	4.565	14.65	8572	1789	found in faint-star QLP search; v-shaped
2814.01	1	11.09	5.479	15.18	9196	1403	found in faint-star QLP search; CTOI from Olmschenk et al
2817.01	1	12.12	6.28	9.97	10240	1071	found in faint-star QLP search
2818.01	1	11.32	4.04	14.23	15110	1515	found in faint-star QLP search; CTOI from Olmschenk et al. (2021)
2820.01	1	13.28	13.345	12.03	24630	620	found in faint-star QLP search
2821.01	1	12.92	0.286	13.69	1990	1571	V-shaped; found in faint-star QLP search
2824.01	1	13.09	2.209	13.79	4710	2901	found in faint-star QLP search
2825.01	1	13.02	5.949	11.62	7490	1284	found in faint-star QLP search
2832.01	1	12.97	2.689	13.09	10930	1655	found in faint-star QLP search; CTOI from Olmschenk et al. (2021)
2833.01	2	13.07	4.39	0.0	6550	1113	no radius; found in faint-star QLP search
2833.02	2	13.07	1.895	6.72	4247	1473	no stellar radius; two stars within 1 sigma of centroid
2837.01	1	13.5	0.86	0.0	14559	1916	no stellar parameters; V-shaped; found in faint-star QLP search; TFOP BEB/APC
2841.01	1	12.63	2.166	14.46	5930	3298	found in faint-star QLP search
2846.01	1	13.37	2.679	14.0	10530	1636	found in faint-star QLP search
2847.01	1	12.22	2.649	11.66	16770	1194	found in faint-star QLP search; CTOI from Olmschenk et al. (2021)
2850.01	1	10.66	6.633	7.47	3190	440	V-shaped; found in faint-star QLP search
2851.01	1	13.09	4.826	14.79	7650	1648	found in faint-star QLP search
2852.01	1	13.4	0.401	10.06	2000	2214	found in faint-star QLP search
2853.01	1	13.46	3.292	21.08	26840	1062	slightly V-shaped; found in faint-star QLP search
2856.01	1	12.7	0.599	11.59	1290	1950	found in faint-star QLP search
2857.01	1	12.46	0.622	8.64	2345	3263	found in faint-star QLP search; possible secondary; period updated to 2x alerted period (0.3 days) with spoc-s61-b0A
2858.01	1	13.36	2.418	0.0	4150	1299	no radius; found in faint-star QLP search
2859.01	1	12.94	3.959	20.25	13190	1505	found in faint-star QLP search
2861.01	1	13.03	6.627	11.13	5105	1202	found in faint-star QLP search
2862.01	1	13.04	11.487	15.52	16360	868	found in faint-star QLP search
2864.01	1	12.82	0.478	0.0	2690	2020	no radius; V-shaped; found in faint-star QLP search; multiple stars in pixel; distant host; period likely too short to be planetary companion
2865.01	1	12.68	0.452	9.83	1660	1751	found in faint-star QLP search
2867.01	1	13.49	5.639	14.2	7320	1308	found in faint-star QLP search
2868.01	1	12.97	9.38	12.15	8600	1103	found in faint-star QLP search
2872.01	1	12.89	5.22	14.75	6040	2058	found in faint-star QLP search
2873.01	1	12.66	1.252	0.0	8690	0	no radius; V-shaped; found in faint-star QLP search
2880.01	1	13.29	4.78	13.19	5250	1808	found in faint-star QLP search
2883.01	1	12.37	3.706	0.0	4710	1572	V-shaped; found in faint-star QLP search
2887.01	1	13.3	4.918	17.01	20620	1320	found in faint-star QLP search
2888.01	1	11.03	4.219	0.0	9198	0	no radius; V-shaped; found in faint-star QLP search
2889.01	1	12.97	3.658	0.0	32300	1512	found in faint-star QLP search; no stellar radius
2890.01	1	12.62	3.196	16.46	10760	1314	found in faint-star QLP search; v-shaped; possible odd-even
2891.01	1	11.75	17.308	17.42	8880	873	found in faint-star QLP search
2892.01	1	13.38	14.95	15.17	8070	950	found in faint-star QLP search
2893.01	1	13.3	10.363	7.37	5880	796	found in faint-star QLP search
2896.01	1	12.8	1.348	18.09	2570	1632	found in faint-star QLP search
2897.01	1	13.34	12.004	7.95	6890	826	found in faint-star QLP search
2898.01	1	13.43	3.613	17.57	9702	1786	found in faint-star QLP search
2903.01	1	12.73	3.595	5.1	3070	1015	found in faint-star QLP search; low SNR
2904.01	1	12.55	7.501	7.05	2550	1339	found in faint-star QLP search
2905.01	1	12.41	11.879	0.0	8580	780	found in faint-star QLP search; possible depth aperture correlation; v-shaped; variable host; host is distant and likely evolved so $R_p$ may be too large to be planetary; multiple stars in pixel
2910.01	1	13.34	3.308	0.0	11856	1223	found in faint-star QLP search

Table B.2. Continued.

TOI ID	$N_p$	$T$ [mag]	$P$ [days]	$R_p/R_\oplus$	depth [ppm]	$T_{\text{eq}}$ [K]	comment
2911.01	1	13.38	1.77	10.95	49803	922	found in faint-star QLP search; likely M-dwarf host; Rp from qlp-s36-tois as spoc is assuming Rstar is solar
2912.01	1	11.38	8.761	11.81	4200	1037	found in faint-star QLP search
2914.01	1	13.21	3.052	15.53	5836	2154	found in faint-star QLP search
2915.01	1	12.52	5.13	0.0	7670	992	found in faint-star QLP search; no stellar radius
2921.01	1	12.88	3.004	13.45	11000	1596	found in faint-star QLP search; CTOI from Olmschenk et al. (2021)
2923.01	1	12.85	4.323	12.22	9090	1246	found in faint-star QLP search
2924.01	1	12.15	7.35	10.95	5727	1175	found in faint-star QLP search
2932.01	1	12.64	3.257	15.97	5960	1956	found in faint-star QLP search
2944.01	1	13.31	7.793	25.45	16340	1164	found in faint-star QLP search; ~2000-3000 ppm secondary in SPOC s1-s65 at half phase
2945.01	1	12.95	3.201	15.36	5500	2123	found in faint-star QLP search
2948.01	1	13.18	2.756	14.79	14830	1261	slightly V-shaped; found in faint-star QLP search; possible secondary at half phase; no stellar radius in TIC; Gaia DR2 Rstar ~1.18 Rsun
3002.01	1	13.3	7.797	22.98	23150	603	found in faint-star QLP search
3003.01	1	11.92	1.622	7.13	1250	2204	found in faint-star QLP search; noisy but strong BLS
3006.01	1	11.96	8.613	20.68	12840	1009	found in faint-star QLP search; large Rp for orbital period; "The Gaia DR3 NSS SB1 list has a 51 km/s signal at same period as planet candidate."; v-shaped
3007.01	1	13.16	4.277	12.03	5000	1508	found in faint-star QLP search
3009.01	1	12.91	3.365	16.72	7700	2373	found in faint-star QLP search
3010.01	1	11.97	9.554	18.04	18260	933	found in faint-star QLP search
3011.01	1	13.25	1.842	0.0	10500	1478	V-shaped; found in faint-star QLP search; no stellar radius; ~1300 ppm secondary in SPOC s1-s65; Gaia DR3 RV error ~7.3 km/s; parallax and temperature and log g suggest host star is distant evolved F star
3013.01	1	12.7	5.472	11.57	1800	1619	found in faint-star QLP search; low SNR; some depth aperture correlation
3014.01	1	13.26	1.795	8.71	2860	2288	found in faint-star QLP search
3015.01	1	13.24	4.275	10.75	3620	1625	found in faint-star QLP search
3016.01	1	13.18	5.114	12.99	7090	1069	found in faint-star QLP search; slight depth aperture correlation
3017.01	1	12.54	3.053	16.92	14090	1727	found in faint-star QLP search
3019.01	1	13.48	5.959	12.8	15090	891	V-shaped; found in faint-star QLP search
3020.01	1	13.44	3.033	19.69	12000	1608	found in faint-star QLP search
3021.01	1	13.56	11.265	0.0	10110	1055	found in faint-star QLP search; no stellar radius
3348.01	1	11.4	2.616	4.05	2340	1614	found in faint-star QLP search
3354.01	1	10.96	46.381	5.75	1108	696	
3355.01	1	10.82	15.66	2.14	400	904	low SNR
3360.01	1	10.69	16.738	16.01	2570	521	
3363.01	1	10.15	9.743	0.0	1566	0	B9 host; possibly a large planet
3368.01	1	12.83	7.261	15.44	3980	1628	found in faint-star QLP search
3370.01	1	12.02	2.351	6.4	1940	1832	found in faint-star QLP search; multiple stars in pixel
3374.01	1	13.1	2.654	23.74	18470	2022	found in faint-star QLP search
3376.01	1	13.42	4.726	14.79	6910	2218	potential weak secondary at phase 0.5; found in faint-star QLP search
3378.01	1	11.97	2.61	15.94	2844	2540	found in faint-star QLP search
3386.01	1	12.48	0.886	5.05	1900	1811	found in faint-star QLP search
3391.01	1	13.51	4.713	19.76	10493	1643	found in faint-star QLP search; Gaia DR2 Rstar ~2.23; large Rp
3393.01	1	13.62	5.206	11.13	9210	1139	found in faint-star QLP search
3394.01	1	12.14	7.837	7.62	2880	1113	found in faint-star QLP search; possible centroid offset to S
3395.01	1	12.68	3.273	0.0	4030	1069	found in faint-star QLP search
3403.01	1	11.97	11.221	17.09	10721	1032	found in faint-star QLP search
3407.01	1	13.06	1.385	11.98	4150	2006	found in faint-star QLP search
3410.01	1	11.58	3.979	0.0	4000	0	found in faint-star QLP search
3411.01	1	13.14	7.063	0.0	13490	0	found in faint-star QLP search
3413.01	1	12.59	4.711	15.65	5410	1588	V-shaped; found in faint-star QLP search
3414.01	1	11.89	9.736	9.29	2590	1250	found in faint-star QLP search
3429.01	1	12.45	13.931	14.02	6720	806	found in faint-star QLP search
3432.01	1	13.79	9.148	0.0	22476	871	V-shaped; found in faint-star QLP search; no stellar parameters; Gaia DR2 color and parallax suggest host is a red giant
3437.01	1	13.07	4.987	12.45	16931	1039	found in faint-star QLP search



Table B.2. Continued.

TOI ID	$N_p$	$T$ [mag]	$P$ [days]	$R_p/R_\oplus$	depth [ppm]	$T_{\text{eq}}$ [K]	comment
4180.01	1	8.26	1.595	4.32	474	2578	possible odd-even or secondary; variable star
4189.01	1	8.76	46.962	2.47	758	468	
4212.01	1	11.97	2.349	0.0	3070	1987	found in faint-star QLP search
4223.01	1	12.8	7.265	13.01	13930	1022	found in faint-star QLP search
4224.01	1	12.28	1.161	10.76	4320	2501	found in faint-star QLP search; v-shaped; possible centroid offset to E
4231.01	1	12.36	3.297	13.46	6550	1885	found in faint-star QLP search
4233.01	1	13.57	1.82	16.63	7330	1898	found in faint-star QLP search
4234.01	1	13.54	0.908	8.54	5020	2617	found in faint-star QLP search
4242.01	1	12.47	3.058	14.25	7765	1613	found in faint-star QLP search; CTOI from Olmschenk et al. (2021)
4243.01	1	10.75	1.089	8.71	412	3762	found in faint-star QLP search
4244.01	1	12.4	1.867	10.21	3606	2050	found in faint-star QLP search
4245.01	1	11.61	3.153	5.72	4103	1076	found in faint-star QLP search; multiple stars in pixel
4246.01	1	12.9	12.886	12.1	11435	848	found in faint-star QLP search
4247.01	1	13.56	4.354	23.03	41586	1176	found in faint-star QLP search
4249.01	1	13.55	6.773	19.13	8606	963	V-shaped; found in faint-star QLP search
4250.01	1	13.42	4.019	13.96	6230	1897	found in faint-star QLP search
4252.01	1	12.66	2.609	13.9	10432	1694	found in faint-star QLP search
4253.01	1	12.9	3.419	0.0	19415	1210	found in faint-star QLP search
4254.01	1	12.54	1.146	14.12	4058	2697	found in faint-star QLP search
4255.01	1	12.52	2.506	12.97	3170	1956	found in faint-star QLP search; possible centroid centered near TIC 82302236
4259.01	1	11.86	8.961	17.09	11334	1000	V-shaped; found in faint-star QLP search
4262.01	1	11.19	5.998	11.36	7349	1234	found in faint-star QLP search
4265.01	1	12.12	3.735	8.62	2360	1085	found in faint-star QLP search
4286.01	1	13.52	1.027	3.28	1430	1925	found in faint-star QLP search
4288.01	1	13.18	6.06	8.07	8270	603	found in faint-star QLP search
4303.01	1	9.46	8.611	4.31	543	1320	
4313.01	1	9.6	6.823	3.6	226	1370	L1 candidate
4319.01	1	10.82	0.0	6.55	6743	379	alert as single transit on second event
4322.01	1	10.16	13.419	2.42	348	851	weak signal; possibly off-target; odd transits might not be real
4328.01	1	7.77	703.794	1.86	602	190	two transits; actual period likely shorter than 704 days
4343.01	1	11.26	11.542	1.88	416	791	
4344.01	1	9.48	731.481	3.25	245	291	check neighbor TIC 6649664; low MES; possibly a single transit at $\sim 1507$ TBJD
4348.01	1	8.4	602.245	2.87	220	305	period may be half the max period of $\sim 602$ days
4351.01	1	11.02	20.146	2.44	576	589	
4355.01	1	7.23	0.0	3.07	186	291	low SNR; updated to single transit at $\sim 1507.586$ TBJD base don s1-s69 not finding original second event at TBJD $\sim 2181$
4356.01	1	9.25	579.647	4.05	564	306	period could be half; low SNR; bad transit shape; only two transits
4362.01	1	8.46	7.548	2.83	249	1272	possible odd-even; some bad difference images; possibly SV
4369.01	1	9.33	13.577	3.58	263	1090	two stars in pixel of similar magnitude; L1 candidate; this star is listed as spectroscopic binary with period of 516.83 days (Gaia DR3 NS) and also a visual binary with TIC 278862747
4403.01	1	10.74	4.462	3.04	290	1456	potential L1 planet; 2 sectors show significant centroid offsets not centered on other stars
4404.01	1	10.71	39.624	16.76	4511	673	possible secondary at QLP at phase=0.25 ruled out by later SPOC data
4408.01	1	13.29	2.054	3.51	1994	938	
4409.01	1	11.81	92.492	7.77	11488	305	
4503.01	1	9.04	710.698	2.09	691	244	two transits; actual period likely shorter than 710.697 days; first event is after momentum dump
4504.01	2	12.55	82.929	11.48	13068	183	8 hour TTV; potential multi
4504.02	2	12.55	2.426	2.66	755	1234	potential multi; L1 candidate
4505.01	1	10.38	19.472	17.33	7063	1052	Gaia DR2 RV error 3.76 km/s; strong stellar pulsations; large PC for period
4507.01	1	10.23	104.616	15.82	6111	562	some odd-even in spoc-s01-s65; may be affected by variable host; possibly too large for insolation
4508.01	1	11.84	3.467	2.11	3657	493	potential L1 planet; low MES
4509.01	1	11.4	0.0	10.49	3178	530	still a single transit as of s69
4510.01	1	10.36	194.243	4.47	811	478	weak signal; just 2 transits

Table B.2. Continued.

TOI ID	$N_p$	$T$ [mag]	$P$ [days]	$R_p/R_\oplus$	depth [ppm]	$T_{\text{eq}}$ [K]	comment
4558.01	1	8.71	6.581	1.68	55	1006	weak signal; evolved host star
4562.01	1	11.53	225.104	13.21	10850	341	TOI-4562 b
4567.01	2	11.92	0.841	1.67	549	1088	potential multi
4567.02	2	11.92	23.542	2.31	1412	358	possible multi; L1 candidate
4663.01	1	13.0	5.292	10.13	17870	745	found in faint-star QLP search
4670.01	1	14.87	15.501	10.83	90070	254	found in faint-star QLP search
4676.01	1	13.22	13.292	8.66	7360	652	found in faint-star QLP search
4680.01	1	13.17	17.431	9.82	8180	714	found in faint-star QLP search
4691.01	1	13.36	8.573	10.41	4880	1076	found in faint-star QLP search
4692.01	1	13.28	4.052	10.72	5310	619	found in faint-star QLP search
4706.01	1	11.38	735.982	12.54	9100	0	period may be several times shorter than max period of ~736 days; found in faint-star QLP search
4710.01	1	12.9	1.48	8.37	3090	1909	found in faint-star QLP search
4746.01	1	11.9	7.54	4.39	2920	759	found in faint-star QLP search
4747.01	1	11.81	5.219	3.83	1500	1035	found in faint-star QLP search
4755.01	1	12.02	22.727	19.08	6510	677	found in faint-star QLP search
4757.01	1	13.5	2.08	11.55	5260	2165	found in faint-star QLP search
4759.01	1	12.26	9.658	9.98	2300	1117	found in faint-star QLP search
4765.01	1	13.05	16.373	0.0	7810	799	found in faint-star QLP search; no stellar radius; Rp be too large to be planetary depending on Rstar
4767.01	1	13.19	2.732	13.24	3880	1927	found in faint-star QLP search
4768.01	1	10.44	7.264	15.08	7988	1295	found in faint-star QLP search
4770.01	1	12.98	1.949	15.83	11670	2165	found in faint-star QLP search; possible offset on TIC 112110893 (Tmag~16)
4774.01	1	12.54	8.6	4.56	1620	1020	found in faint-star QLP search
4775.01	1	11.53	2.473	15.5	2740	1826	found in faint-star QLP search
4778.01	1	12.93	3.807	15.42	8644	1359	found in faint-star QLP search
4779.01	1	13.48	10.749	11.47	9240	639	star marker in diffimage does not look accurate; found in faint-star QLP search
4780.01	1	12.46	4.694	16.49	5310	1546	found in faint-star QLP search
4788.01	1	12.48	4.393	14.03	11110	1134	found in faint-star QLP search
4789.01	1	13.16	7.5	11.25	8750	812	found in faint-star QLP search
4795.01	1	12.92	2.743	0.0	8230	1901	star marker in diffimage does not look accurate; found in faint-star QLP search; no stellar radius
4796.01	1	13.15	3.578	15.32	8730	1415	found in faint-star QLP search
4799.01	1	13.1	4.023	12.89	7560	1496	found in faint-star QLP search
4801.01	1	12.96	3.251	0.0	7880	1348	found in faint-star QLP search; no stellar radius; Rp may be too large to be planetary if Rstar is evolved
4804.01	1	10.23	5.065	8.29	915	1514	found in faint-star QLP search; possible offset to S
4806.01	1	11.75	8.448	4.98	2000	1033	found in faint-star QLP search
4807.01	1	11.97	17.687	8.8	10310	333	V-shaped; found in faint-star QLP search
4812.01	1	12.97	3.314	8.16	3550	1753	found in faint-star QLP search
4816.01	1	13.31	11.247	15.75	10340	920	found in faint-star QLP search
4819.01	1	13.08	1.589	14.03	22530	1245	V-shaped; found in faint-star QLP search
4821.01	1	12.78	5.469	12.67	5940	1137	found in faint-star QLP search
4822.01	1	12.66	4.471	15.89	5140	2415	found in faint-star QLP search
4825.01	1	11.23	2.818	0.0	7916	1290	found in faint-star QLP search; no stellar radius in report; Gaia DR2 has Rstar ~ 2 Rsun which would indicate companion is planetary in size
4828.01	1	13.35	19.029	8.14	8910	536	found in faint-star QLP search
4842.01	1	11.74	5.337	16.55	2780	889	found in faint-star QLP search
4844.01	1	12.54	4.543	11.92	8670	1489	found in faint-star QLP search
4848.01	1	13.1	3.724	18.05	8089	1733	crowded field; found in faint-star QLP search
4851.01	1	9.4	21.609	2.13	320	888	found in faint-star QLP search
4858.01	1	14.81	1.751	16.68	70067	666	found in faint-star QLP search; v-shaped; Rp likely too large for M dwarf host
4879.01	1	13.33	5.376	9.72	4040	1099	found in faint-star QLP search
4888.01	1	12.07	9.419	8.09	2670	1076	found in faint-star QLP search; weak transit shape due to poor detrending
4906.01	1	13.37	11.977	8.82	6760	845	found in faint-star QLP search
4908.01	1	13.22	19.711	10.0	4150	889	found in faint-star QLP search
4923.01	1	12.26	12.918	9.96	4615	805	found in faint-star QLP search
4940.01	1	11.76	25.866	6.76	2613	643	found in faint-star QLP search

Table B.2. Continued.

TOI ID	$N_p$	$T$ [mag]	$P$ [days]	$R_p/R_\oplus$	depth [ppm]	$T_{\text{eq}}$ [K]	comment
4980.01	1	12.93	16.157	0.0	13030	466	found in faint-star QLP search; no stellar radius
4981.01	1	12.48	0.21	11.96	1250	2489	found in faint-star QLP search; short period duration (~5 hours)
4988.01	1	14.88	2.37	21.17	46129	843	found in faint-star QLP search
5151.01	1	12.83	92.195	16.01	27400	298	source of signal previously alerted as TOI-2239.01 /TIC-388130235 (now retired as FP); this is the real star
5402.01	1	12.38	3.317	1.45	462	810	small star small planet
5541.01	1	12.29	9.018	5.61	3480	892	actual source of signal previous alerted as TOI 2448.01 on TIC 231721005
6093.01	1	10.04	1.271	7.86	1115	2380	V-shaped; possible odd-even
6095.01	1	10.1	2.161	1.87	529	1187	variable host
6098.01	1	8.77	2.73	2.12	362	1048	
6100.01	1	11.94	1.228	3.2	1317	1448	Weak signal; short duration; nearby TIC 770748659 (delta Tmag ~ 5) about 1.5 '' away
6102.01	1	13.58	5.371	12.06	14601	1041	
6103.01	1	10.67	3.242	13.81	10616	1596	nearby bright star (Tmag~8) 35'' away contaminating difference image but signal appears to be on this star
6105.01	1	10.77	3.112	14.38	14170	1204	
6107.01	1	11.73	3.79	23.93	7609	2671	large planet around large star
6108.01	1	13.75	3.878	12.53	7843	1330	
6264.01	1	10.2	5.693	3.81	291	1529	L1 candidate; possible offset E; slight depth aperture correlation
6271.01	1	13.7	1.604	13.86	19169	1557	multiple stars in pixel; no stellar radius but Gaia DR2 Rs=1.22 so Rp~17 Re
6401.01	1	12.68	3.02	0.0	11319	0	found in faint-star QLP search
6407.01	1	12.12	8.991	10.91	3320	1295	found in faint-star QLP search
6409.01	1	12.24	1.53	19.19	9499	2220	found in faint-star QLP search
6411.01	1	13.08	8.217	7.33	5304	1010	found in faint-star QLP search
6415.01	1	13.42	20.838	10.5	10875	689	found in faint-star QLP search
6416.01	1	13.29	8.233	0.0	29859	0	found in faint-star QLP search
6421.01	1	13.28	3.751	17.42	13942	1527	found in faint-star QLP search
6424.01	1	13.25	2.04	7.5	4429	1863	found in faint-star QLP search
6425.01	1	11.96	12.142	11.8	4584	903	found in faint-star QLP search
6427.01	1	12.46	18.373	8.41	4311	764	found in faint-star QLP search
6428.01	1	13.18	1.676	17.74	13272	1463	found in faint-star QLP search
6435.01	1	11.05	6.116	6.7	3588	754	found in faint-star QLP search
6437.01	1	11.62	8.31	18.26	5667	1603	found in faint-star QLP search
6442.01	1	11.04	2.828	18.52	14846	1611	found in faint-star QLP search
6443.01	1	11.8	9.987	10.29	2884	893	found in faint-star QLP search
6444.01	1	13.34	12.293	14.02	10299	991	found in faint-star QLP search
6448.01	1	12.32	14.844	7.05	7245	641	found in faint-star QLP search
6451.01	1	13.39	5.495	10.08	5504	1296	found in faint-star QLP search
6453.01	1	13.05	6.869	12.82	4404	1506	found in faint-star QLP search
6455.01	1	10.87	0.897	15.85	2703	2622	V-shaped; evolved host
6459.01	1	10.36	5.149	2.77	737	1302	found in faint-star QLP search; possible centroid offset
6471.01	1	13.14	3.076	5.1	2346	1354	found in faint-star QLP search
6472.01	1	13.3	2.681	14.35	6451	2525	found in faint-star QLP search
6475.01	1	12.32	26.599	15.71	8222	1093	found in faint-star QLP search
6480.01	1	11.84	750.24	9.69	6713	135	found in faint-star QLP search; period likely shorter
6483.01	1	12.47	5.208	6.03	4315	570	found in faint-star QLP search
6484.01	1	12.08	18.246	3.87	3157	579	found in faint-star QLP search
6488.01	1	11.82	8.085	3.89	1521	864	found in faint-star QLP search
6493.01	1	12.48	3.067	3.39	3497	687	found in faint-star QLP search
6513.01	1	14.82	2.421	9.94	20899	670	found in faint-star QLP search
6520.01	1	12.72	7.602	19.35	2969	719	found in faint-star QLP search
6521.01	1	14.92	3.581	12.25	41493	661	found in faint-star QLP search
6523.01	1	12.8	7.809	14.05	11239	1065	found in faint-star QLP search
6524.01	1	14.48	0.852	16.07	51018	689	found in faint-star QLP search
6535.01	1	11.74	20.836	7.56	2451	704	found in faint-star QLP search
6549.01	1	12.23	6.108	19.14	14668	1222	Gaia DR3 NSS SB1 list has a 13 km/s signal at P ~7.6 d
6550.01	1	10.81	6.915	15.96	5765	1965	found in faint-star QLP search
6552.01	1	12.39	3.271	13.58	7559	1551	
6601.01	1	14.65	32.544	12.0	101822	167	found in faint-star QLP search
6614.01	1	12.57	25.071	11.99	12286	532	found in faint-star QLP search

Table B.2. Continued.

TOI ID	$N_p$	$T$ [mag]	$P$ [days]	$R_p/R_\oplus$	depth [ppm]	$T_{\text{eq}}$ [K]	comment
6618.01	1	11.28	35.789	9.21	2256	796	CTOI from Montalto et al.; found in faint-star QLP search
6621.01	1	12.81	4.281	2.84	2031	778	found in faint-star QLP search
6622.01	1	13.33	37.858	7.36	5180	664	found in faint-star QLP search
6633.01	1	12.18	6.548	2.29	988	878	found in faint-star QLP search
6640.01	1	12.39	16.936	3.6	2618	633	found in faint-star QLP search
6644.01	1	12.57	42.731	4.04	2711	499	found in faint-star QLP search
6654.01	1	10.1	9.516	17.81	487	610	evolved host; Rstar may be smaller ( $\sim 5.8 R_{\text{sun}}$ in Sharma+2018); possible depth aperture correlation
6670.01	1	8.89	0.0	9.39	2390	309	single transit; long duration; CTOI from Guoyou Sun
6690.01	2	10.3	761.709	2.56	545	200	two events; real period likely shorter than 761 days; somewhat v-shaped; low MES/SNR
6690.02	2	10.3	904.535	2.73	603	238	alerted as single at TBJD $\sim 1433$ ; now have second transit with max period of $\sim 904.534$ d; actual period could be shorter
6691.01	1	8.62	0.0	2.95	184	340	single transit; possible additional transits at $\sim 2119$ and $\sim 2367$ TBJD; still a single transit as of s69
6700.01	1	12.23	15.518	9.48	3717	942	CTOI from Marco Montalto (Montalto et. al 2020)
6701.01	1	11.3	10.018	12.32	1791	1313	v-shaped; some events on/near momentum dumps potentially causing apparent odd-even
6702.01	1	12.98	2.187	3.33	769	960	crowded field; many fainter stars in pixel; v-shaped; possible odd-even
6703.01	1	8.44	49.618	2.47	88	745	low MES/SNR; possible L1 planet; slightly evolved host
6704.01	2	11.53	2.861	0.0	928	1284	potential multi; equally bright neighbor 2 arcsec away; no stellar radius but host is likely K dwarf which would allow for possible L1 Rp
6704.02	2	11.53	6.828	5.09	1559	961	potential multi; likely K dwarf host; equally bright star in same pixel
6707.01	1	12.33	3.835	5.66	1112	1509	possible odd-even
6710.01	1	9.69	2.067	1.51	394	1127	low SNR; variable host
6716.01	1	11.77	4.719	1.01	1735	375	low SNR; flaring host; some transits close to flares
6725.01	1	9.76	2.148	0.0	136	0	no stellar radius; host is likely nearby late K dwarf; Rp likely $< 2 R_{\text{e}}$ based on transit depth
6728.01	1	9.61	24.964	4.53	461	768	slightly evolved host star
6813.01	1	12.07	2.356	1.98	740	1150	found in faint-star QLP search
6820.01	1	12.9	2.014	2.55	971	1261	found in faint-star QLP search
6826.01	1	12.18	6.438	2.11	730	879	found in faint-star QLP search
6847.01	1	13.13	1.394	8.87	5131	1545	found in faint-star QLP search; variable host
6851.01	1	12.47	12.01	2.29	1204	513	found in faint-star QLP search
6854.01	1	13.11	2.766	6.36	2476	1258	found in faint-star QLP search
6900.01	1	11.59	13.922	1.72	552	534	low SNR; inconsistent centroids; many fainter stars nearby
6902.01	1	5.68	36.436	2.87	384	705	variable host; interior to HR2562 b
6957.01	1	10.85	160.676	3.22	960	320	some asymmetry in some transits; only 4 events
7047.01	1	11.77	5.273	2.57	1177	1140	L1 candidate; some depth aperture correlation; CTOI from Marco Montalto

**Notes.** The columns give: the TOI identifier of the planet, the multiplicity of the system, the TESS magnitude  $T$ , the orbital period  $P$  in days, the planetary radius  $R_p$  in Earth units, the planetary equilibrium temperature in K, and a comment field. All the columns except the second one were copied from the TOI database, 2024-08-20 release (Guerrero et al. 2021)